Development and Evaluation of Effective Turbidity Monitoring Methods for Construction Projects

Bruce Wilson, Principal Investigator
Departments of Bioproducts/Biosystems and Civil Engineering
University of Minnesota

July 2014

To request this document in an alternative format call 651-366-4718 or 1-800-657-3774 (Greater Minnesota) or email your request to ADArequest.dot@state.mn.us. Please request at least one week in advance.

Technical Report Documentation Page

1. Report No. MN/RC 2014-24	2.	3. Recipients Accession No.	
4. Title and Subtitle Development and Evaluation of Effective Turbidity Monitoring Methods for Construction Projects		5. Report Date July 2014	
		6.	
7. Author(s) R. Perkins, B. Hansen, B. Wilson and J. Gulliver		8. Performing Organization Report No. CTS Project #2011108	
9. Performing Organization Name and Address Departments of Bioproducts/Biosystems and Civil Engineering University of Minnesota 1390 Eckles Avenue St. Paul, MN 55108		10. Project/Task/Work Unit No.	
		11. Contract (C) or Grant (G) No. Contract number: (c) 89261 (wo) 250	
12. Sponsoring Organization Name and Address Minnesota Department of Transportation Research Services & Library 395 John Ireland Boulevard, MS 330 St. Paul, MN 55155		13. Type of Report and Period Covered Final Report	
		14. Sponsoring Agency Code	
15. Supplementary Notes http://www.lrrb.org/pdf/201424.pdf			

16. Abstract (Limit: 250 words)

Various agencies have discussed the possibility of using turbidity as an effluent standard for construction site. Turbidity monitoring can be difficult for dynamic construction sites. This project investigated turbidity relationships for conditions of Minnesota and developed protocols for the design and installation of cost-effective monitoring systems. Turbidity characteristics of fourteen different soils in Minnesota were investigated using the laboratory protocols. Trends in turbidity with sediment concentrations were well represented by power functions. The exponent of these power functions was relatively constant between soils and the log-intercept, or scaling parameter varied substantially among the different soils. A regression analysis for the scaling parameter was a function of percent silt, interrill erodibility, and maximum abstraction. A power value of 7/5 was chosen to represent all soils. The field studies were also used to develop turbidity monitoring systems that would be adaptable to construction sites and to collect turbidity data on construction site runoff. Construction site turbidities often exceeded 1000 NTUs and sometimes surpassed 3000 NTUs.

17. Document Analysis/Descriptors Turbidity, construction management, erosion, best practices	18. Availability Statement No restrictions. Document available from: National Technical Information Services, Alexandria, VA 22312
19. Security Class (this report) Unclassified	20. Security Class (this page) Unclassified	21. No. of Pages 158	22. Price

Development and Evaluation of
Effective Turbidity Monitoring Methods for
Construction Projects

Final Report

Prepared by:

Rebekah Perkins
Department of Civil Engineering

Brad Hansen
Department of Bioproducts and Biosystems Engineering

Bruce Wilson
Department of Bioproducts and Biosystems Engineering

John Gulliver
Department of Civil Engineering
University of Minnesota

July 2014

Table of Contents

List of Tables

List of Figures

Executive Summary

Stormwater runoff from construction sites can transport eroded sediment to nearby water bodies degrading water quality and impairing biotic communities. The use of turbidity as measure of the sediment loads leaving construction sites has been of interest in Minnesota and elsewhere. The project examined turbidity relationships and monitoring systems to measure field turbidity data. Laboratory protocols have been developed herein for studying the factors that impact turbidity from construction site soils. Experimental procedures include the use of a rainfall simulator to generate runoff and turbidity values from soils carefully packed in appropriate test boxes. Turbidity characteristics of fourteen different soils in Minnesota were investigated using the laboratory protocols. Trends in turbidity with sediment concentrations were well represented by power functions. The exponent of these power functions was relatively constant between soils and the log-intercept, or scaling parameter varied substantially among the different soils. Multiple soil properties were evaluated for each soil. An extensive regression analysis resulted in a model using percent silt, interrill erodibility, and maximum abstraction that best represented the intercept term. A power value of 7/5 was chosen to represent all soils. A second laboratory experiment was performed to determine how particle settling affects the coefficients of the turbidity -TSS relationship. The scaling parameter increased with sediment deposition and the power value decreased.

The field studies were also used to develop turbidity monitoring systems that would be adaptable to construction sites and to collect turbidity data on construction site runoff. Two different monitoring systems were developed from this project. The first was a turbidity flume designed to monitor turbidity levels from overland flows and the second was designed to monitor turbidity values during de-watering activities. Turbidity values were measured at two different construction sites. Both turbidity values generated from onsite erosion control practices and runoff leaving the construction site were recorded. Turbidities easily exceeded 1000 NTUs and often surpassed 3000 NTUs for most of the runoff events recorded.

To better understand the accuracy of turbidity measurements on construction site soils in Minnesota a laboratory analysis of five different turbidity sensors on five different soil

textures was conducted . As expected both differences in soil texture and probe configuration impacted the accuracy of the turbidity readings.

Chapter 1
Introduction

Background Information

Stormwater runoff from construction sites needs to be managed to avoid undesirable off-site impacts. This runoff contains eroded sediment from the exposed, barren ground which is often transported to nearby water bodies causing water quality impairment, degrading their biotic communities and reducing their capacity to store water with sediment deposition. Reducing these negative impacts is dependent on determining the mass and concentration of eroded sediment in runoff. The quickest and a cost effective method of assessing these impacts is to measure the turbidity of the runoff.

Construction sites by nature have the potential to create high turbidity values related to suspended sediment loads during storm events. For example, NCHRP (2012) estimated that using conventional best management practices would still result in turbidities of 500 to 1000 NTU's leaving the site. This is substantially larger than standard suggested by the EPA (Environment Protection Agency) in 2011 of 280 Nephelometric Turbidity Units (NTUs). Other states have considered implementing turbidity standards (California, 250 to 500 NTUs, Georgia 75 to 750 NTUs and reportable limits of 25 NTUs in Vermont and Washington). The usefulness of turbidity standards rests upon the validity of the turbidity data collected at construction sites.

The use of using measured turbidity data to accurately represent sediment load leaving construction sites faces a number of challenges. Extensive variability in soils, slopes, compactions and erosion control methods increases the difficulty of calibrating turbidity probes and in selecting sites for data collection. The rapidly changing conditions result in a moving target for monitoring sites. The location of roads, stock piles, sediment basins, culvert outfalls, and ditches changes as the construction site moves to completion. The long-term monitoring over the life of the construction process at a single location is rarely possible. Construction site runoff can leave a site using a number of different conduits such as; culverts outfalls, ditches, side slopes, storm water pond overflows and dewatering activities. No single monitoring design can fit all these different locations or processes. Proper calibration, maintenance and installation

procedure are also important to help reduce the effects of high turbidity values or excessive bed loads that can overwhelming equipment.

Measurement of Turbidity

Turbidity is an optical property of water associated with the light scattering properties of the particles suspended in water. This measurement can be used as a surrogate to determine the concentration of sediment in construction site runoff. A turbidity meter is a device that is comprised of at least one light source and one photo-detector. The light source is beamed through a sample, and the light is scattered as it interacts with the particles in the water and the water itself. The photo-detector then reads how much light reaches it and at what angle, thus determining the turbidity of the sample. There are many kinds of turbidity meters. One of the goals of the project is to evaluate the differences in measured turbidity obtained from these different sensors.

Turbidity meters have been different features depending on their uses. Bench top turbidity meters are laboratory based meters that measure the turbidity of grab samples taken from the site. There are also portable turbidity meters. Portable meters measure the turbidity of grab samples, but are more durable for travelling and on-site weather conditions. There are also turbidity meters designed to continuously monitor and record turbidity on-site. These turbidity meters only measure turbidity at a point, and need to be positioned at optimal places at a site. However, they capture the changes in turbidity as runoff occurs, creating a better temporal representation of turbidity (Sadar, 2007).

Turbidity meters can have many different light/photo-detector set-ups. The U.S. Environmental Protection Agency (EPA) (1999) describes three standard turbidity meters. A standard single beam turbidity meter is comprised of one light source and one photo-detector situated 90° from the light source. This type of turbidity meter uses a tungsten filament light source that can generate a wide range of light wavelengths, measures in nephelometric turbidity units (NTU) directly, and is accurate for samples of colorless water with low turbidity. However, this design

has many limitations. This meter has a low range of applicability and needs frequent calibration because of changes in the tungsten filament light source.

A ratio turbidity meter uses one light source and several photo-detectors that detect forward scatter, transmitted light, backscatter, and light scattered at 90°. The light scatter readings are mathematically combined to determine turbidity in NTU's. This limits the effect of water color, allowing for a turbidity reading that better captures the turbidity caused by the suspended particles themselves. This turbidity meter design is more accurate, but it still has a low NTU range. Also, depending on what light source is used, this turbidity meter design may still require frequent calibration (EPA 1999).

A modulated four beam turbidity meter uses two light sources and two photo-detectors all located 90° around the sample volume with each light source directly across from a photo-detector. This design alternates using each light source, measuring transmitted light and 90° scattered light with each light beam. The light scatter readings are mathematically combined using an algorithm to determine turbidity in NTU's. This algorithm uses an equation such that the effect of water color completely cancels out, allowing for a turbidity reading only based on the effect of suspended particles. This design is accurate from 0 to 100 NTU's. The NTU range for this type of turbidity meter is higher, but it is not as high as needed for construction site runoff. Also, depending on the light source, it may need frequent calibration (EPA, 1999).

Because construction site runoff can contain significant amounts of eroded sediment, this project is interested in turbidity meters that can read high turbidities upwards of 4000 NTU. This range can be accomplished by using multiple light sources and photo-detectors, different types of light sources, and different turbidity meter technologies. As said before, tungsten filament light sources have been widely used because they produce many wavelengths, but this source also has many limitations. Because of this, they are most suitable for water treatment effluent monitoring or monitoring water with low turbidity. Infrared light has been determined to minimize the effect of particle size and water color on turbidity readings (Jastram, 2009; Patil, 2011). However, actually achieving reliable infrared light from a light source can be difficult. Another light source that has been explored is monochromatic light. Monochromatic light uses a small range of light

wavelengths. For the best result, these wavelengths can be chosen based on how they react with the suspended particles. Monochromatic light is not greatly affected by water color, but due can often produce inaccurate readings because it is insensitive to small particles. Other turbidity meter technologies have been researched. One such technology is optical fiber sensing. Even though this technology is still being developed, it is already found to have many advantages such as absolute measurement, excellent resolution and range, and modest cost (Omar and MatJafri, 2009). The fiber optic sensing technology currently is not widely available.

A concern in comparing the results from different meters is their technique for measuring light scatter. This is a problem because an NTU is defined by measuring only light scattered 90° from the light source (Anderson, 2005). The addition of multiple photo detectors and angle measurements cause variance in turbidity readings. Some meters are designed to measure attenuation, backscatter, or a combination of many angles. Each of these instruments defines turbidity using a new unit and it becomes increasingly more difficult to compare measurements to a NTU. Knowing the specifications of the meter being used and how it is set to report turbidity is essential to determining the applicability of turbidity measurements.

Calibration is important to obtain accurate turbidity measurements. Calibration is based on a 20 NTU formazin solution (Sadar, 2007). For a turbidity meter to be accurate, it needs to be calibrated with a solution that is expertly prepared. The slightest mistake due to bubbles or dirty glassware can cause significant error in the use of the meter. It is also essential that meters are frequently calibrated in the field. They can become inaccurate if not calibrated for conditions at the construction site (Patil et al., 2011). Calibration has been made easier through the use of standard solutions and well-defined specific procedures given for the meters.

Factors Affecting Turbidity

The factors that affect turbidity can be broken down into two groups: factors related to the sample itself and factors tied to the measuring device. Sample variability is most often caused by particle size, particle shape, particle color, water color, and organic matter. Variability caused by

the measuring device is attributed to the angle of detection, photo detectors, incident light beam wavelength, and color sensitivity of the photocell (Omega Engineering, 2011).

Particle size impacts turbidity measurements. For particles smaller than the incident light's wavelength, light will be scattered in all directions. For particles larger than the incident light's wavelength, light will be scattered mostly forward (Omar and MatJafri, 2009). This becomes important because light scattered forward may appear to be transmitted and not scattered, skewing the overall turbidity reading. It is also important to note that light is not scattered in all directions equally. Particles larger than incident wavelength, usually 1 micron, will scatter light in all directions, but primarily forward. Particles smaller than 1 micron tend to scatter light in all directions, but in a peanut type shape. Particles smaller than 0.05 microns will generally scatter light evenly in all directions. Because particles smaller than 0.45 microns are considered dissolved, even dissolved particles have the capability of scattering light that will affect turbidity measurements (Omega Engineering, 2011). Most of the mass of sediment in a runoff from a construction site will likely be larger than 1 micron; however, dissolved particles may still be present. Particle size distributions are important in understanding turbidity readings.

When describing the effects of size on scattered light, an equivalent diameter corresponding to a spherical shape is widely used to estimate the size of the particles. However, this is rarely an accurate assumption. Particles that are spherical will produce more predictable light scattering patterns. Irregularly shaped particles, corresponding to most soil particles, will produce many light scattering patterns, causing unpredictable effects on turbidity (Omega Engineering, 2011). When working with construction site runoff, it is likely that the particles will be irregularly shaped.

Particles can have a variety of different colors. These colors absorb and scatter light differently. It is important to know the type of soil that is eroded, so the soils can be evaluated for their absorption capabilities. Dark colored sediment has the potential to absorb light causing less light to reach the photo detectors. This will lead to higher turbidity readings (Anderson, 2005). Particle color is also important when choosing incident light wavelengths because different colored particles will absorb different wavelengths of light. The more recent use of near infrared

5

light (λ=860 nm) seems to limit particle color affects (Sadar, n.d.). For naturally occurring soils, color variation is inevitable, and needs to be considered when interpreting turbidity data and choosing measurement devices. Water color, much like particle color, skews turbidity results because of its ability to absorb light wavelengths. The use of near infrared light will limit these effects as well.

Organic matter and organisms are important when measuring turbidity in lakes and streams. Organic matter has a higher tendency to absorb light, causing skewed turbidity measurements (Ankcorn, 2003). Organic matter can also be dissolved easier into water, causing water color to change. These effects are largely a concern when monitoring lakes and streams. Construction site runoff is expected to have less organic matter and organisms, reducing possible error. Other sample variables that could affect turbidity readings that have been considered but not thoroughly researched include water pH, water temperature, and particle mineral composition.

The wavelength of the incident light source is vital in determining accurate values of turbidity. The size of the wavelength of incident light will determine the light scatter pattern (Ankcorn, 2003; Omega Engineering, 2011). As previously mentioned, particle size and its relation to the size of the light wavelength cause different scatter patterns. If wavelength is varied between instruments, its reaction to different sized particles will also be different, causing a spectrum of turbidity values. Wavelength is also important because wavelengths in the visible light spectrum are absorbed readily by different colored water and particles. Due to this problem, research has concluded that infrared or near infrared light is less susceptible to absorption. Using such wavelengths will limit variability (Ankcorn, 2003). In general, the nearer the incident light's color spectrum is to being a single wavelength, the more consistent the light scatter patterns (Omega Engineering, 2011). When monitoring construction site runoff, it will be important to use turbidity meters that use the same wavelength light range so that values are comparable.

Variability among turbidity meters is well known, but adjusting their values so that they correspond to any common standard is not easy. A turbidity meter is manufactured with specific specifications, light sources, and photo detectors. These characteristics vary among the meters.

When using a turbidity meter, it is vital to know exactly how to calibrate it, read measurements, what units are used, and what factors in the sample may affect the measurements.

Turbidity and Sediment Concentration

Turbidity is often used as a surrogate for sediment concentration or total suspended solids (TSS) in runoff. However, the relationship between turbidity and TSS is dependent on several factors. As discussed in the previous section, turbidity is affected by water color, particle concentration, temperature, and shape, size and mineral concentration of sediment particles in the water (Packman et al., 1999). Because of these factors, it becomes difficult to relate turbidity values to TSS.

Holliday et al. (2003) performed laboratory research to find a correlation between turbidity and TSS. From measuring turbidity and settling times of water samples, they found a strong power relationship and a potential for a linear relationship between turbidity and TSS. It was found that turbidity to TSS was 1:1 for samples of silt plus clay but lower for whole soil samples. Rasmussen et al. (2009) took their turbidity analysis a step further and began to use continuously monitored stream flow data to analyze turbidity and suspended sediment concentration (SSC). Their experiment used site specific regression analysis to develop a linear regression model to compute SSC values based on turbidity readings. However, their approach required samples from every season and over a large range of turbidities. Other problems they experienced were skewed turbidity values because of large particles, black or very dark colored particles, and microorganisms. Jastram et al. (2009) used a more comprehensive approach to related measured turbidity in rivers to estimate SSC. Their study included the use of both univariate and multivariate approaches to identify variables to predict SSC. In the univariate approach, SSC is only a function of turbidity. In the multivariate approach, SSC is a function of several variables such as turbidity, stage, organic matter, and water temperature. Their best relationship for predicting SSC used turbidity and stage depth.

While much research has been done to relate turbidity to TSS in streams and rivers, less work has been done to explore this relationship for runoff from construction sites. Turbidity in a

stream is likely caused by sediment, dissolved materials, organic matter, and organisms. Runoff on a construction site primarily contains water and sediment. Many of the variables that affect stream turbidity can be disregarded on construction sites; however, the relationship between turbidity and TSS is still complex because of the many soil types and land uses at construction sites. Patil et al. (2011) used a linear relationship between turbidity and TSS. They measured the turbidity and TSS of samples for different soil types and different particle classes. For their limited number of samples, they found that the total turbidity could be obtained by adding the individual turbidity corresponding to that obtained for individual particle size classes.

Rasmussen et al. (2009) reported that the relationship between NTU and TSS varies because of different meter configurations, measurement methods, and color effects. Careful planning and consideration must therefore be done to determine the best instruments and measurement methods for a specific application. After choosing an instrument, it is also vital that consistent measurement techniques be utilized so that measurements can be comparable. Even with careful planning and consistent measurement, it is generally stated that turbidity can still only be considered a relative value, more useful for revealing trends in information, than an absolute value (Ankcorn, 2003; Omega Engineering, 2011).

Scope of Project

EPA and other agencies have discussed the possibility of using turbidity as an effluent standard for construction site. Turbidity monitoring has the potential to be expensive in terms of equipment costs as well as salaries for proper installation and maintenance and for data collection. This is especially true for linear highway construction projects where the flow is often discharged at many locations. The overall goals of the research are (1) to investigate turbidity relationships for conditions of Minnesota and (2) to develop protocols for the design and installation of cost-effective monitoring systems. The first goal is achieved by relying largely on collection of data in a laboratory setting. Chapters 2, 3 and 4 are used to describe the methodology and analysis of the results for the laboratory component of the project. The second goal is obtained by using both field and laboratory data. This material is covered in Chapters 5 and 6.

Chapter 2
Experimental Design of Laboratory Component

Introduction

An important activity of this study is to determine a general relationship between turbidity and TSS for Minnesota soils on construction sites. Ideally, this relationship will utilize soil properties which can be easily determined on a construction site. Such a relationship can provide an estimation of the turbidity values and sediment loading from construction sites. It also provides a simple way to compare the TSS loads on a site and the TSS loads corresponding to a potential turbidity standard.

A multitude of soils and runoff samples are required to develop a reliable relationship between turbidity and TSS. Because of the variability in weather and expense of collecting field data, the relationship was developed using data collected in a laboratory setting. This setting allowed us to control the environment and enable us to a repeatable process. Synthetic runoff was created using a rainfall simulator. The experimental methods for the laboratory study are presented in Chapter 2. The analysis of the turbidity and TSS is given in Chapter 3. In additional to this analysis, further analysis of turbidity data was performed to determine the impact of particle settling on the turbidity and TSS relationship. The theoretical development and analysis of this approach is given in Chapter 4. The turbidity for this part of the study was obtained using the Hach 2100N bench top turbidity meter. To better understand potential errors when applying these relationships to field turbidity meters, laboratory analysis was also performed to evaluate the differences in turbidity among five sensors. The experimental design for this component of the study is given in Chapter 2. Analysis of the results is given in Chapter 3.

Soil Acquisition

A large and diverse group of soil samples is useful to determine the impact of soil characteristics on turbidity. With the assistance of Dwayne Stenlund of the Minnesota Department of Transportation, 14 soils from 8 construction sites around Minnesota were

acquired for the laboratory study. Figure 2.1 shows the locations from which the soils were acquired. Of these fourteen soils, eight of them were subsoil samples and six were taken from the top soil at the locations.
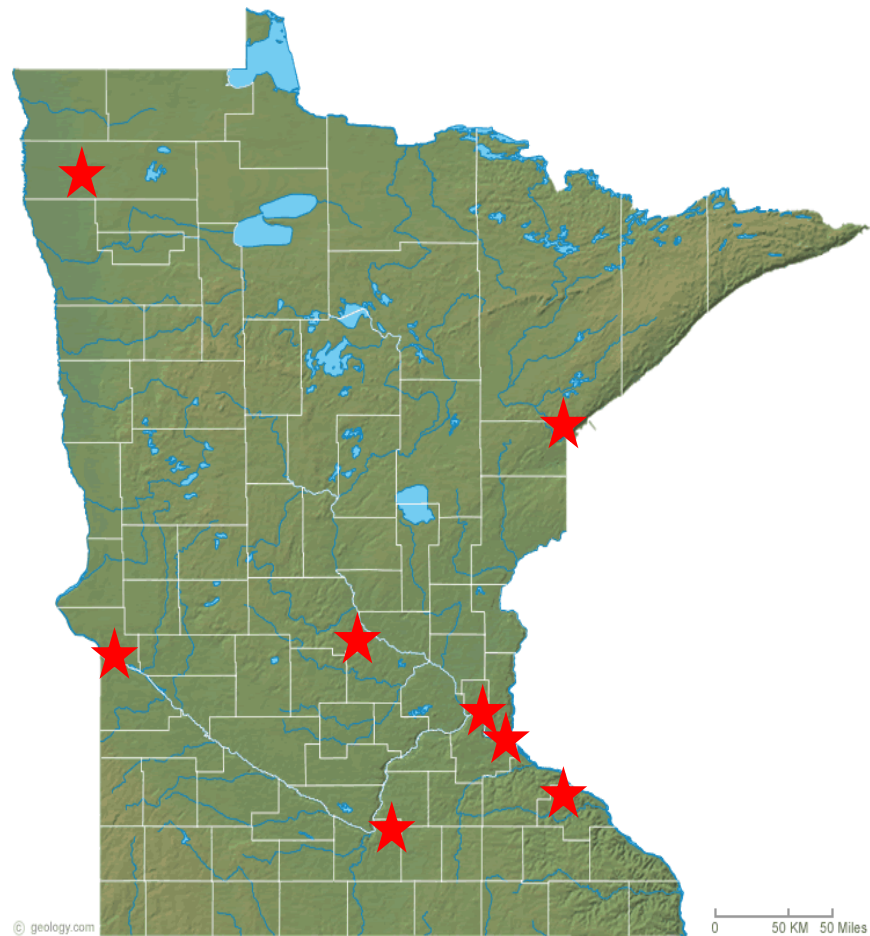
Figure 2.1: Soil site locations marked with red stars.

Soils were classified using the USDA soil triangle (Coduto, Yeung, and Kitch, 2010). The percent of sand, silt, and clay in each soil was determined from a particle size graph created for each soil from standard hydrometer test data. Of these soils, all were classified in the loam family, with the most significant portion being sandy loams. The soil visual descriptions and classifications can be seen in Table 2.1

Table 2.1. Characteristics of the Soil.

Name	Type	Location	Description	Classification
AH T	Topsoil	Arden Hills, MN	Silty, dark colored soil	Sandy Loam
AH S	Subsoil	Arden Hills, MN	Silty, yellow colored soil	Sandy Loam
CTY 14 T	Topsoil	Mankato, MN	Silty, dark colored soil	Sandy Loam
CTY 14 S	Subsoil	Mankato, MN	Silty, yellow colored soil	Sandy Loam
Dul T	Topsoil	Duluth, MN	Sandy, dark colored soil	Loamy Sand
Dul S	Subsoil	Duluth, MN	Silty, red colored soil	Silt Loam
Hast T	Topsoil	Hastings, MN	Sandy, dark colored soil	Loamy Sand
Hast S	Subsoil	Hastings, MN	Silty, rust colored soil	Sandy Loam
OV T	Topsoil	Ortonville, MN	Silty, dark colored soil with gravel	Sandy Loam
OV S	Subsoil	Ortonville, MN	Silty, dark colored soil with gravel	Silt Loam
TH-23 T	Topsoil	St. Cloud, MN	Silty, grey colored soil	Loam
TH-23 S	Subsoil	St. Cloud, MN	Silty, red colored soil	Sandy Loam
Soil A	Subsoil	Redwing, MN	Silty, tan colored soil	Silt
Soil B	Subsoil	Red Lake Falls, MN	Very fine, tan/grey soil	Silty Clay Loam

Rainfall Simulator

A rainfall simulator was calibrated and used for this experiment (Figure 2.2). The rainfall simulator is a 0.61 m by 0.91 m aluminum box that contains 96 hypodermic needles. These needles were designed to allow water pressure to push water droplets out through them (Figure 2.2). Droplets fall from the tip of needle and accelerate with gravity to achieve the desired velocity at impact. Onstad et al. (1981) describe the design of this rainfall simulator in greater detail. The rain falls a total distance of 2.6 m from the tip of the needle to the box of soil underneath it.

The rainfall simulator was calibrated to replicate the peak hour of a 2 year, 24 hour storm. For Minnesota, that rainfall intensity is 1.27 in/h using TP-40 (United States Weather Bureau, 1961). The volume and collection area were measured and rainfall rate was calculated with the following equation:

$$I = \frac{V_f}{A_f\ t} \tag{2.1}$$

where I is the rainfall intensity, V_f is the rainfall volume collected, A_f is the surface area, and t is the amount of time rainfall was collected.
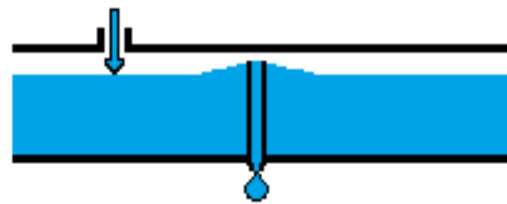
Illustration of raindrop created by rainfall simulator needle.

Figure 2.2. Rainfall simulator used for the laboratory experiments.

The simulator was also calibrated to replicate natural raindrop size. Sheppard (1990) and Marshall and Palmer (1948) both note that natural raindrop diameters are less than 4 mm. To measure the raindrop size for this experiment, rain volumes were collected for each needle over 10 minutes of rain. The raindrop rate in drops/min was measured for each needle. The raindrop diameter was calculated assuming spherical raindrops with the following equations:

$$V_n = t\,V_d\,n_d \tag{2.2}$$

$$V_d = \frac{1}{6}\,\pi\,D_d{}^3 \tag{2.3}$$

where V_n is the total rain volume associated with a single needle of the rainfall simulator, t is the rainfall time, n_d is the number of drops rained from that needle in a unit of time, V_d is the volume of an individual raindrop, and D_d is the equivalent raindrop diameter.

13

Details of the total rain volumes, raindrop rates, and raindrop diameters for each needle respectively are given in Perkins (2013). She found that the average raindrop diameter of 3.53 mm which falls within the reported raindrop diameter range in the literature. To ensure that the simulator was raining evenly over the surface of the soil, oscillating fans were installed around the simulator to push the raindrops in random directions. The uniformity of the rainfall pattern is given by Perkins (2013). Her results indicates that there is an adequate distribution of rainfall below the simulator and the raindrop diameters are of reasonable size.

Soil Box and Runoff Collection

A platform was constructed under the rainfall simulator to hold the soil sample during rain events. This platform was placed at a 9% slope. There are many possible slopes at construction sites. This slope corresponds to the standard slope used by USDA in developing relationships to estimate the impact of slope steepness in the Universal Soil Loss Equation (United States Department of Agriculture, 1978).

The soil is contained in a long plywood box as shown in Figure 2.3. The box is 91.4 cm by 25.4 cm by 15.2 cm and can hold approximately 19 liters of soil. Soil was weighed, placed into the box, and was compacted evenly over the area of the box using a standard packing method developed for this study. The box had 12 holes drilled into the bottom and perforated fabric was placed over the holes. This allowed the soil to soak in water and drain prior to rainfall.

A 15.2 cm PVC pipe with an elbow joint was connected to a circular drain on the box to collect runoff. This can be seen in Figure 2.3.

Figure 2.3. Collection of runoff samples.

Soil Processing

The soil collected from the construction sites needed to be processed to remove organic matter and large rocks. Large rocks were removed because they are unlikely to be transported with runoff, and would settle out quickly if transported, and therefore would have little impact on the turbidity from construction sites. The soil was broken down and run through a 6.35 mm sieve to remove large rocks, clumps of dirt, and sticks. Each soil was processed with the following procedure:

1) If soils are moist, let air dry
2) Separate soil into 5 gallon buckets
3) Remove large chunks (larger than a fist) and break down with a sledge hammer
4) Add 2 buckets (of the same soil) at a time to a cement mixer
5) Mix soil for 30 minutes

6) Place ¼ in. sieve on top of a 5 gallon bucket and place bucket inside a tub or   larger container to collect excess soil

7) Pour a little soil at a time through sieve and separate chunks larger than ¼ in.

8) Break down large chunks using sledge hammer

9) Re-sieve broken down chunks

10) Repeat steps 7 and 8 if needed

11) Discard rocks > ¼ in.

Rainfall Procedure

Soil Box Preparation

The soils were compacted into a soil box. Three methods of soil packing were deliberated because of the many soil conditions found on a typical construction site. To attain a highly compacted soil, the soil is compacted while wet. A medium compacted soil is compacted while dry. A loose soil has no compaction. A medium compaction was chosen as an average of these three conditions. The soils were then allowed to soak up water for a day and drain for a day while in the box. The soils were prepared with the following procedure:

1) Use dry, processed soil (see soil processing procedure) and a plywood box

2) Weigh out enough soil to fill box to top and fill box

3) Compact soil into box using a metal plate that spans the entire width of the box and a proctor hammer

4) Place plate at one end of box and strike it with 25 blows from a proctor hammer

5) Move plate to the next uncompact section and repeat steps 3 and 4 until the entire length of the box has been compacted

6) Using a shallow pool, place box inside and fill with enough water to saturate soil in box

7) Leave box in pool for 24 hours to allow water to soak into soil profile

8) Remove box from pool and place on blocks

9) Leave box on blocks for 24 hours, letting excess moisture drain from soil

Pre-rainfall

Although the rainfall simulator was calibrated to rain at specific rainfall intensity, the subtle fluctuations in flow rate from the faucet supplying the water caused discrepancies in the actual rainfall intensity. At the start of the experiment, rainfall intensity was measured to assure the rainfall was within range of the desired rainfall intensity. This procedure is outlined below:

1) Set rainfall simulator to rain at desired rainfall intensity
2) Place rainfall gauges under simulator and rain for 30 minutes
3) Measure volume of water
4) Convert to rainfall intensity

Rainfall

The following procedure describes the steps done immediately before and during rainfall on each soil:

1) Turn fans on
2) Place soil box under rainfall simulator
3) Place plate in front of runoff opening and remove when sample is ready to runoff (can take 1-15 minutes depending on the drainage capability of the soil)
4) Place 5 gallon bucket under opening to collect runoff
5) Attach PVC pipe to runoff opening to guide runoff to 5 gallon bucket (Figure 2.3)
6) Once sample begins to runoff, begin taking 5 minute runoff samples of 50 mL (Figure 2.3)
7) After 30 minutes of rainfall, remove box
8) Repeat for next soil box

Aliquot Sample Analysis

During the rainfall on each soil, six 50 mL samples of runoff were collected. These samples were used to determine the relationship between turbidity and TSS for each soil. The procedure used to analyze these samples is described below:

1) Dilute 50 mL runoff samples (see rainfall procedure) to 4000 NTU, recording the amount of water used

2) Slowly dilute sample to 280 NTU (using 4-6 dilutions), recording turbidity and water added every time sample is diluted. Dilute as far as the beaker will allow.

3) To take turbidity measurements using a Hach 2100N bench top turbiditimeter:
   a. Put sample in 500 mL beaker
   b. Place beaker on magnetic stirrer and mix completely
   c. Fill 30 mL vial with sample
   d. Use bench top turbidity meter to measure turbidity
   e. Take 3 turbidity measurements to get an understanding of the range of turbidity of the sample
   f. Empty vial back into beaker and rinse with dilution water for next dilution

4) Dry out sample in oven and find mass of sample

5) Plot turbidity vs. concentration curve

Total Runoff Sample Analysis

Aside from the 50 mL samples that were collected for each soil, a 5 gallon bucket of remaining runoff was collected. This sample contained a majority of the runoff from the soil and was analyzed to determine the effect of particle settling on the turbidity and TSS relationship. The analysis procedure is described below:

1) Measure volume of runoff in 5 gallon bucket used in Rainfall Procedure

2) Dilute sample to under 4000 NTU by adding water to the runoff sample. Determine the amount of water needed from the dilution curve created in Dilution Procedure.

3) Prepare 4 sets of 6, 30 mL vials by adding 0, 5, 10, 15, 20, 25 mL of water to the 6 vials

4) Pipette out enough runoff to fill one set of diluted vials while mixing sample with paint stirrer. Pipette at a consistent depth for all samples.

5) Stop mixing, start stop watch or other timing device, and allow sample to settle

6) Pipette out enough runoff at 3 minutes, 6 hours and 52 minutes, and 24 hours and fill the other 3 sets of vials. These samples represent the breaks between sand, silt, clay, and colloidal particles.

7) Pipette out enough runoff to fill a single, empty vial at 0.25, 0.5, 1, 2, 3, 4, 5, and 6 hours. These samples represent different sizes of silts.

8) Measure turbidity of the vials using bench top turbidity meter and record values

9) Using filter paper procedure, measure the weight of soil in the 0 mL vials for the 0 min, 3min, 6:52 hour, and 24 hour samples and for each silt sample. Use these weights to determine the soil concentration in the sample.

Determination of Rainfall Duration

The duration of rainfall should be long enough to achieve steady state conditions but short enough to be time and cost efficient. To determine this duration, a trial run was done with one of the soils. Using the 50 mL sample analysis, a set of time dependent, turbidity vs. concentration curves was acquired for 5, 10, 15, 20, 25, and 30 minutes after the start of runoff.

Conditions corresponding to steady state were assessed by examining changes in the power coefficient with the successive combination of collected data with cumulative time. The power coefficient was determined using the log slopes (Nater et al., 1996). Therefore, when the regression is finished, there is a common slope value for the 5 minute data, the combined data corresponding to sampling times of 5-and-10 minute data, to sampling times of 5-10-and-15 minutes and so forth for each subsequent sampling time. The common slope for different cumulative sampling time is shown in Figure 2.4. The scatter significantly decreased between the 5 minute intervals over the 30 minute time period. The slope collapsed to a robust value of approximately 1.41 after 15 minutes. It was decided that 30 minutes is a satisfactory duration of rainfall.

Soil Properties

To determine how the turbidity and TSS relationship varies between soils, soil parameters were determined for each soil. For ease of analysis and application, the selection of soil

properties was limited to those that can be gathered or estimated directly from soil samples from construction sites. These soil properties are described below.
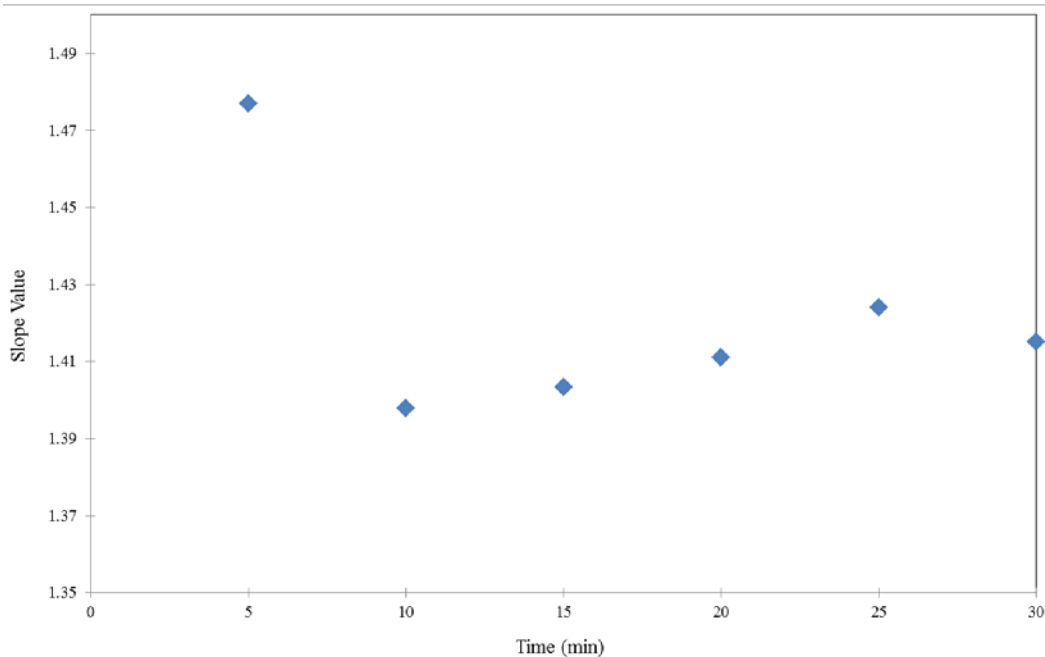
Figure 2.4. Same slope regression for trial run.

A standard hydrometer test was performed to determine the particle-size distribution for each soil prior to packing the soil in the test apparatus. Using the USDA particle size scale, percent sand is defined as the percent of the sample that is 0.05-10 mm in diameter. Percent silt is the percent of the sample that is 0.002-0.05 mm in diameter. Percent clay is the percent of the sample that is < 0.002 mm in diameter (Coduto et al., 2010). Because sand can easily settle out of suspension, the percent sand in the runoff treated by an effective sediment control plan is likely quite small. It was decided to use a statistical analysis with a variable that is not nearly equal to zero. Therefore, the role of percent sand was represented by the summation of percent silt and percent clay. The term percent silt plus clay is the mathematical equal to one minus percent sand. Nonetheless, problems with relationships using the inverse of percent sand can be avoided.

For each rainfall trial of each soil, rainfall intensity was measured by placing a catch basin below the rainfall simulator. This basin collected the rainfall over ½ hour. The volume of water collected in the catch basin was measured in milliliters using a large graduated cylinder. The surface area of the catch basin was measured and the rainfall intensity was evaluated using Equation 2.1.

Dry bulk density was determined after the previously described soil preparation procedure was completed. Dry bulk density is measured in g/cm³. The mass of soil placed into the soil box was first determined. The soil was then evenly compacted into the soil box. The volume of compacted soil was measured using the box dimensions and subtracting the empty space above the soil from the depth of the box. The equation used to evaluate dry bulk density is as follows:

$$BD = \frac{M_B}{A_B H} \tag{2.5}$$

where BD is the dry bulk density, M_B is the mass of soil in the box, A_B is the surface area of the soil box, and H is the depth of soil in the box.

The volume of runoff was measured directly by collecting the total runoff from the boxes in a bucket and measuring the total runoff volume in the bucket using a graduated cylinder. A volume of 300 mL was added to this volume to account for the six 50 mL samples that were collected over the rainfall period.

The runoff flow rate was calculated using the volume of runoff and the duration runoff. The average runoff flow rate was calculated using the following equation:

$$Q = \frac{V_t}{t_t} \tag{2.6}$$

where Q is the flow rate of runoff, V_t is the total volume of runoff, and t_t is the duration of runoff.

The NRCS Curve Number Method uses following equations:

$$Z = \frac{(P-0.2S)^2}{P+0.8S}, P \geq I_A = 0.2S \tag{2.7}$$

$$Z = 0, P \leq I_A = 0.2S \tag{2.8}$$

$$S = \frac{1000}{CN} - 10 \qquad (2.9)$$

where Z, P, S, and I_A are in inches and CN is dimensionless. Z is the depth of runoff. P is the total depth of precipitation. S is the maximum abstraction during runoff. I_A is the initial abstraction prior to runoff (Wurbs and James, 2001). P and Z were solved for using data collected prior and during rainfall. S needed to be found using solver software. The equations used for P and Z are as follows:

$$P = I\,t \qquad (2.10)$$

$$Z = \frac{V_t}{A_B} \qquad (2.11)$$

where V_r is the total runoff volume and A_B is the surface area of the box.

Moisture content was determined for each sample after the samples were soaked in water and drained, as described in the previous Soil Preparation section. A sample of soil from the middle of the soil box was extracted, quickly weighed, and then dried overnight in an oven and weighed again. Moisture content was determined with the following equation:

$$w = 100\,\frac{M_w}{M_d} \qquad (2.12)$$

where w is the soil moisture content as a percent, M_w is the mass water in a soil in grams, and M_d is the mass, in grams, of soil after it was dried (Coduto et al., 2011).

The optimum moisture content was found for each soil using a standard proctor test (Coduto et al., 2011).

The total amount of eroded sediment was determined from the total runoff sample that was collected in a bucket. The majority of the water in the bucket was decanted and the excess water and sediment was transferred into pre-weighed containers to be dried at 45° C in an oven over night. The container and sediment was then weighed and the total eroded sediment (TES) was determined The same procedure was used for the 50 mL samples, and the mass of soil in the six samples was added to the mass of soil in bucket to determine the TES for each soil.

Three replicate cohesive strength meter (CSM) tests were performed on each soil. Using the data collected with this test, a soil shear stress in Pascals was determined (Tolhurst et al., 1999).

Interrill erodibility is a measurement of the erosion caused by raindrop impact (Elliot, Liebenow, Laflen, & Kohl, 1989). To determine interrill erodibility, the interrill detachment and the dimensionless slope factor, S_f, were calculated with known values:

$$D_i = \frac{TES}{A_B\, t} \tag{2.13}$$

$$S_f = 1.05 - 0.85e^{(-4\sin(\% \, Slope))} \tag{2.14}$$

where A_B is the surface area of the soil box and t is the duration of runoff. The interrill erodibility constant, Ki, could then be determined using the following equation:

$$K_i = \frac{D_i}{I^2\, S_f} \tag{2.13}$$

Maximum abstraction, S, was previously described in the curve number section. Equation 2.9 shows the relationship between curve number and maximum abstraction.

Comparison of Turbidity Meters

All turbidity readings in the previous sections were obtained using the Hach 2100N bench top turbidimeter. To better understand potential errors in using these results for field conditions, a laboratory comparison experiment was conducted. The laboratory study explored the range of turbidity values expected for both an individual sensor for differing soil textures and differences between sensors for a single soil texture. The five different sensors used in this experiment and their specifications are shown in Table 2.2.

Table 2.2. List of turbidity sensors and specifications.

Sensor	Light Source	Detector angle	Method	NTU range
Campbell Sci. OBS 3+	850 nm	90-165	Side scatter	0-4000
Campbell Sci.OBS500	850 nm	90, 125 to 170	Side and Back Scatter	0-4000
McVan Analite NEP495	860 nm	90	Back scatter	0-1000

| YSI 6136 | 860 nm | 90 | Back scatter | 0-1000 |
| Hach 2100N | Tungsten | 90, 135, 180 | Forward scatter | 0-4000 |

Five soils representing a range of soil textures from our laboratory study were used for this comparison and are described in Table 2.3. They are a subset of the soils previously reported in Table 2.1.

Table 2.3 List of soils and soil properties used in turbidity probe comparison.

Name	Type	Location	Description	Classification
AH T	Topsoil	Arden Hills, MN	Silty dark grey soil	Sandy Loam
TH-23 T	Topsoil	St. Cloud, MN	Silty, greyish brown soil	Loam
TH-23 S	Subsoil	St. Cloud, MN	Silty, reddish orange soil	Sandy Loam
Soil A	Subsoil	Redwing, MN	Sticky, tan soil	Silt
Soil B	Subsoil	Red Lake Falls, MN	Sticky, greyish tan soil	Silty Clay Loam

The testing apparatus and procedures were patterned after Lewis (2007). A black bucket with a capacity of twelve liters was used for a test chamber. A drill, with attached paint stirrer, was mounted above the bucket at a height that allowed the paint stirrer to spin approximately 2 cm above the bottom of the bucket and 2 cm from the side of the bucket. A bracket was then attached to the sensors so that they could be mounted in the same location for each measurement. Each of the meters was inserted separately into the bucket opposite the stirrer so that the sensor was 8 cm from the base of the bucket. A drill speed was chosen that retained the sediment particles in suspension over the range of sediment concentrations needed to attain a turbidity of 1000 NTUs for all soils. The test apparatus is shown in Figure 2.5.

Figure 2.5. Measuring turbidity with test apparatus

Prior to starting the experiment, each meter was calibrated according to their specific manufacturer's instructions. Twelve liters of water were added to the bucket and the OBS-3+ meter was mounted. The drill was turned on and three turbidity readings were taken. The OBS-3+ was then un-mounted, and the next meter was mounted in its place. This was repeated for all portable meters. The YSI 6136, Campbell scientific OBS500 and Analite NEP495 are each pre- programmed to take a series of readings and output an average value. The OBS3+ was programmed to average 10 readings taken every five seconds. Each probe was allowed to go through its scan interval three times and an average of the three readings was recorded. A 30 mL sample was extracted from the bucket at the depth of the sensor face. The turbidity of this sample was determined with the Hach 2100N bench top turbidimeter. The OBS-3+ was remounted and a measured amount of soil was added to the suspension until

the meter read 25 NTUs. Again, each meter was allowed to read three times. The experiment was repeated for 50, 100, 200, 400, 800, and 1000 NTUs.

Chapter 3
Evaluation of Turbidity-Concentration Relationships

Introduction

The experimental methods of Chapter 2 were used to obtain a data set to investigate the relationship between turbidity and concentration. The analysis is based largely on the six 50 mL aliquot samples. The first section of the chapter will evaluate the samples using a general power relationship. This evaluation will be done for all of the soils. Trends in the coefficients of this power relationship will be further explored. Predictive relationships are proposed and their usefulness is evaluated.

General Power Relationship

Insight into turbidity readings was obtained by plotting the turbidity data as a function of sediment concentration. An example of turbidity-concentration trends is shown in Figure 3.1. Each soil had six sets of data and six separate relationships to describe the data. Several regressions were performed on the data to determine the correct form of the turbidity and TSS relationship. A power relationship for turbidity and sediment concentration was clearly suggested from these plots.

All of the soils in the study were well represented by a power function. The general relationship used to describe turbidity as a function of TSS is as follows:

$$\text{Turbidity} = \alpha\,\text{TSS}^{\beta} \tag{3.1}$$

where α and β are scaling and power coefficents, respectively. They are considered to be soil dependent. In the above equation, turbidity and TSS are measured in NTUs and mg/L respectively. Equation 3.1 was evaluated for each of the six samples collected at different times during the runoff event. The power coefficent, β, remained relatively stable while the scaling coefficient, α, varied among samples.
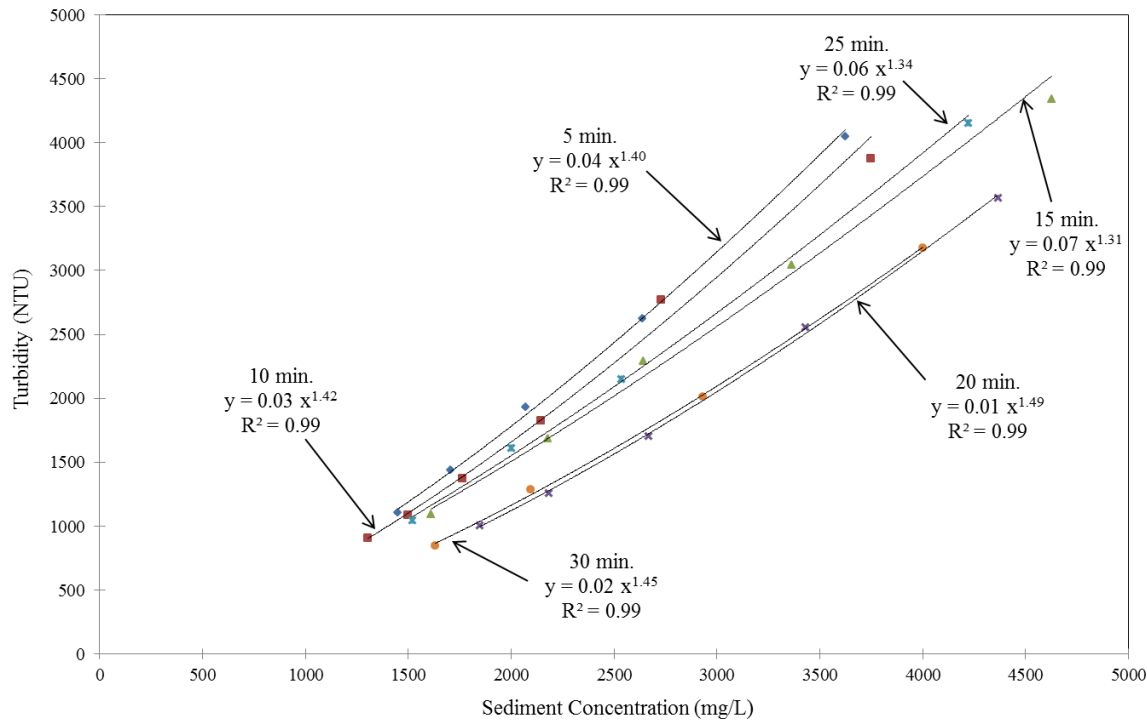
Figure 3.1. Time Dependent 50 mL sample dilution curves for one soil.

In addition to variation of α and β with samples of a particular soil, possible trends for α and β were further investigated by comparing values between soils. Turbidity and concentration data for all fourteen soils are plotted on a single graph in Figure 3.2. The data for all of the soils are well represented by the general power relationship of Equation 3.1. Between all of the soils, the β value varied between 1.3 and 1.5 and the α values varied between 0.001 and 0.1. The time dependent variation in α in Figure 3.1 is small in comparison to its variation between soils. Investigation into possible trends of α will be limited to measurable soil properties. This investigation is given later in this section.

Estimation of β

Investigations were done to estimate β when observed turbidity and concentration data are unavailable for a construction site. The first step was to select a single value β for each of the soils. This value was obtained using the regression analysis for common slope. The result of this analysis is a β value for each soil which varied between 1.3 and 1.5. The mean and median of the β values are 1.38 and 1.39, respectively.

28
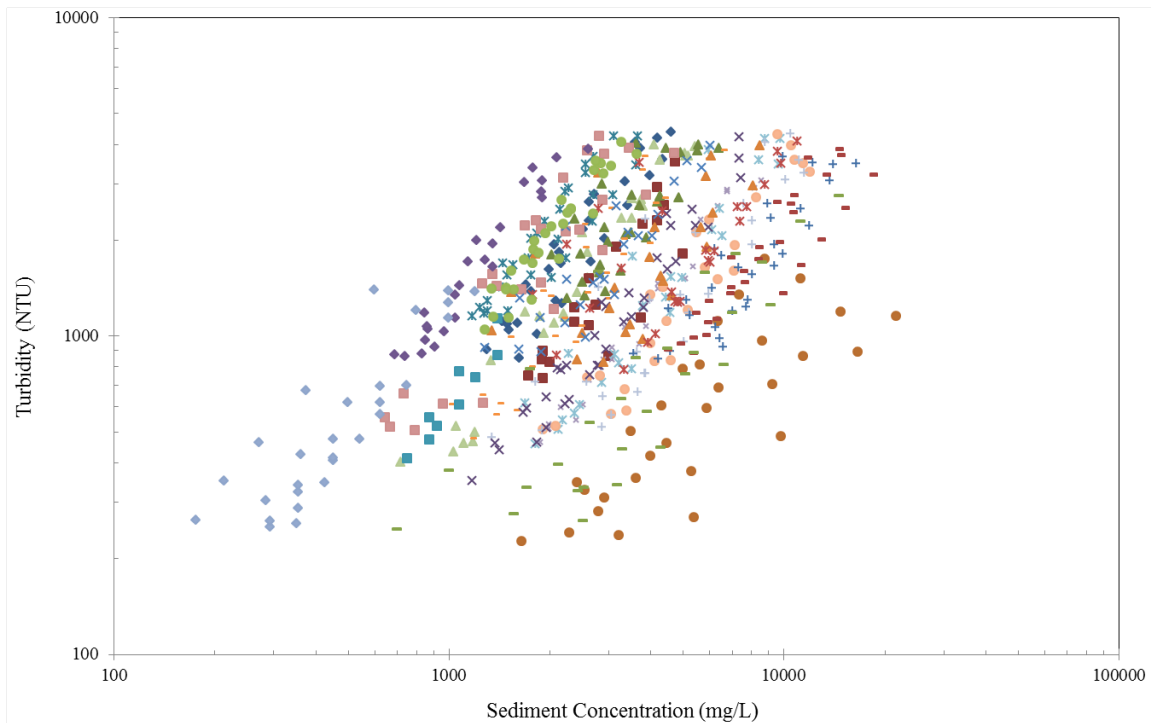
Figure 3.2. Dilution curves for all soils.

Since the range in β is relatively small between soils, the possibility of a single power value that can represent the range of soils was tested. The mean and median values of β are well represented by a power value of 1.4 or 7/5. This fraction is also simple to use and communicate to others. A standard hypothesis test was performed using a null hypothesis of $b_1 = 1.4$, and an alternate hypothesis of $b_1 \neq 1.4$. Using a standard normal distribution, 9 of 19 soils were found to have a β value significantly different from 1.4 at a 95% confidence level.

The effect of setting β to a constant value was also evaluated using standard hypothesis tests on changes in α. Hypothesis tests were performed for each soil where the null hypothesis was that the median α using β = 7/5 equals the median α using the least-square estimate of β. This test was repeated using the mean instead of median values. The results of these hypothesis

29

tests show that there is no statistically significant difference between using β =7 /5 and the least-square estimate.

Because there were nine β values significantly different from 7/5, a multiple linear regression was done on the β using the soil properties described in Chapter 2. No discernible trend was found for β between soils. Because of this, β was set at a constant value of 7/5.

Estimation of α

The determination of α for construction sites without observed turbidity-concentration data was also investigated. Since the value of α varied by nearly two orders of magnitude for our experimental methods, a predictive relationship for this factor as a function of measurable soil properties is needed.

The soil properties previously described were used in a multiple linear regression (Neter et al., 1996) to determine a relationship for α. The log transformed multiple linear regression was performed using the median α values when β was set at 7/5. Nearly 40 regression models were evaluated, and the most useful regression models are given in this section. The correlation matrix and details of the best regression models are given by Perkins (2013). The most significant variables in the model are percent silt plus clay, percent silt, interrill erodibility, and curve number.

Multiple regression models are used to determine a relationship between significant independent variables that describe the dependent variable. The independent variables are the soil properties in Table 2.1, and the dependent variable is the median α values for each soil. The three independent variables of percent silt, curve number, and interrill erodibility were identified as important indicators of physical processes of particle detachment and transport and well represented the observed α values having a $R^2 = 0.69$. Percent silt represents the available particles on a site that can be easily eroded and transported in stormwater, curve number is a measurement of runoff potential on a site, and interrill erodibility is a value that quantifies the detachment and transport of soil by raindrops and overland flow. Both the percent silt and interrill erodibility were significant at the 10% level. However, the curve number was not significant at a 10% level. It was significant at the 30% level. Because of its

30

importance in the erosion process, it was decided to still include it in the regression model. The regression model using these three parameters explained 70% of the variability in α. The equation for this model is as follows:

$$\alpha = 1.68\text{E-}16 \; \text{Silt}^{1.20} \; CN^{8.15} \; K_i^{-0.66} \tag{3.2}$$

This model is highly nonlinear with respect to the curve number. Although curve number is a variable that can be easily determined with simple calculations and table values, it is still a dimensionless index of runoff. Because of this, maximum abstraction depth, a physical property of the site that is used in curve number calculations, was substituted for curve number in the regression models. This substitution had little effect on the overall fit of the regression model, but it did decrease the nonlinearity of the regression model. The equation for this model is as follows:

$$\alpha = 0.43 \; \text{Silt}^{1.19} \; S^{-0.31} \; K_i^{-0.56} \tag{3.3}$$

Although Equation 3.3 is the preferred prediction model for α, the interrill erodibility and maximum abstraction may not be readily available for soils at construction sites. An alternative and simpler predictive model was obtained using only percent silt. This regression model explained 55% of the variability of α. The equation for this model is as follows:

$$\alpha = 1.94\text{E-}4 \; \text{Silt}^{1.22} \tag{3.4}$$

Equation 3.4 provides a simple estimate of α if only particle size distribution is available for the site. The fit of these two models will be described later in this chapter.

Evaluation of Regression Models

The usefulness of the regression models of Equation 3.3 (Model 1) and Equation 3.4 (Model 2) was evaluated by comparing the predicted α to those observed. For all soils, the observed α values correspond to the minimum, maximum, and median obtained using a β of 7/5. The results of this comparison are shown in Figure 3.3 for the predicted α using Equation 3.3 and in Figure 3.4 for the predicted α using Equation 3.4.
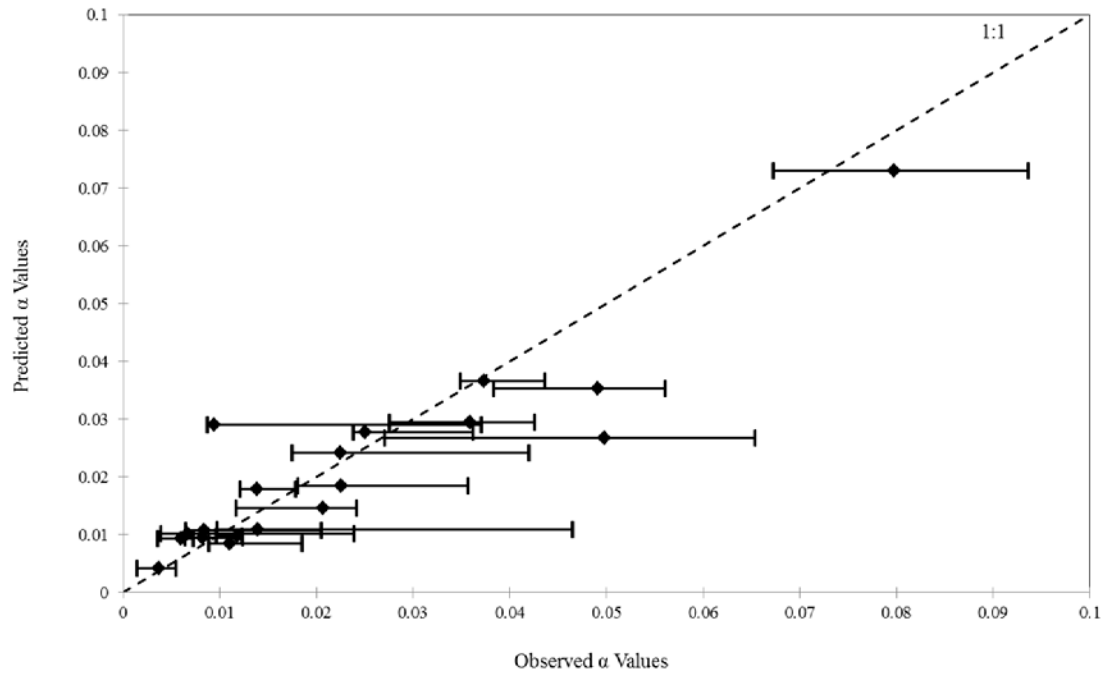
Figure 3.3. Observed α values plotted against predicted α values for Model 1.
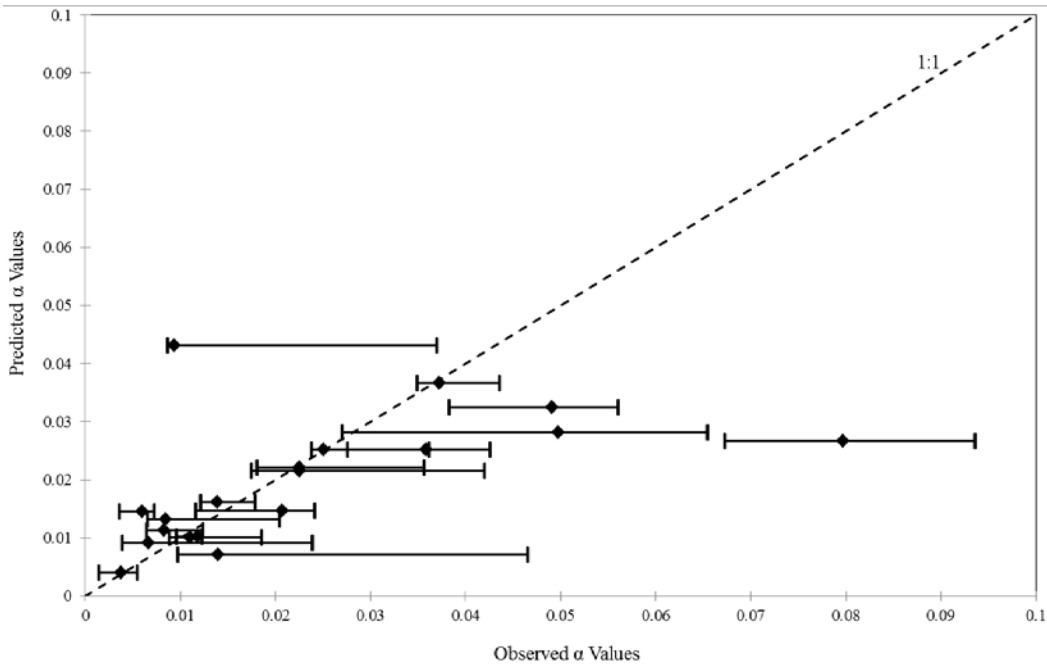
Figure 3.4. Observed α values plotted against predicted α values for Model 2.

Model 1 and Model 2 are evaluated using the normalized mean square error (NMSE) and the relative mean error (RME). When NMSE = 0, the model has a perfect fit, but when NMSE ≥ 1, the mean describes α as good as or better than the regression model. The RME shows a bias in the models. A model with a positive RME over estimates α and a model with a negative RME underestimates α. NMSE and RME were calculated with the following equations:

$$NMSE = \frac{\sum(P_i - O_i)^2}{\sum(O_i - \bar{O})^2} \tag{3.5}$$

$$RME = \frac{\sum(P_i - O_i)}{n\,\bar{O}} \tag{3.6}$$

where P_i and O_i are the predicted and median of observed α values for each soil, i. $\bar{O}$ is the mean of the observed α values and n is the number of soils used in the analysis. The error of each model is summarized in Table 3.1.

Table 3.1. Model error values.

Error	Model 1	Model 2
NMSE	0.19	0.72
RME	-0.02	-0.15

The NMSE of Model 1 is smaller than Model 2, indicating a better fit. Both models have NMSE values <1 indicating that the Models better represent α then the mean of observed α values. The negative RME values indicate that both models are slightly under-predicting α.

The α regression-based predictions were then applied to each soil to demonstrate how turbidity would be predicted based on collected TSS data. This analysis shows the impact of potential errors in α on predicted turbidities. Further application will be discussed later in the report. Figure 3.5 shows the turbidity-TSS relationships for a soil with α estimated using both Equation 3.3 and 3.4. Turbidity was then determined by using the estimated α value in Equation 3.1 with a β value of 7/5.

Data Normalization

A single dimensionless curve is useful in representing the turbidity-concentration data. The power functions for the different soils can be collapsed into a single curve using a turbidity defined for an index concentration. The index concentration can be set by a turbidity standard or it can be a known value collected from a site.
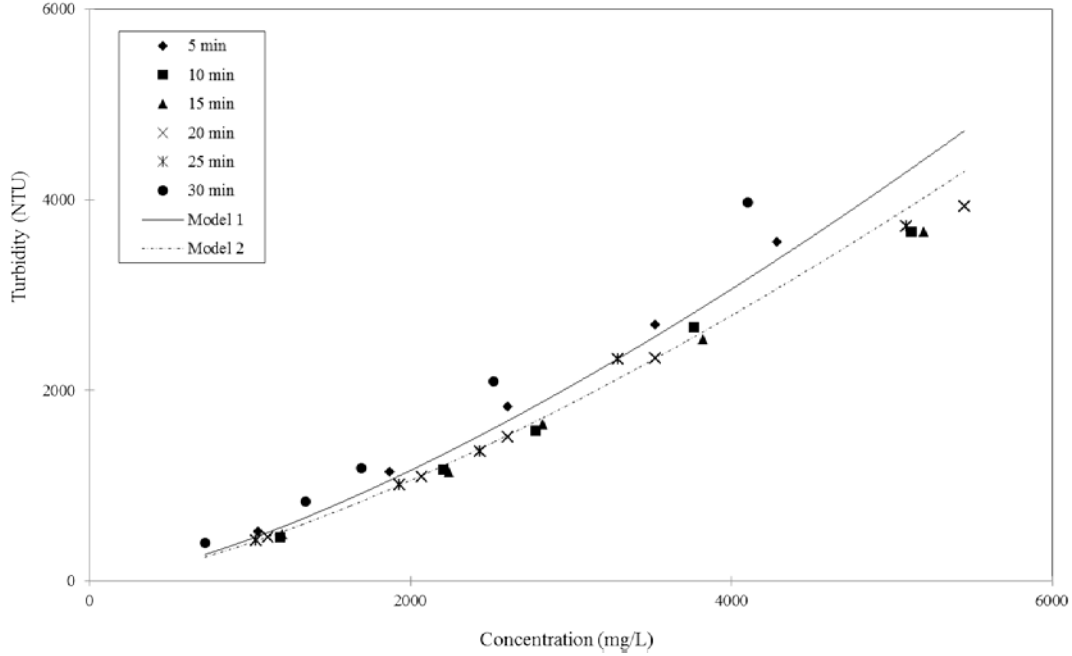
Figure 3.5. Estimated α for an example soil.

Normalization by a Standard

Turbidity-concentration data can be normalized with a chosen turbidity standard, T_{std}. Using Equation 3.1, T_{std} can be used to determine the corresponding standard concentration, C_{std}, with an appropriate estimate or known α. Equation 3.1 can then be normalized with these standard values as seen in Equation 3.7.

$$\frac{T_{site}}{T_{std}} = \frac{\alpha_{site}}{\alpha_{std}}\left(\frac{C_{site}}{C_{std}}\right)^{7/5} = \left(\frac{C_{site}}{C_{std}}\right)^{7/5} \tag{3.7}$$

Because α_{site} and α_{std} are both deterimined using the same site data, they are the same value and would cancel out in Equation 3.7. With the removal of α, the data collapses nicely on a single curve. A dimensionless plot of all of the laboratory data is shown in Figure 3.6. A single dimensionless curve was able to accurately represent the observed data.

35
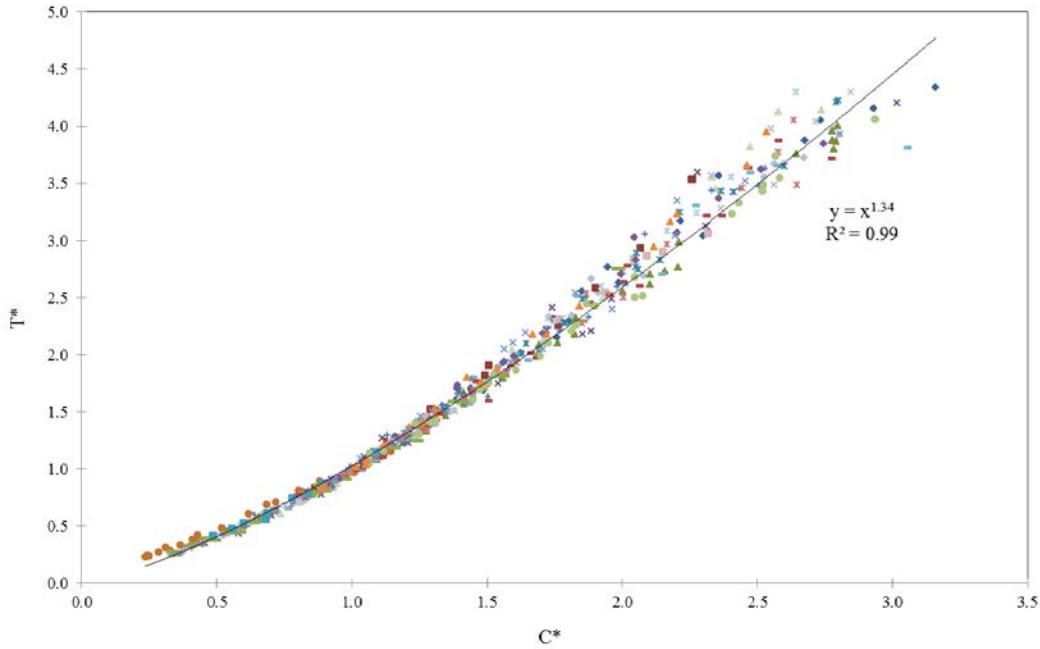
Figure 3.6. Laboratory turbidity and concentration data normalized by a 1000 NTU turbidity standard.

Normalization with a Single Known Data Value

A single measured pair of turbidity and concentration values for a storm event can be used to establish the relationship between turbidity and concentration. This approach is preferred if resources allow the collection of a single sample but are insufficient to allow multiple sampling during a storm event. The use of this known data avoids the uncertainty in estimating α from regression equations. In addition, as discussed in Chapter 5, α values change with deposition along the flow path, which further complicates the determination of α from regression equations.

Let's define a single sample from the site from which a known turbidity, T_{known}, and corresponding concentration sample, C_{known}, are obtained. Using Equation 3.1, T_{known} and C_{known} can be used to determine α_{known}. Equation 3.1 can then be normalized with these values as seen in Equation 3.8.

$$\frac{T_{site}}{T_{known}} = \frac{\alpha_{site}}{\alpha_{known}}\left(\frac{C_{site}}{C_{known}}\right)^{7/5} = \left(\frac{C_{site}}{C_{known}}\right)^{7/5} \tag{3.8}$$

36

Again, α_{site} and α_{known} are equal. For measured or predicted concentrations, the turbidity can then be computed by Equation 3.8. The α value is inherently embedded in the known turbidity and concentration values.

Analysis of Turbidity Meters

The experimental design for the comparison of turbidity meters was given in Chapter 3. Once again, the YSI 6136, Campbell scientific OBS500 and Analite NEP495 take a series of readings and output an average value. The OBS3+ was programmed to average 10 readings taken every five seconds. Each probe was allowed to go through its scan interval three times and an average of the three readings was recorded.

Figures 3.7 through 3.11 show the average turbidity values recorded by each meter for each soil type. As expected a wide range of turbidities were recorded by each sensor dependent on the soil type. Differences in particle diameters, shape and color all can affect the turbidity readings (Anderson, 2004). The location of each soil on the plot for all five sensors was consistent. For given sediment concentration the highest turbidity values were produced by the finer textured soils. The coarser textured soils produced the lowest turbidities for a given sediment concentration. The range in turbidity at the lower concentrations ranged from 30 to 90 NTUs and at the higher concentrations 300 to 430 NTUs.
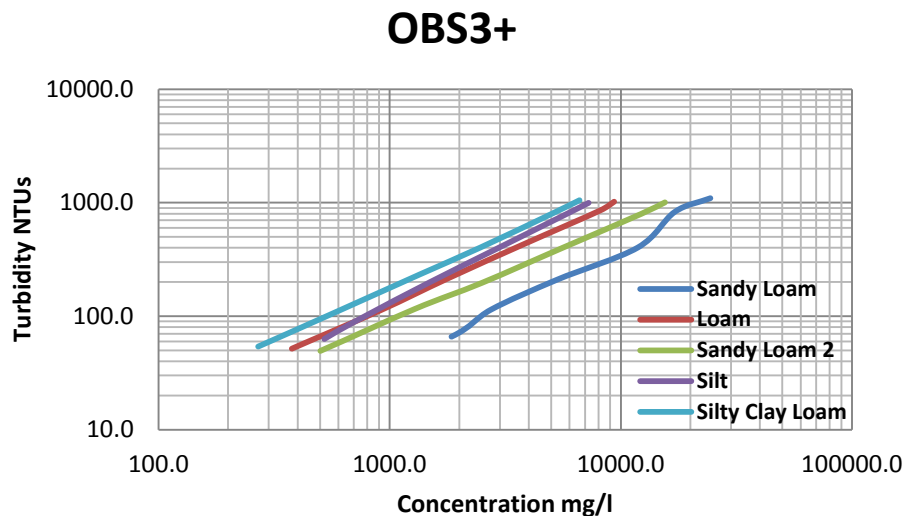
Figure 3.7. Turbidity values measured by the OBS3+ for all five soils.
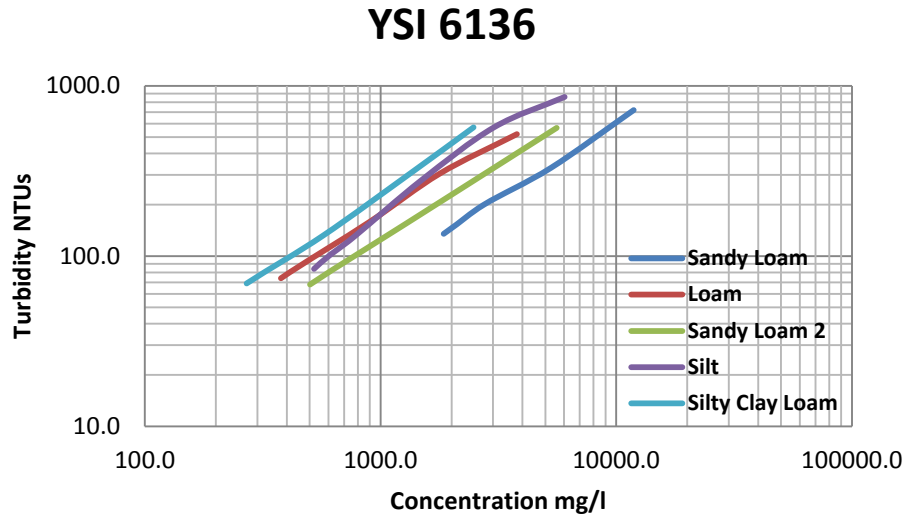
YSI 6136

Figure 3.8. Turbidity values measured by the YSI 6136 for all five soils
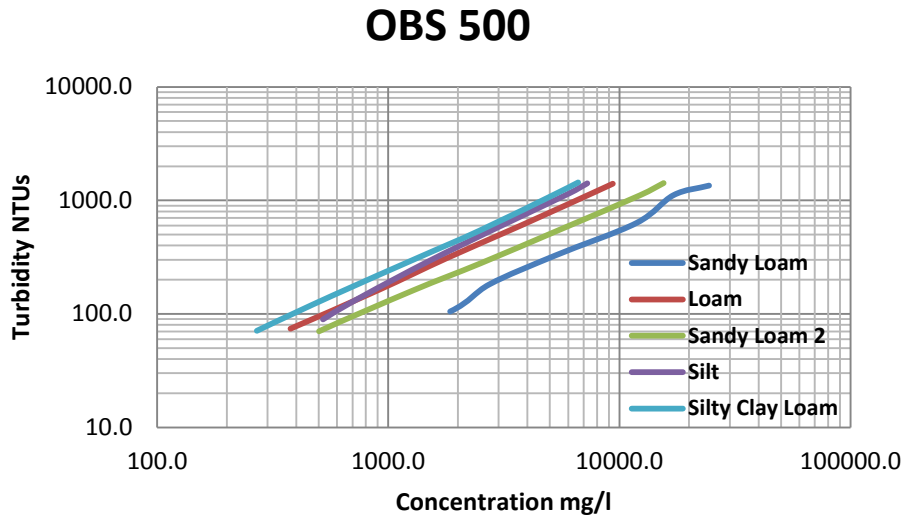
OBS 500

Figure 3.9. Turbidity values measured by the OBS500 for all five soils

Analite 495
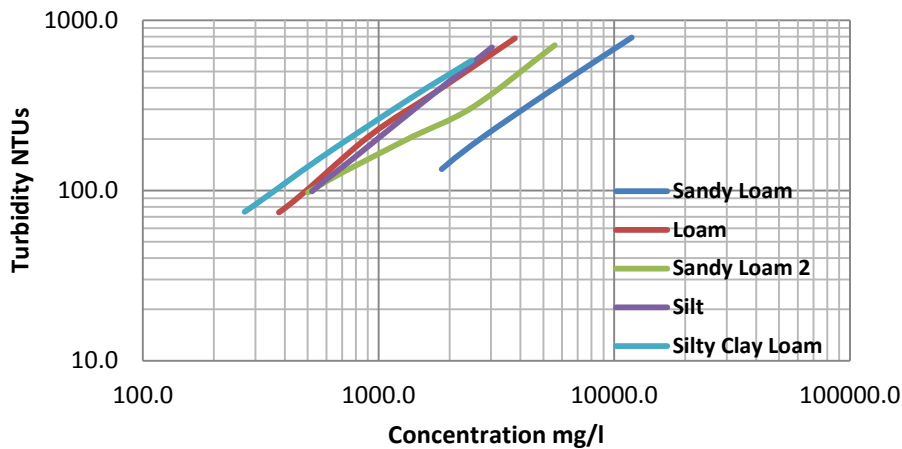
Figure 3.10. Turbidity values measured by the Analite NEP495 for all five soils

2100N
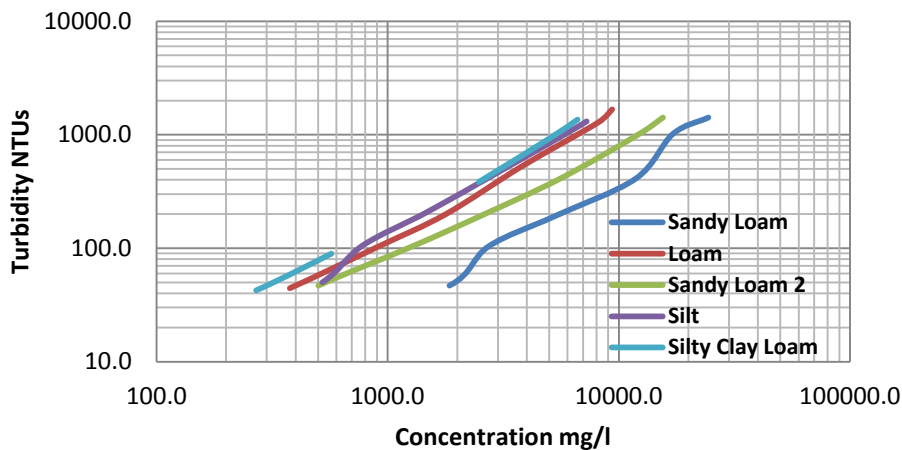
Figure 3.11. Turbidity values measured by the 2100N for all five soils

Figures 3.12 through 3.16 show the differences in turbidity values generated by each sensor for a given soil type. Differences in wave length, detection angles, and method used, back scatter versus side scatter, can explain the range of turbidities recorded from different sensors for the same soil (Anderson 2004). The 2100N and OBS3+ measured the lowest turbidity values per soil type and the Analite NEP495 recorded the highest turbidity for each soil. The percent sand, percent silt and percent clay correspond to the primary particle sizes.

39
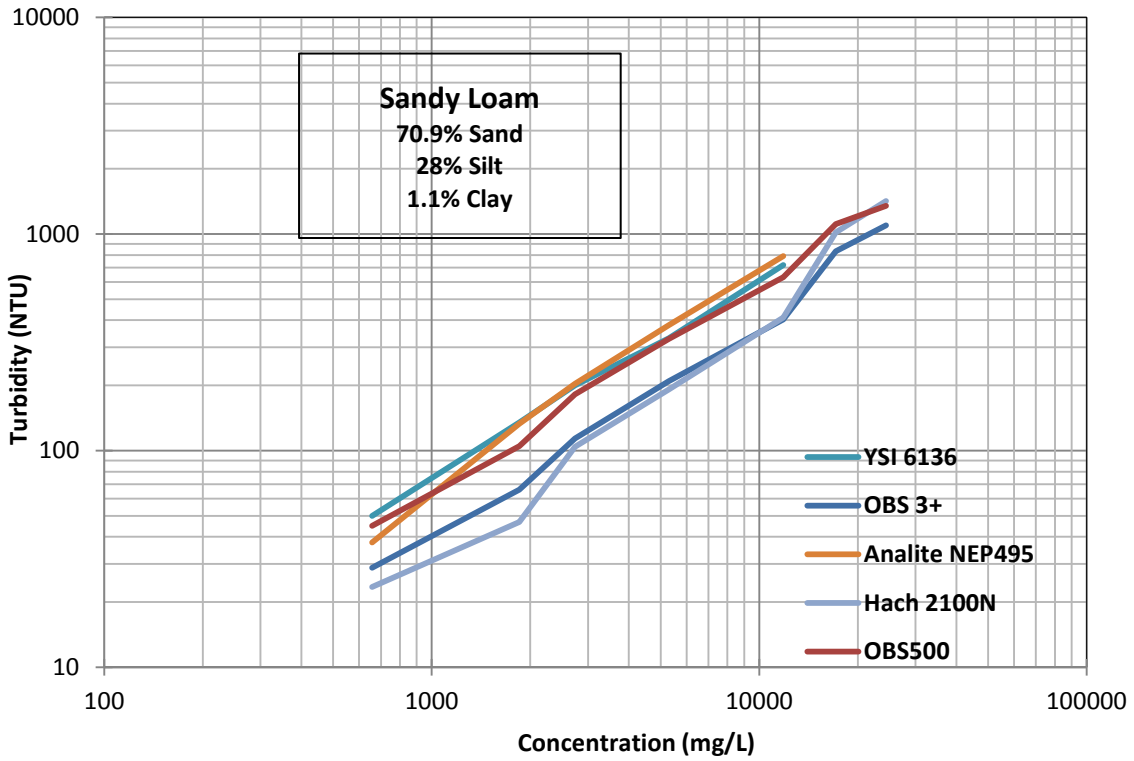
Figure 3.12. Turbidity values measured by each sensor on the sandy loam soil
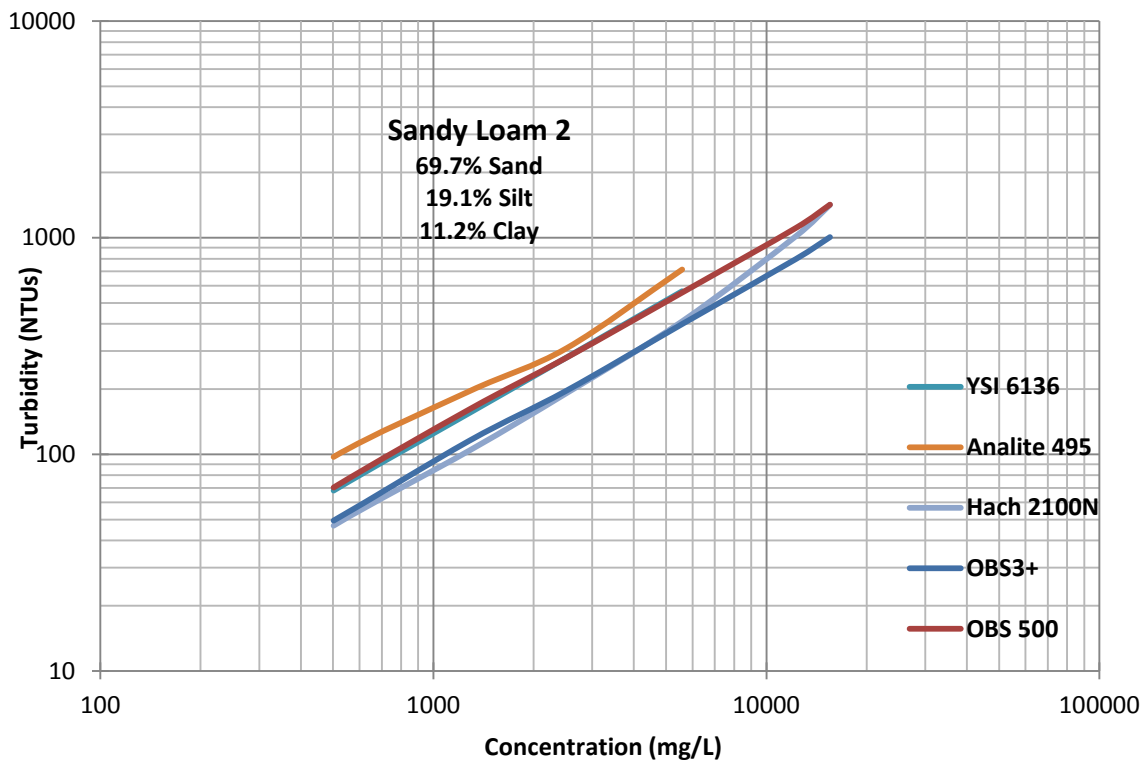
Figure 3.13. Turbidity values measured by each sensor on the sandy loam 2 soil
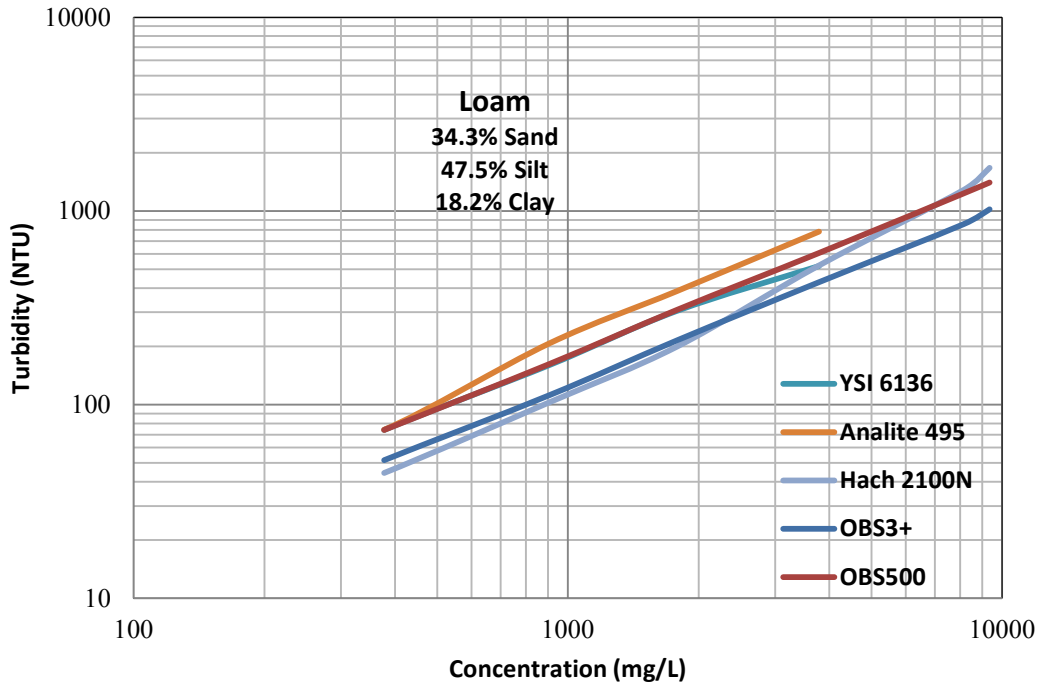
Figure 3.14. Turbidity values measured by each sensor on the loam soil
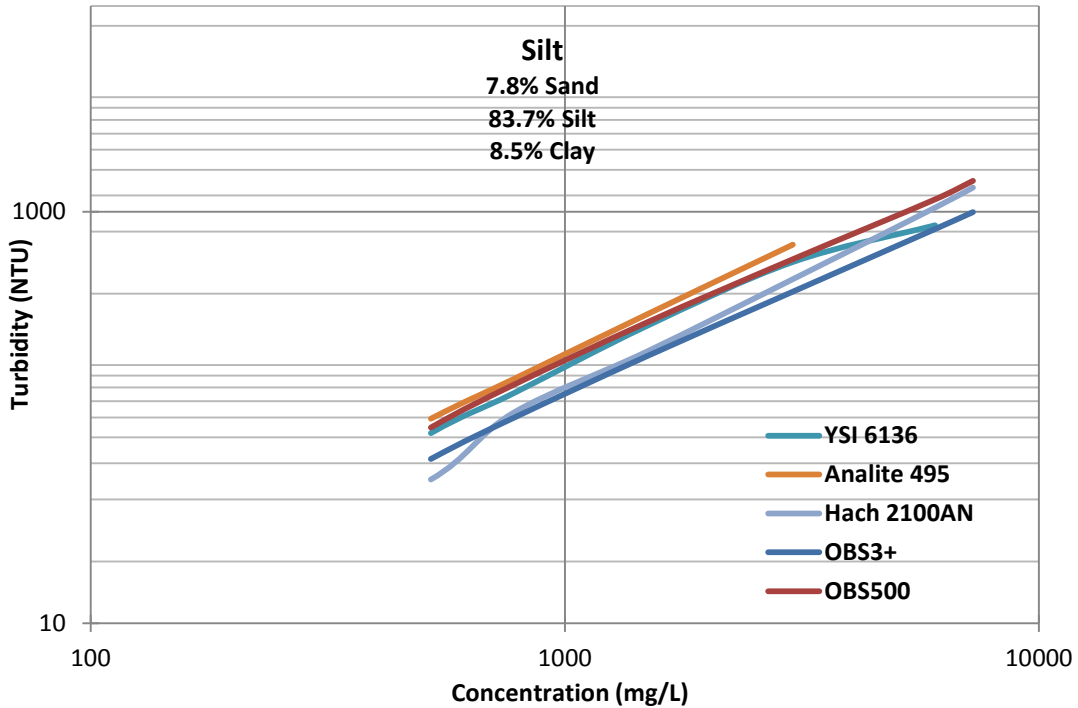
Figure 3.15. Turbidity values measured by each sensor on the silt soil

41
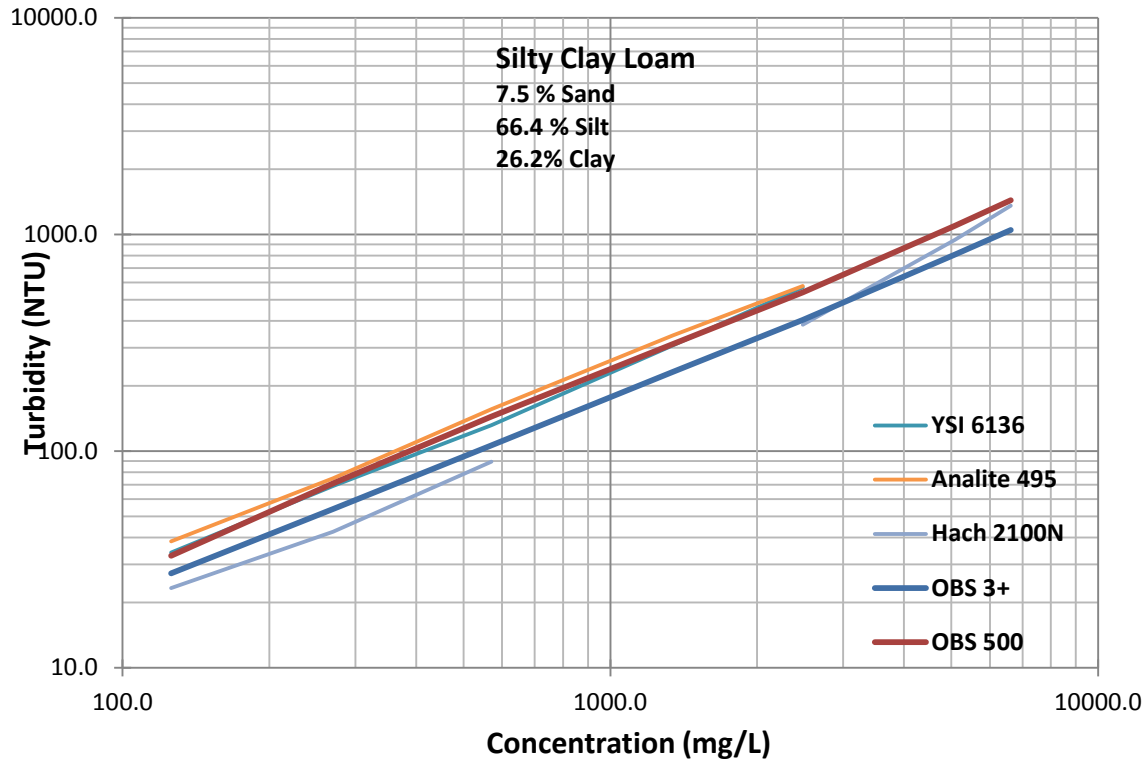
Figure 3.16. Turbidity values measured by each sensor on the silty clay loam soil

To provide a better comparison between sensors, the difference between the turbidity values recorded by the 2100N and each sensor were calculated and plotted in Figure 3.17. The differences were calculated at a sediment concentration of 2500 mg/l.
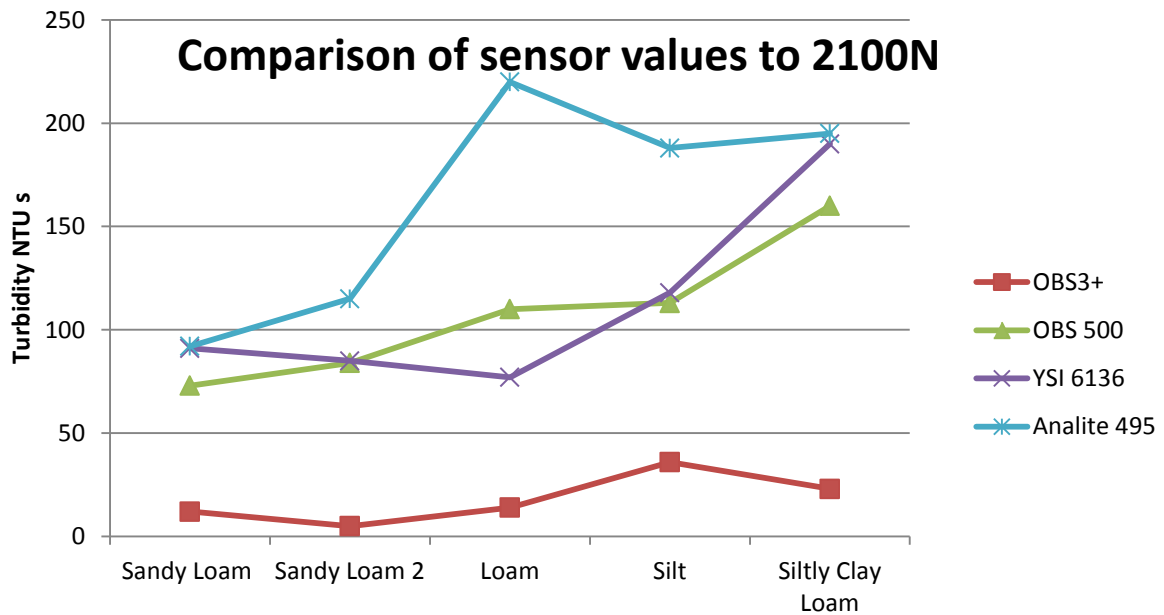
Figure 3.17. Difference between turbidity values of each probe and the 2100N

The OBS3+ varied less than 36 NTUs from the 2100N values. The YSI 6136 and OBS500 differences were similar and ranged from 70 to 180 NTUs. The Analite NEP495 differences trended highest of the four probes ranging from 90 to 220 NTUs.

An average value of the difference between the 2100N and all the sensors for each soil type and the average value for all the soil textures by individual sensors was calculated. The data is shown in Table 3.2 and Figure 3.18.

Table 3.2. The average value of the difference between the 2100N and all the sensors for each soil type and the average value for each sensor for all the soils

Difference between 2100N and all sensors at a concentration of 2500mg/l					
	Sandy Loam	Sandy Loam 2	Loam	Silt	Silty Clay Loam	**Ave**
OBS3+	12	5	14	36	23	**18**
OBS 500	73	84	110	113	160	**108**
YSI 6136	91	85	77	118	190	**112**
Analite 495	92	115	220	188	195	**162**
Ave.	**67**	**72**	**105**	**113**	**142**	
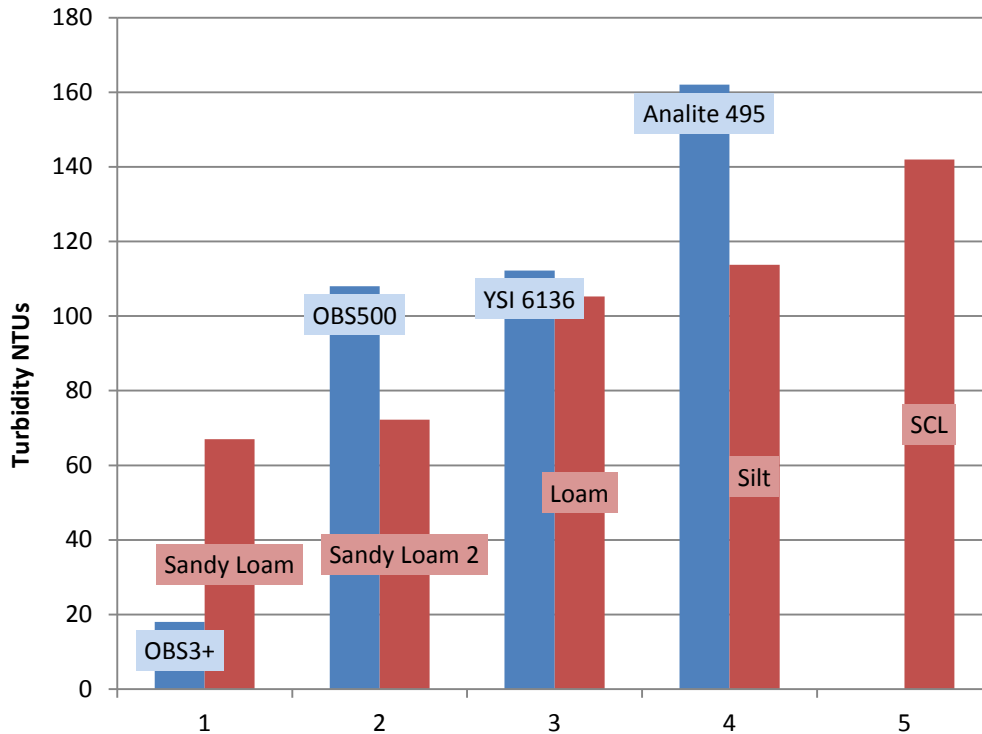
Figure 3.18. Average difference between sensors and the 2100N turbidities.

The bars labeled with soil texture represent the difference between all the sensors and the 2100N averaged together for a single soil. They represent the expected range of turbidity values generated by the four different probes on the same soil. Soil texture affected the ability of probes to predict turbidity with an average range across sensors trending upward as the soils went from coarser textured sandy loams to the highest clay content of the silty clay loam soil.

The bars labeled with sensor names represent the average difference between an individual turbidity sensor and the 2100N for all of the five soils. The OBS3+ had the least amount of variability across soil textures with an average difference of 18 NTUs. The Analite had the highest variability at 162 NTUs.

Summary

A set of laboratory experiments was conducted to determine the relationships between turbidity and sediment concentrations. Fourteen different soils were considered. Each soil

was rained on for thirty minutes and runoff was collected every five minutes in 50 mL vials. These samples were then analyzed to determine time dependent relationships between turbidity and TSS. Each soil exhibited a strong power relationship with varying coefficients, α and β. These coefficients were then evaluated to determine suitable relationships for each coefficient. Using soil properties, a regression analysis determined a relationship to define the widely variable α coefficient. Due to the complicated process to attain the proper soil properties to use the regression model for α, a second, simpler, model was given that gives a suitable, yet less accurate approximation of α. Because β varied significantly less than α and had no visible trends with soil properties, it was set to a constant value of 7/5.

The relationships of the chapter were able to predict turbidity based on known soil concentration. Turbidity-concentration data can also be normalized into a single curve with a turbidity standard and corresponding standard concentration or a known turbidity and corresponding concentration value from the site being monitored.

The impact of turbidity sensors was also evaluated using laboratory procedures. Turbidity values were measured using five different turbidity sensors on five different soil textures. Soil texture and probe configuration had an impact on the turbidity readings. For the Hach 2100N sensor, the range in turbidity with soil texture varied from 60 to 142 NTUs for concentration of 2500 mg/L. Differences in probe configurations generated a range of turbidities between 18 and162 NTUs. The difference between theOBS3+ sensor and the 2100N turbidities was the least of the four sensors at 18 NTU's compared to 108 NTUs for the OBS500, 112 NTUs for the YSI 6136 and 162 NTUs for the Analite NEP495.

45

Chapter 4
Evaluation of Turbidity with Particle Settling

Introduction

Most sediment control practices remove eroded particles by gravitational settling. The larger sediment particles are then deposited and finer sizes are more likely discharged from the construction sites. Sediment control practices not only change the mass of sediment but also the particle size distribution. The analysis given in Chapter 3 can be used to evaluate changes in sediment mass on turbidity. The focus of this chapter is to investigate the impact of changes in the size of particles in the sample on turbidity.

A theoretical framework for changes in turbidities with sediment deposition will first be given. Data collection methods for this part of the study will then be explained. The collected data will be analyzed to determine parameters established by the theoretical framework. The chapter will conclude with recommendations on methods for changing turbidity with sediment deposition.

Theoretical Framework

Turbidity-Fraction-Finer Relationship

The distribution of mass with particle sizes is widely represented using the fraction finer. The fraction finer can be defined as

$$F_d = \frac{M_d}{M_T} = \frac{M_d/V}{M_T/V} = \frac{C_d}{C_i} \tag{4.1}$$

where M_d and C_d is the cumulative mass and corresponding concentration for a particle diameter of d, M_T is the total mass of a sample volume V without any deposition, and C_i is the initial concentration of the sample without any deposition.

The turbidity relationships developed in Chapter 3 are applicable to the initial concentration. For this chapter, the relationship is written as

$$T_i = \alpha_0 C_I^{\beta_0} \tag{4.2}$$

where T_I is the turbidity without deposition and α_0 and β_0 can be determined using the methods given in Chapter 3.

To allow for changes with sediment deposition, the turbidity relationship will be written in a more general form as

$$T_d = \alpha_d C_d^{\beta_d} = \alpha_d (F_d C_I)^{\beta_d} \tag{4.3}$$

where T_d is the turbidity with deposition corresponding to a diameter for F_d. In the above relationship, α_d and β_d vary with sediment deposition. Equation 4.1 was used for C_d.

A normalized turbidity can be obtained by using Equation 4.2 to obtain

$$T_d^* = \frac{T_d}{T_I} = \frac{\alpha_d (F_d C_I)^{\beta_d}}{\alpha_0 C_I^{\beta_0}} = v_d F_d^{\beta_d} C_I^{\beta_d - \beta_0} = v_d F_d^{\omega_d \beta_0} C_I^{\beta_0(\omega_d - 1)} \tag{4.4}$$

where dimensionless parameters of v and ω are defined as

$$v_d = \frac{\alpha_d}{\alpha_0} \tag{4.5}$$

$$\omega_d = \frac{\beta_d}{\beta_0} \tag{4.6}$$

As an alternative formulation, the relationship for T_d can be determined directly as

$$T_d = v_d F_d^{\omega_d \beta_0} C_I^{\beta_0(\omega_d - 1)} \left(\alpha_0 C_I^{\beta_0} \right) = v_d \alpha_0 F_d^{\omega_d \beta_0} C_I^{\omega_d \beta_0} \tag{4.7}$$

The experimental analysis in this chapter is done using the fractions of sand, silt, and clay in the initially eroded sediment. The upper limit of sand-sized particles corresponds to $F_d = 1$, and the lower limit of clay-sized particles corresponds to $F_d = 0$. The subscript "c" will be used to identify the breakpoint between clay-sized particles, that is, F_c corresponds to the finer fraction for the upper limit of clay-sized particles (and the lower limit of the silt-sized particles). Similarly the subscript "s" will be used for the breakpoint between silt and sand, and therefore F_s is the fraction finer corresponding to the upper limit of silt-sized particles. By using this notation, the initial turbidity can then be divided into clay, silt, and sand components as

$$T_I = \Delta T_{Clay} + \Delta T_{silt} + \Delta T_{Sand} \tag{4.8}$$

where each component is defined by Equation 4.7 as

$$\Delta T_{clay} = v_c \alpha_0 F_c^{\omega_c \beta_0} C_I^{\omega_c \beta_0} \tag{4.9}$$

$$\Delta T_{silt} = v_s \alpha_0 F_s^{\omega_s \beta_0} C_I^{\omega_s \beta_0} - v_c \alpha_0 F_c^{\omega_c \beta_0} C_I^{\omega_c \beta_0} \tag{4.10}$$

47

$$\Delta T_{sand} = \alpha_0 C_I^{\beta_0} - v_s \alpha_0 F_s^{\omega_s \beta_0} C_I^{\omega_s \beta_0} \tag{4.11}$$

For the upper limit of sand-sized particles, $\omega_d = v_d = 1$. The use of these relationships requires particle size distribution information to define F_s and F_c. Experimental data were collected and are analyzed in this chapter to obtain insight into v_d and ω_d.

Simplified Forms

Insight into the role of deposition can be obtained by simplifying Equation 4.7. Let's first consider the special case where $\omega_d = v_d = 1$. The parameters of the turbidity relationship are then independent of the deposition processes. Equation 4.7 can be written as

$$T_d = \alpha_0 F_d^{\beta_0} C_I^{\beta_0} = \alpha_0 C_d^{\beta_0} \tag{4.12}$$

The turbidity is now defined using the relationships of Chapter 3. The turbidity is only a function of changes in the sediment mass. Mathematically, change in turbidity with size of sediment can now be directly written as

$$\frac{dT_d}{dF_d} = \alpha_0 (\beta_0 - 1) F_d^{\beta_0 - 1} C_I^{\beta_0} \tag{4.11}$$

Relationships are further simplified if the turbidity varies linearly with concentration, which corresponds to $\beta_0 = 1$. With this condition, and again using $\omega_d = v_d = 1$, the clay silt and sand components of turbidity can be evaluated as

$$\Delta T_{clay} = T_{clay} = \alpha_0 F_c C_I = \alpha_0 C_{clay} \tag{4.12}$$

$$\Delta T_{Silt} = T_{silt} = \alpha_0 F_s C_I - \alpha_0 F_c C_I = \alpha_0 (F_s - F_c) C_I = \alpha_0 C_{silt} \tag{4.13}$$

$$\Delta T_{Sand} = T_{sand} = \alpha_0 C_I - \alpha_0 F_s C_I = \alpha_0 (1 - F_c) C_I = \alpha_0 C_{sand} \tag{4.14}$$

where the turbidity for each component varies linearly with its concentration. The initial turbidity can be written as

$$T_I = T_{clay} + T_{silt} + T_{sand} \tag{4.15}$$

that is, it is a linear combination of the turbidities of each of its component. This relationship corresponds to the results obtained by Patil et al. (2011). It is limited to a linear relationship between turbidity and concentration and to a scaling factor, α, that remains constant for all particle sizes.

Data Collection

Data were collected to further investigate the effect of particle settling on the relationships developed in Chapter 3. The initial sediment concentration and turbidity data were obtained using the same experimental design given in Chapter 2. Each soil was allowed to run off for 30 minutes. However, in addition to collecting the 50 mL samples used in Chapter 3, the runoff was collected in a bucket. This relatively large sample of runoff was used to investigate the effect of particle settling on the v_d and ω_d coefficients.

To analyze particle settling, a pipette experiment (Klute [Ed.], 1986) was performed on each runoff sample. To do this, each sample was mixed thoroughly with a paint stirrer to adequately suspend all of the sediment in the sample. As the sample was being mixed, an initial 120 mL sample was extracted at a depth of 10 cm from the water surface level. This sample represented the total turbidity of the bucket sample. The sample was then allowed to settle and samples were extracted according to the settling rate of the primary sediment particles sand (> 50 µm), silt (2-50 µm), and clay (< 2 µm). The universal grain settling equation developed by Ferguson and Church (2004) was used to determine the equivalent spherical diameters of the extracted particles based on settling time and extraction depth.

Each 120 mL sample was mixed and divided into six 30 mL vials containing 0, 5, 10, 15, 20, and 25 mL of water. Each vial was then mixed and the turbidity of the sample was taken. The TSS concentration was determined for each sample, and the values were plotted on a TSS vs. Turbidity plot. Figure 4.1 shows an example plot of this information.
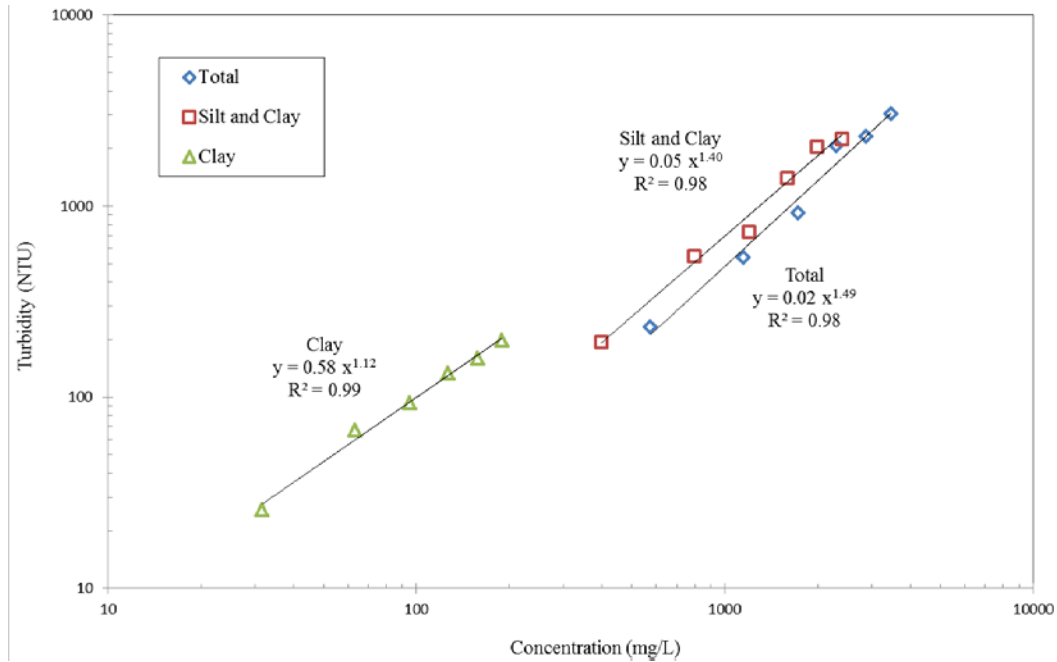
Figure 4.1. Example of turbidity and concentration data corresponding to a total runoff sample.

Data Analysis

For the total runoff sample, three turbidity relationships were developed using Equation 4.2 corresponding to sand-silt-clay, silt-clay, and clay sized particles. A typical set of curves is shown in Figure 4.1. As shown by this figure, both power and scaling coefficients vary with changes in the size of particles in the sample. Using the theoretical framework described in Section 4.2, each soil was evaluated to quantify these changes with the adjustment parameters, ν and ω.

Estimation of ω_d

To start the analysis, a relationship for ω with fraction finer, F_d, was sought, where, as given by Equation 4.1, F_d represents the fraction of the total mass smaller then diameter, d. A relationship between these two variables then represents changes in ω_d as particles are removed from suspension. To determine this relationship, ω_d was determined for the each soil using Equation 4.6. The upper limit for ω is $\omega_d = F_d = 1$.

50

Each individual soil showed a strong logarithmic trend between the ω_d and F_d values of the following form

$$\omega_d = \gamma \ln(F_d) + 1 \qquad (4.16)$$

where the coefficient γ varied between 0.05 and 0.16.

Further analysis was performed to determine if the coefficient γ could be estimated using the soil properties described in Chapter 2. A multiple linear regression, similar to the regression performed on α in Chapter 3, was used to analyze the coefficient γ. This analysis showed a slight trend in γ with dry bulk density. A regression on all of the soil's ω_d and F_d values to develop a constant relationship that uses a constant γ. This regression can be seen in Figure 4.2. The two regression models are

$$\omega_d = (0.23 - 9.20E\text{-}2\ BD)\ Ln(F_d) + 1 \qquad (4.17)$$

$$\omega_d = 0.09\ Ln(F_d) + 1 \qquad (4.18)$$

where F_d is the fraction finer and BD is the dry bulk density of the soil in g/cm^3.

Figure 4.2. Overall logarithmic regression between ω_d and F_d for all soils.

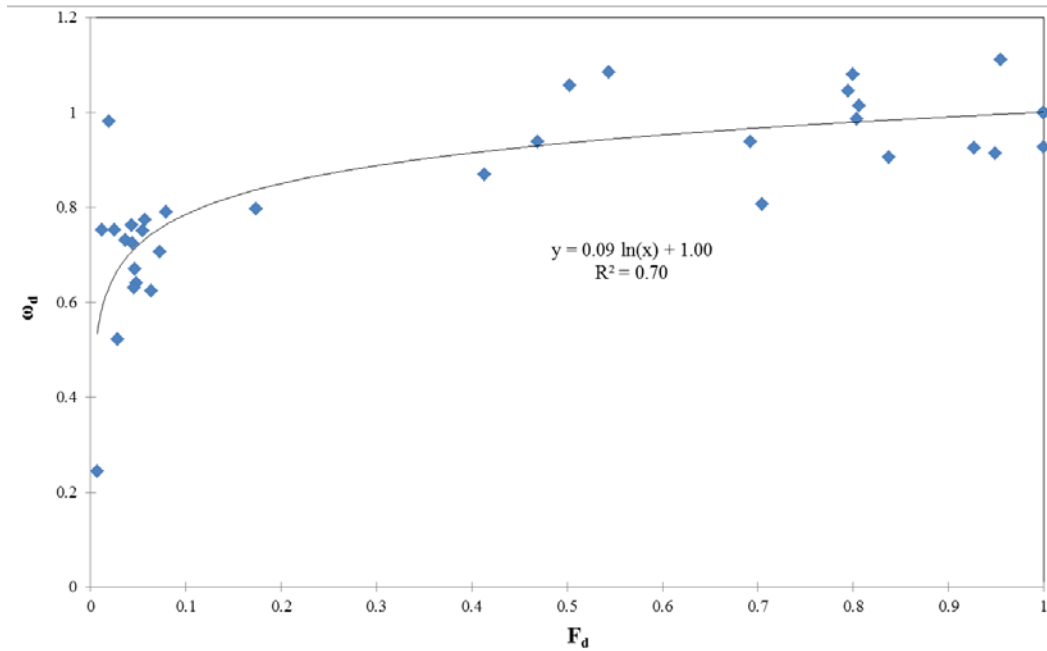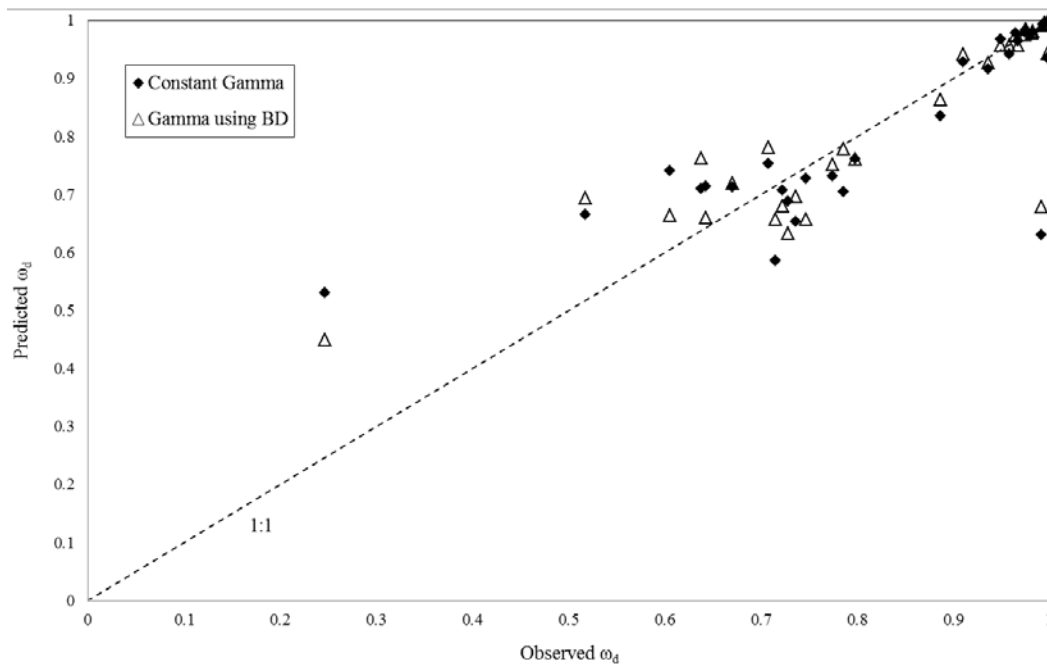Figure 4.3. Observed vs. Predicted ω_d using Equation 4.17 and Equation 4.18

Figure 4.3 shows the observed ω_d values plotted against ω_d predicted with Equations 4.17 and 4.18. This figure has a 1:1 line that represents a model that perfectly predicts ω_d. The

normalized mean square error (NMSE) of each model was determined with Equation 4.5 for just the ω_s and ω_c values. Predictions of ω_t contain no error because $\omega_t = 1$ at all times. Using dry bulk density to estimate γ and using a constant γ had an NMSE of 0.23 and 0.31, respectively.

Predicting ω_d using bulk density (Equation 4.17) has less error then an overall regression with a constant γ; however, the error is not considerably smaller than using a constant relationship for ω_d. The next section will use Equation 4.18 to predict ω_d and determine a relationship for ν_d.

Estimation of ν_d

The scaling factor is adjusted for the size of particles using the ν_d parameter. This adjustment parameter was determined for each soil using Equation 4.7. The ω_d parameter in this equation was estimated using Equation 4.18 developed in the previous section. Once again, three ν_d values were obtained for the sand-silt-clay, silt-clay, and clay sized particles. Results for all soils were plotted together to determine how the parameter varied with particle settling (see Figure 4.4). The best least square fit to the ν_d data is

$$\nu_d = F_d^{-0.85} \tag{4.19}$$

The ν_d parameter varied between 1 and 45 for our soils. This range is consistent with that obtained for the observed variability in α for our analysis given in Chapter 4. This analysis showed that the range in the x-intercept values was approximately 50, with the soil containing the least amount of clay on the far right of Figure 4.2. Likewise, Figure 4.2 shows that the α value and x-intercept can vary significantly as large particles are removed from suspension. The range in ν_d is consistent with the variability found in α in the other components of our study.

53
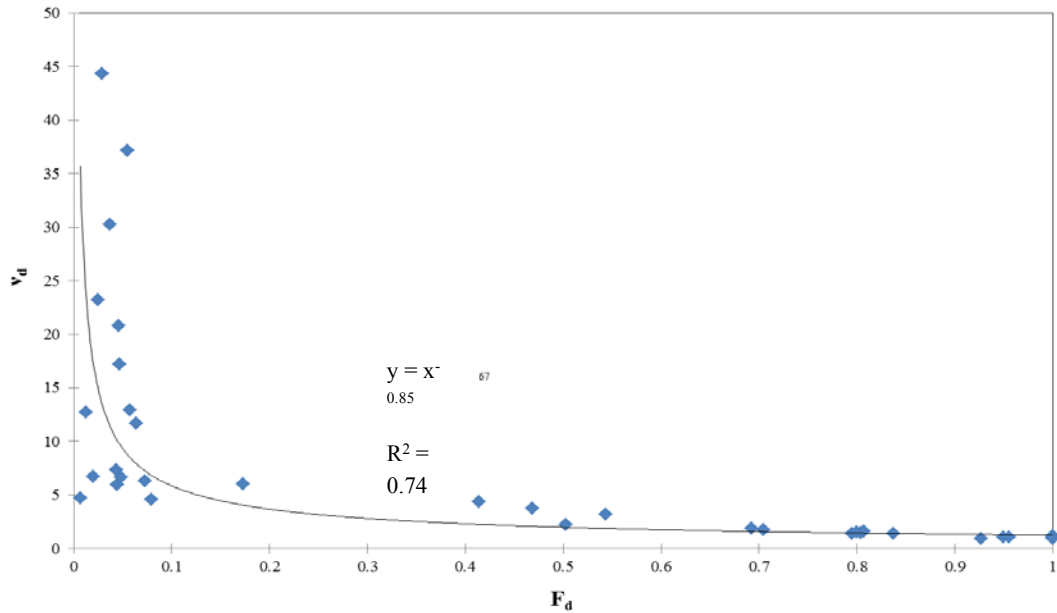
Figure 4.4. Overall power relationship between v_d and F_d for all soils.

Dimensionless Turbidity

Equation 4.4 defines dimensionless turbidity, T_d^*, as the ratio of the turbidity corresponding to particle size d to the initial turbidity corresponding to the sample. It is a function of the initial power value, β_0, and concentration, C_I, of a soil, the dimensionless parameters, ω_d and v_d, and the fraction finer, F_d, corresponding to the diameter d. If the initial concentration of the sample does not significantly impact the dimensionless turbidity, then dimensionless turbidity is defined as

$$T_d^* = \frac{T_d}{T_I} = v_d F_d^{\omega_d \beta_0} \tag{4.19}$$

The removal of concentration simplifies the determination of the turbidity with sediment deposition. Equation 4.19 is only a function of fraction finer and fitted coefficients. It provides a simple way to estimate what size particles need to be removed from runoff to meet a specific turbidity, greatly aiding the development of erosion control plans.

The dimensionless turbidities for the sand, silt, and clay particles in each of the laboratory soils were found using both Equation 4.4 and Equation 4.19. ω_d and v_d were estimated using

the relationships shown in Figure 4.3 and Figure 4.4. The minimum, maximum, and median values for fraction finer and both dimensionless turbidities are given in Table 4.1.

Table 4.1. Dimensionless turbidity calculated with and without concentration.

	Sand	Silt			Clay		
		min	max	median	min	max	median
F_d	1	0.1733	0.9998	0.7974	0.0067	0.0795	0.0451
T* w/ conc.	1	0.2401	0.0998	0.7651	0.7416	0.0999	0.0935
T* w/o conc.	1	0.0207	0.1257	0.0465	0.4881	3.896	0.8547

Unfortunately, the simplified equation does not accurately predict the dimensionless turbidity of clay. For most application, it should not be used to evaluate the impact of deposition on turbidity.

Summary

The effect of particle settling on the turbidity-concentration relationship developed in Chapter 3 was evaluated. A theoretical framework was developed to explain how turbidity can be divided into primary particle classes. Dimensionless adjustment parameters ν and ω were developed to represent the change in α and β as sediment is removed from suspension. Relationships for the change in ν and ω with fraction finer were developed. These relationships were used to determine the turbidities of each particle size for each soil evaluated. The sum of those turbidities for each soil, the estimated total turbidity, was compared to the total turbidity found in the laboratory. The median percent error in these estimates was 2.9%.

Chapter 5
Collection and Analysis of Field Data

Introduction

The monitoring of turbidity at construction site has numerous challenges. In Chapters 3 and 4, variability in measured turbidities with soil type, type of sensor and sediment deposition was examined using data collected in a laboratory setting. Factors related to the rapidly changing landscape of construction sites also need to be considered. Locations of roads, stock piles, sediment basins, culvert outfalls, and ditches also impact the turbidity from construction sites. Consideration of these factors clearly requires field work.

Field activities for the project are divided into (1) design and testing of monitoring systems, (2) collection and analysis of field data, and (3) linkage of the laboratory experiments with field turbidities. Two different monitoring systems were developed. The first was a turbidity box designed to monitor turbidity levels from overland flows and the second was designed to monitor turbidity values during de-watering activities. Two different designs were obtained for each of these types of systems. Both designs are presented. Field data were collected and analyzed at two construction sites using the first designs. After the collection of these data, additional work was done to improve the performance.

With the aid of several Minnesota Department of Transportation (MN DOT) employees, monitoring plans were developed and implemented to measure field turbidities. Although a rigorous analysis of all field data with the laboratory data was not possible, dilution curves for a single storm are compared to those results obtained from the laboratory study. The field study is used to illustrate on how our turbidity relationships can be applied to construction sites. Our relationships will then be used (1) to determine the turbidity from observed concentrations and (2) to determine total suspended solids and the total sediment yield from observed turbidities.

Turbidity Monitoring Systems for Surface Runoff

Initial Turbidity Box Design and Assessment

A turbidity box was designed to allow for easy measurement of turbidities for the rapidly changing conditions at construction sites. Design requirements for the turbidity box were:

- Easy installation and removal
- Simple instrumentation
- Measure high turbidity
- Deal with high sediment loads
- Protect turbidity probe from sunlight

Views of the first design for the turbidity box built to meet these criteria are shown in Figures 5.1, 5.2, and 5.3. The turbidity box provides a conduit that increases water depth so that the turbidity probe functions properly. It is designed to pass bed loads up to 12.5 mm in diameter. This slot size was selected to reduce the likelihood that the probe will become buried with sediment deposition. Velocity and sediment suspension is maintained through the box by a 15-centimeter discharge opening in the top of the box. The turbidity probe is mounted through the top of the box and is protected from direct light. The turbidity box is made from 1.9 centimeter treated plywood. The dimensions of the box can be changed to meet a specific application.

Figure 5.1. Turbidity box showing size, probe placement and overflow outlet.

Figure 5.2. Upstream end with 11/2 inch angle iron attached to prevent water undercutting beneath he box.

Figure 5.3. Downstream end with 0.5 inch slot opening for bed load passage

Installation

The turbidity box can be installed on almost any outfall from a construction site with simple installation hardware. Figure 5.4 shows the box held in place by fence posts with a rubber mat at the downstream end to prevent scour. This installation is designed to monitor the settling effects of ponded water behind a soil berm and rock filter. Figure 5.5 shows the box mount in place to measure the trapping efficiency of erosion control product in a ditch. This installation required wing walls to concentrate the ditch flow through the turbidity box. The upstream end of the box was simply screwed to the wing walls to hold it in place. Figure 5.6 shows the box installed in a culvert outfall. It is held in place at the upstream end by concrete screws drilled into the cement culvert. Fence posts were used to support the downstream end. Two sand bags were used to concentrate low flows through the box. Other installation considerations include: (1) install a small section of silt fence or erosion control barrier upstream of the box inlet to capture rocks and sediment debris and (2) provide a small elevation drop at the downstream end of the box to prevent sediment passing through the box from backing up.

Figure 5.4. Turbidity box mounted in rock filter. Rubber mat anchored at downstream end to reduce scouring.

Figure 5.5. Turbidity box with wing walls monitoring ditch

Figure 5.6. Turbidity box mounted in culvert outfall from sediment pond

In general, the turbidity box performs well in the field. Figures 5.7 and 5.8 show the mixing effect of the box under high flows and the bed load opening operating under low flow conditions. More information on the performance of the turbidity box is given later in the section.

Any sized turbidity probe can be adapted to fit into the box by using a rubber coupling reducer that matches the probe diameter. A single sample per storm event can be collected for laboratory analysis via a sample bottle mounted on the outside of the box, shown in the lower left corner of Figure 5.9. If automated water sampling is required at a site, a pressure transducer can be installed to trigger sampling. The sampling tube from the automated sampler can also be mounted about 1.0 inches above the bottom of the box to collect suspended sediment (Figure 5.9).

Figure 5.7. Discharge out the top of the box maintains sediment in suspension

Figure 5.8. Operation of bed load slot under low flow conditions

Figure 5.9. Pressure transducer, automated water sampling tube and single sample siphon bottle installed in turbidity box

Flow Calibration of the Initial Turbidity Box

The original configuration of the turbidity box was designed to concentrate flow to a depth sufficient enough to immerse the turbidity probe, while allowing bedload to pass. Laboratory testing of the turbidity box was conducted to determine its ability to measure flow rates as well. To provide greater precisions in its dimension, a new box was constructed of grey plastic 3/8" PVC. The dimensions of the PVC box were the same as the wooden version with the exception of the overall length of the box which was reduced to fit better into the laboratory test flume.

The results of the flow calibration are shown in Figure 5.10. The turbidity box provides an accurate estimate of flow between 15 and 30 gpm. But there is an unacceptably large gap between 30 gpm and 150 gpm. Below 15 gpm the water is simply flowing out of the box through the slot designed to pass bedload. Between 15 and 30 gpm the flow is great enough to start ponding in the box. At 30 gpm the water starts to flow out of the top of the box at which point a large volume of water is needed to show an increase in stage. The transition between water ponding in the box to discharge through the top causes a substantial gap in the data between 30 to 150 gpm. Once flow is discharged through the top, a small change in flow

depth corresponds to a large change flow rates. Based on these two characteristics, it was concluded the turbidity box in its current configuration would not be useful for flow measurement. An alternative design is given in the next section.
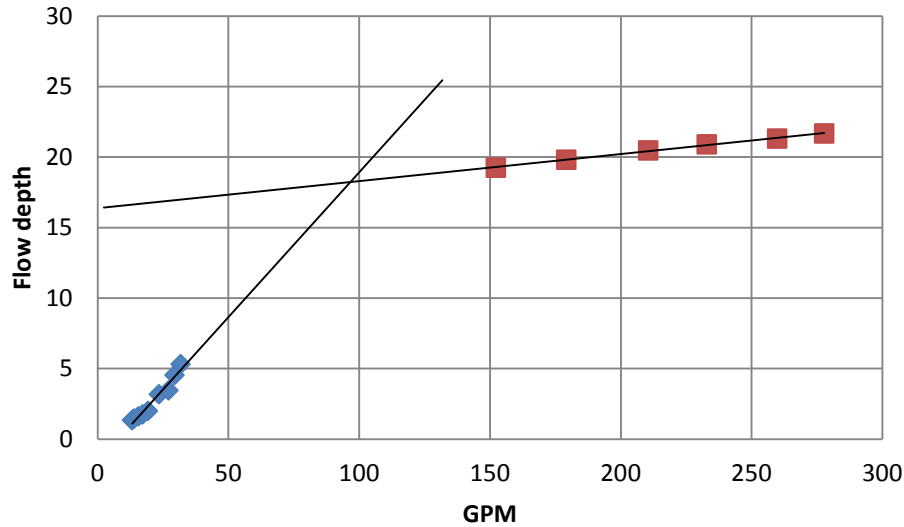

Figure 5.10. Flow calibration of the original turbidity box showing a large gap in flow range due to the configuration of the box

Final Two-Stage Turbidity Box

To allow better measurement of flow rates, an alternative turbidity box was designed and tested in our laboratory flume. This design still concentrates the flow into monitoring section and it uses a bedload slot. However, a two-stage weir is used to improve measurement of flow rate. The new design is shown in Figure 5.11.

The dimensions of the new design are approximately 16 inches by 16 inches. Two side partitions are installed to create a two-stage flow system. These partitions provide for a low flow channel. For small flow rates, flow depths in this channel are generally adequate to immerse the turbidity probe and provide adequate velocities to carry sediment through the bedload slot. For large flow rates, the entire width of the flume is used to carry flows over the weir plate at the downstream end of the box. Design schematics for the two-stage turbidity box are given in Appendix E.

64
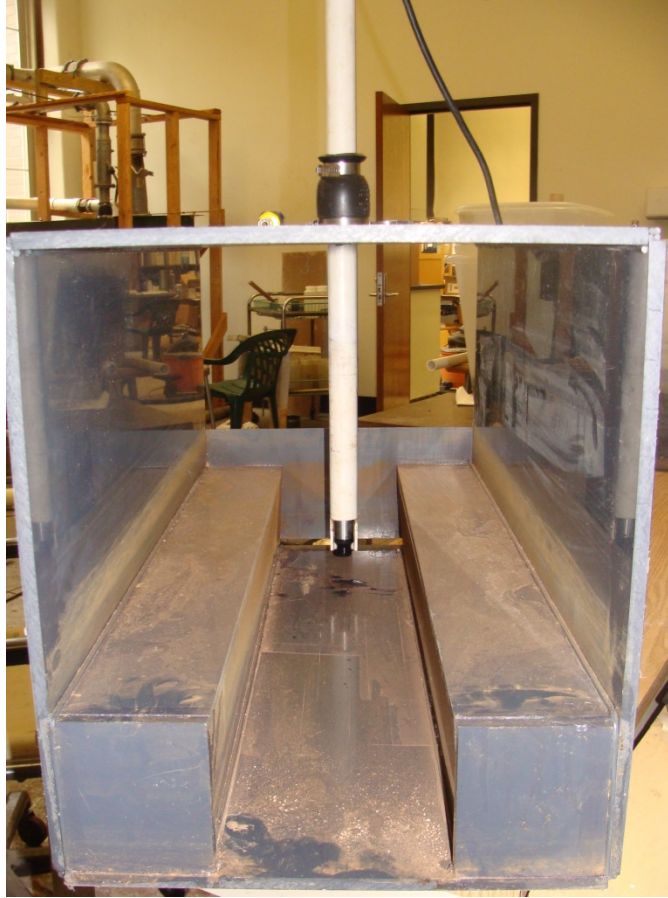
Figure 5.11. View of the two-stage turbidity weir facing downstream. The weir plate and bedload slot can be seen at the downstream end of the box

The two-stage turbidity box was calibrated for flow in a laboratory flume. The results of the calibration are shown in Figure 5.12. The new design still shows the distinct change in slope as the flow transitions from ponding behind the weir to flowing over the weir plate. However, the resolution between the conversion from the flow through the bedload slot and the weir flow is much better than obtained with the original design. With the addition of a pressure transducer or bubbler tube to measure the stage, the two-stage turbidity weir is able to measure both turbidities and flow rates.

Figure 5.12. Calibration curve of the two-stage turbidity box

Turbidity Monitoring Systems for De-watering

Initial Design

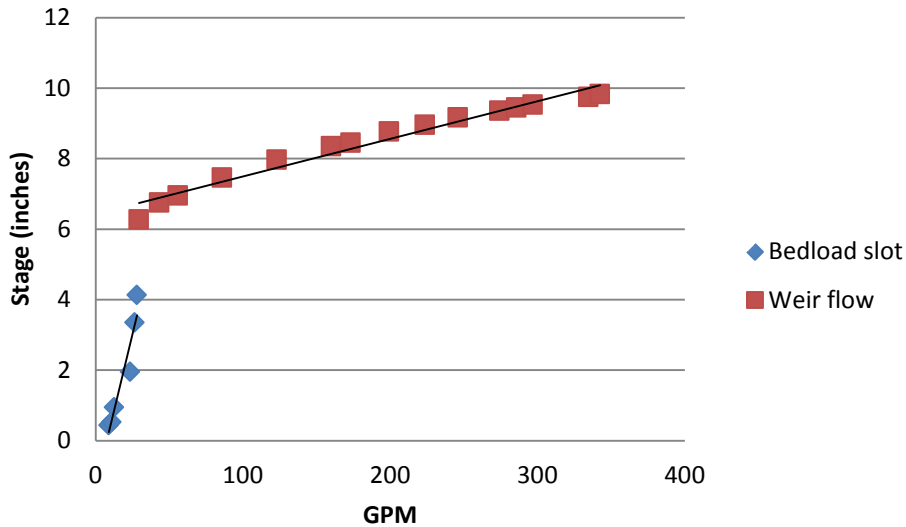De-watering activities occur at construction sites when water is pumped to a discharge location. The water is often pumped into onsite sediment ponds. However, if the water is sufficiently clean, it is discharged off site to increase the available storage in the ponds for treating of storm events. De-watering activities are not static and turbidity levels can quickly change as the water is drawn down or some soil disturbance is introduced near the de-watering site. To better control sediment leaving the construction site via de-watering activities, a monitoring system was developed to measure flow rate and turbidity for de-watering activities. The portable de-watering monitoring system is shown in Figure 5.13. Key components are a Seametrics 4 inch flow meter, Campbell Scientific CR850 data logger and OBS3+ turbidity sensor.

Figure 5.13. Portable de-watering monitoring system

To use the de-watering system in the field, the discharge hose is connected directly to the monitoring pipe. In operation, water first flows through the Seametrics flow meter and then passes through the turbidity chamber (10 centimeter PVC pipe tee). Both flow rates and turbidity data are measured and recorded. This system has a flow range of 12 to 800 gpm and a turbidity range of 0 to 4000 NTUs. For reliable flow rate measurements, the water is then forced through a 4 inch elbow to ensure full pipe flow. The turbidity probe is mounted inside a 30 inch long and a 1 inch diameter PVC pipe. This pipe can be slipped in and out of the 4 inch turbidity chamber for maintenance. The 1 inch pipe provides support for attachment to a fence post, capacity for larger heads, and protection for the turbidity probe from sand and gravel pumped through the system. Details of the placement of turbidity probe are shown in Figure 5.14. This pipe is mounted the 1 inch pipe and is rotated so that the turbidity sensor is protected from abrasion.

Figure 5.14. Turbidity probe mounted inside 2.5 centimeter PVC pipe for protection

The data logging system consists of a CR850 Campbell Scientific data logger and a small 12 volt battery (Figure 5.15). The data logger controls the scan rate of the turbidity probe and logs the data from the turbidity probe and flow meter. It has a small LED screen on the face of the data logger to allow viewing of real time flow and turbidity values. The small battery allows for a more mobile system. If longer data logging times are required a larger 12 volt deep cycle marine battery can be used to power the system.
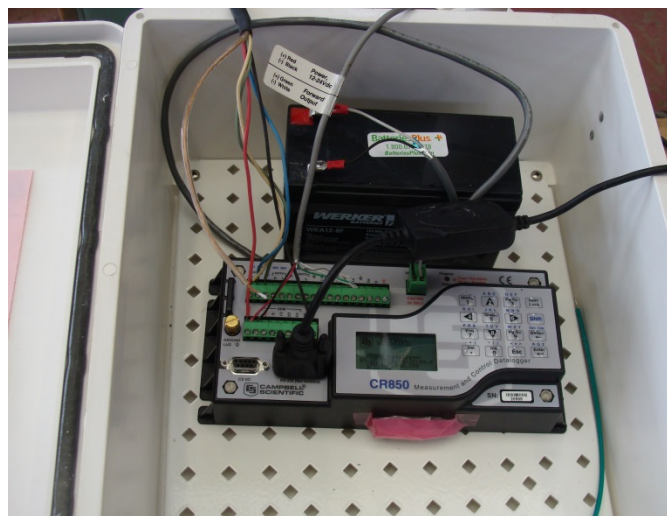

Figure 5.15. Data logger and battery mounted inside weatherproof enclosure

Calibration and Evaluation of the Initial Design

Water was pumped from a holding tank through the system and back into the holding tank. Soil was added to the holding tank to obtain a range in turbidity from 6 to 500 NTU's. A second pump was placed in the holding tank to circulate the water and keep the sediment in suspension. An OBS+3 turbidity probe was used to measure the turbidity in the holding tank. The turbidity in the holding tank was compared to that measured by the same OBS+3 probe inserted into the de-watering system. The results of the comparison are shown in Figure 5.16. The flow rate during the calibration remained unchanged at 20 gpm.
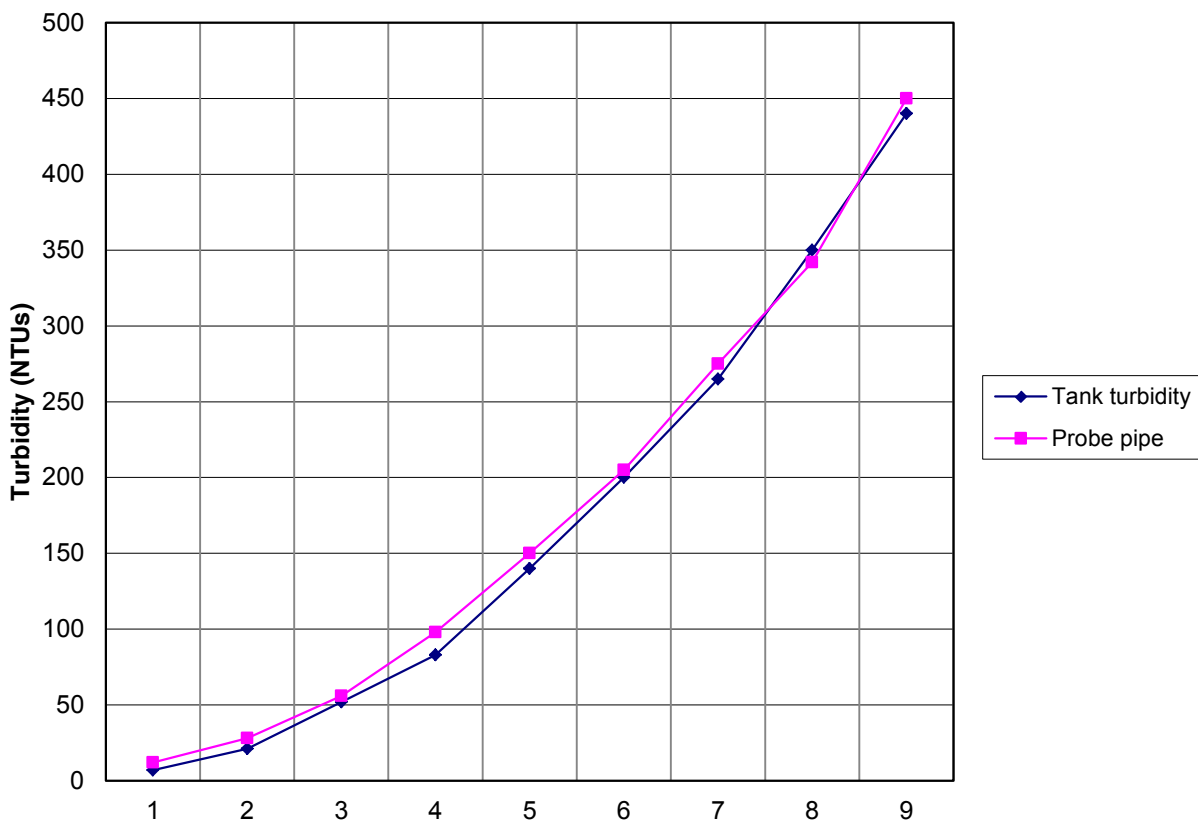
Figure 5.16. Graph depicting the accuracy of the turbidity measurement in the de-watering system compared to tank turbidity.

In August of 2012, the de-watering device was used to monitor water pumped from a settling tank to a stream channel. The laboratory calibration run at 20 gpm shown in Figure 5.16 was unable to provide reliable measurement of turbidities corresponding to higher flow rates measured under field conditions. The turbidity values measured by the turbidity meter mounted in the de-watering device were compared against the turbidity in the settling tank

measured by a HACH 2100Q handheld turbidity meter. The results are shown in Figure 5.17. The turbidity measured by the Campbell Scientific OBS+3 probe mounted in the de-watering device ranged from 45 to 70 NTUs at a flow rate averaging 53 gpm. The settling tank turbidity measured by the HACH 2100Q averaged 25 NTUs. Periodically, the OBS+3 probe was removed from the de-watering device and placed in the settling tank. The average of these readings was 21.6 NTUs. The velocity of the water flowing past the probe appears to have an effect on the turbidity measurement of the probe mounted in the de-watering device.
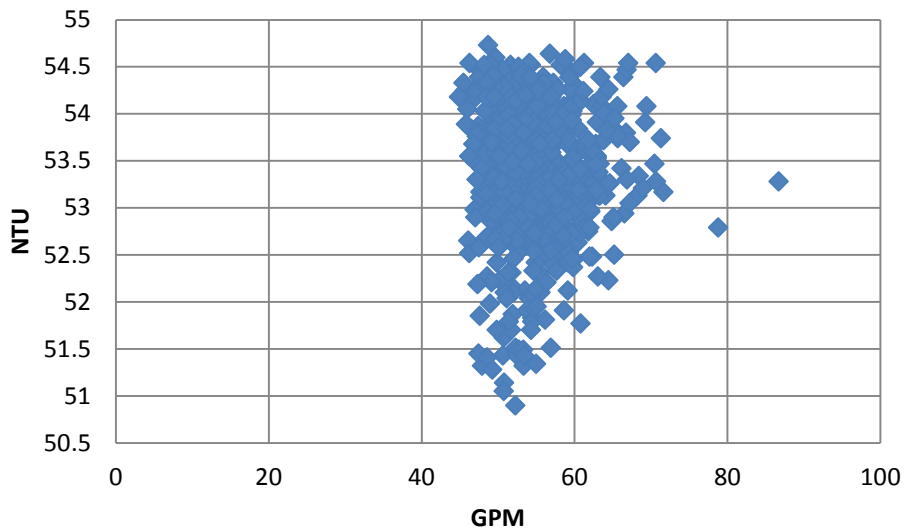
Figure 5.17. Turbidity measured by the de-watering device during pumping of water from a settling tank

The poor performance on the de-watering device in the field resulted in additional testing in the laboratory over a range of larger flow rates. Results of this testing are shown in Figure 5.18. The same OBS+3 probe was used to measure the turbidity in the tank and the de-watering device. As shown by Figure 5.18, the turbidity measured by the de-watering device

over predicted the turbidity of the water.

Figure 5.18. Comparison of turbidity measured in a tank to that in the de-watering device using the same probe

Addition testing of the de-watering device revealed the area of influence of the light signal from the turbidity probe was greater than the area inside the 4 inch pipe tee causing a shift in the turbidity readings.
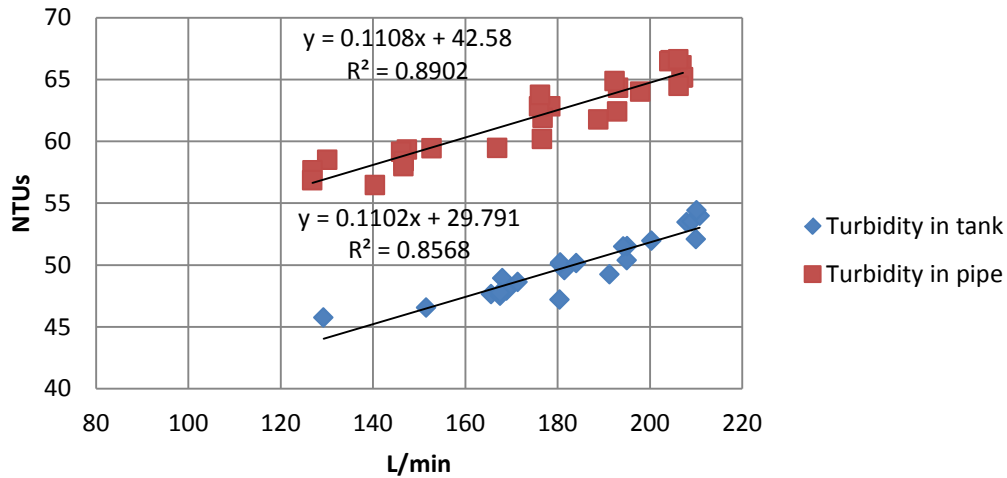
Final Monitoring Design for De-watering

To improve the accuracy of de-watering device, the 4 inch PVC pipe and elbows at the downstream end of the original design was replaced with a PVC box with approximate dimensions of 9 inches by 9 inch with a length of 18 inches. Turbidity is measured for the reduced flow rate within this square box. The flow rate in the box is approximately one-fifth of that in the upstream 4 inch pipe. The new monitoring section also is large enough to reduce errors in turbidity caused by the light signal reflecting off the PVC pipe. A picture of the new design is shown in Figure 5.19.
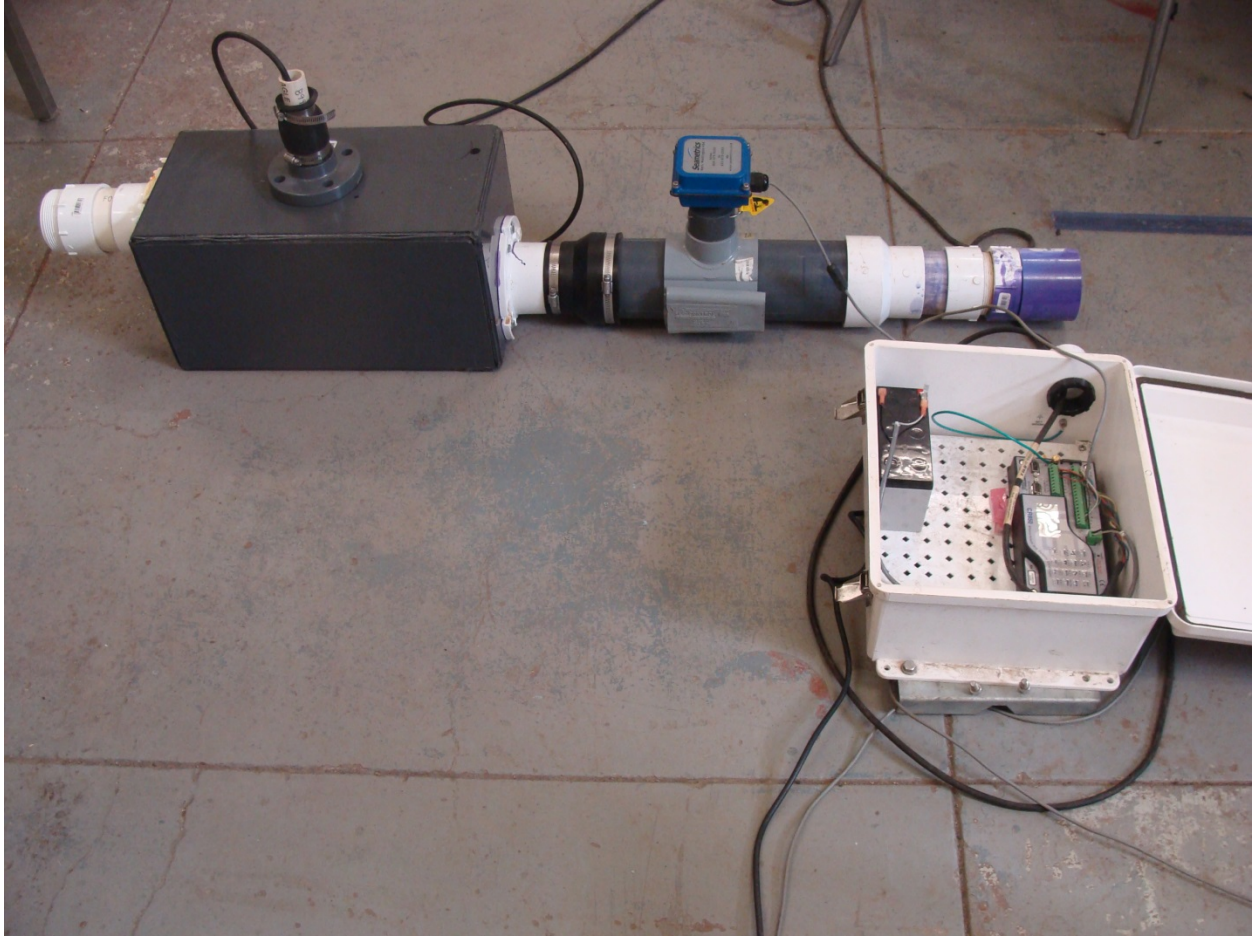
Figure 5.19. De-watering device with PVC box to house the turbidity sensor

The testing of the new de-watering turbidity meter was done in a laboratory flume. Sediment from TH-23 topsoil (34.3% sand, 47.5% silt, 18.2% clay) was incrementally added to the supply tank and turbidity values recorded at six different sediment concentrations. Flow rates were recorded with the in line flowmeter and turbidity values measured by an OBS3+ sensor mounted inside the PVC box. Turbidity values were also measured by a 2100Q HACH handheld field turbidity meter and a second OBS3+ probe mounted in the supply tank. The results of the testing for all 6 concentrations are given in Figure 5.20.

Concentration 1

Average
OBS 18.9
2100Q 19.8
Diff. 0.9

- ◆ 2100Q
- ■ OBS3+

Concentration 2

Average
OBS 33.9
2100Q 51.4
Diff 17.5

- ◆ OBS3+
- ■ 2100Q

Concentration 3

Average
OBS 39.1
2100Q 61.6
Diff 22.5

- ◆ OBS3+
- ■ 2100Q

Concentration 4

Average
OBS 45.3
2100Q 70.5
Diff 25.2

- ◆ OBS3+ Dewater
- ■ 2100Q
- ▲ OBS3+ Tank

Concentration 5

Average
OBS3 54
2100Q 90.3
Diff 36.3

- ◆ OBS3+
- ■ 2100Q
- ▲ OBS3+ Tank

Concentration 6

AverageOB
OBS3 98
2100Q 188
Diff. 90
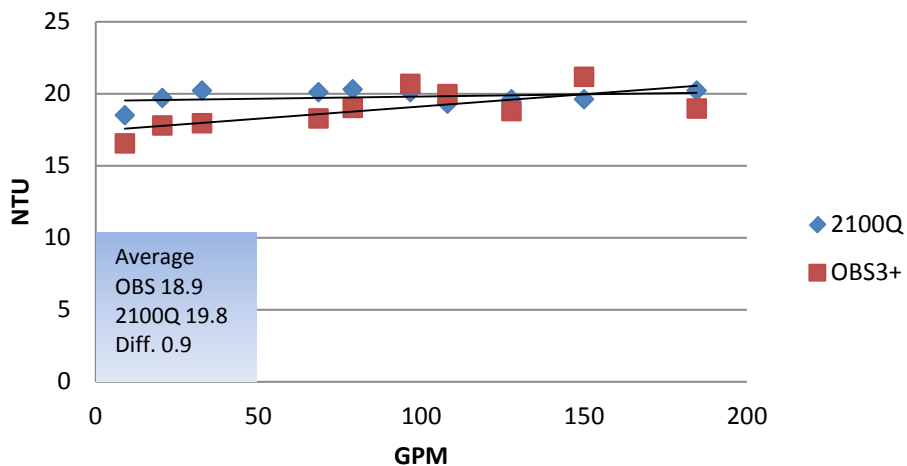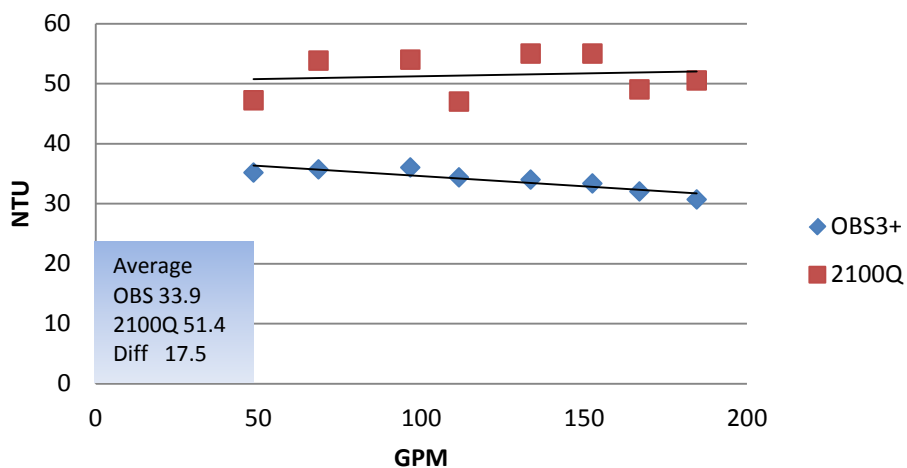
- ◆ OBS3+
- ■ 2100Q
- ▲ OBS3+ Tank
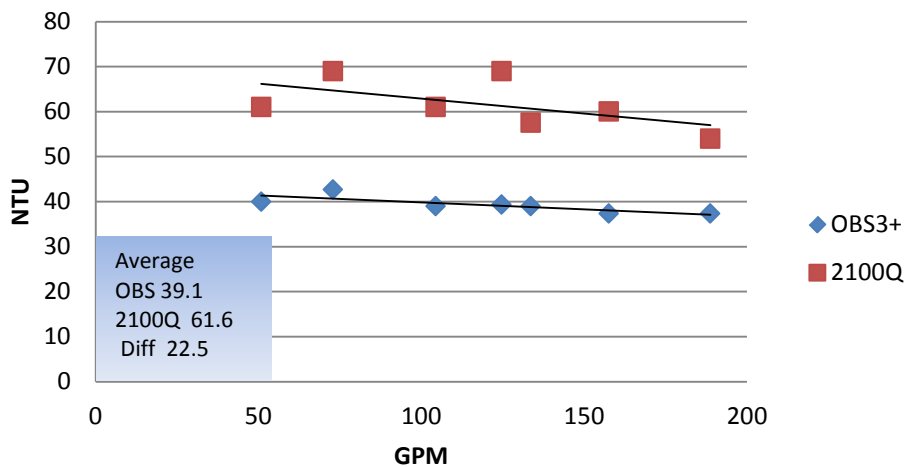
Figure 5.20. Graphs of turbidity values from six different sediment concentrations measured with a 2100Q and OBS3+ probe. The last three graphs also show a comparison between the turbidity values given by the OBS3+ in the de-watering device and the turbidity in the supply tank measured with a second OBS3+ probe

As the sediment concentrations increased from Concentration Test 1 to Concentration Test 6, the difference in the turbidity values between the 2100Q and the OBS3+ probe ranged from near zero at the lowest sediment concentration to a difference of 90 NTU's at the highest sediment concentration. At Concentration Tests 4, 5, and 6 a second OBS3+ probe was installed in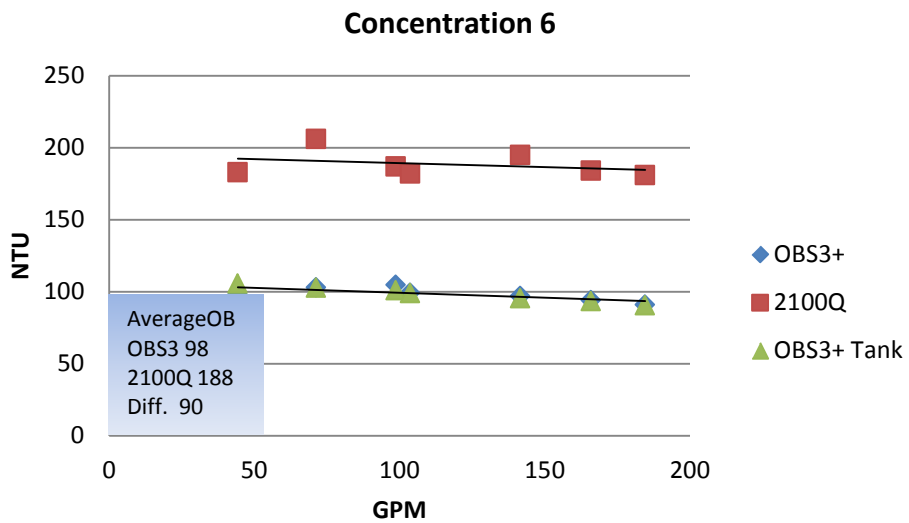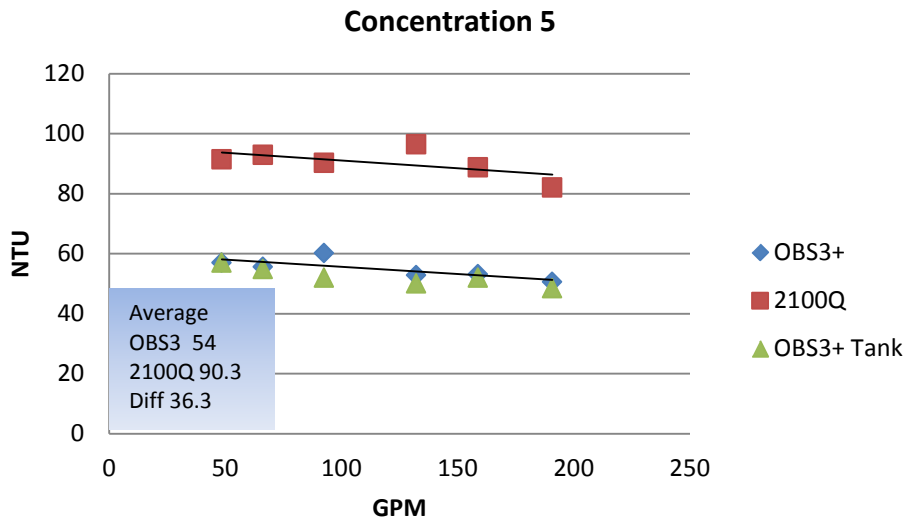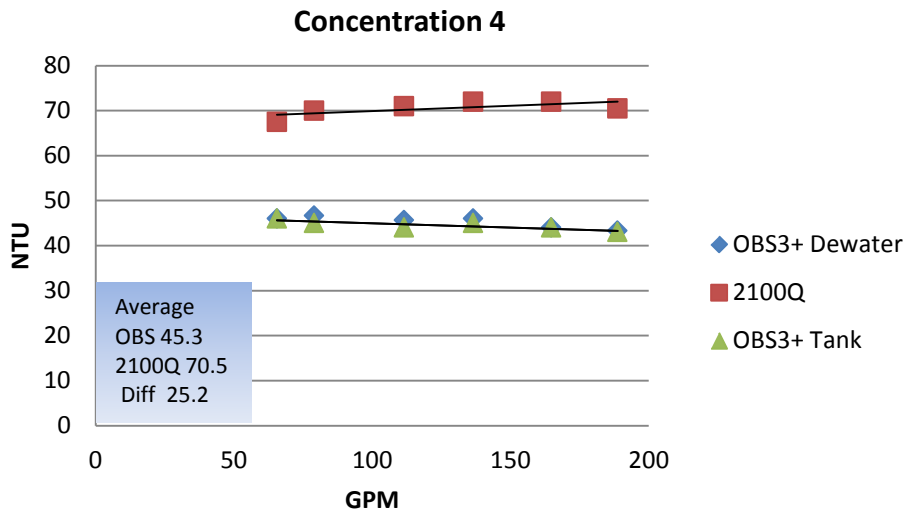 the supply tank to see if there were any effects of water velocity, turbulence or interference from the PVC box on the readings generated from the OBS3+ probe mounted in the de-watering device. The two separate OBS3+ sensors gave nearly identical readings for each of the three sediment concentrations.

To better understand the difference in turbidity values generated by the 2100Q and the OBS3+ as sediment concentrations increased, a second calibration of sediment concentration and turbidity was conducted. The probe from the de-watering device was removed and placed in the supply tank at the same depth as the OBS3+ probe already mounted in the tank. The tank was mixed using the flume pump and turbidity values recorded at different time intervals as the turbidity decreased due to the settling of the sediment in the tank. Turbidity values were also measured with the 2100Q handheld and the 2100N bench top turbidity meters on samples collected at the same depth as the two OBS3+ probes were reading. The results of the calibration are given in Figure 5.21.
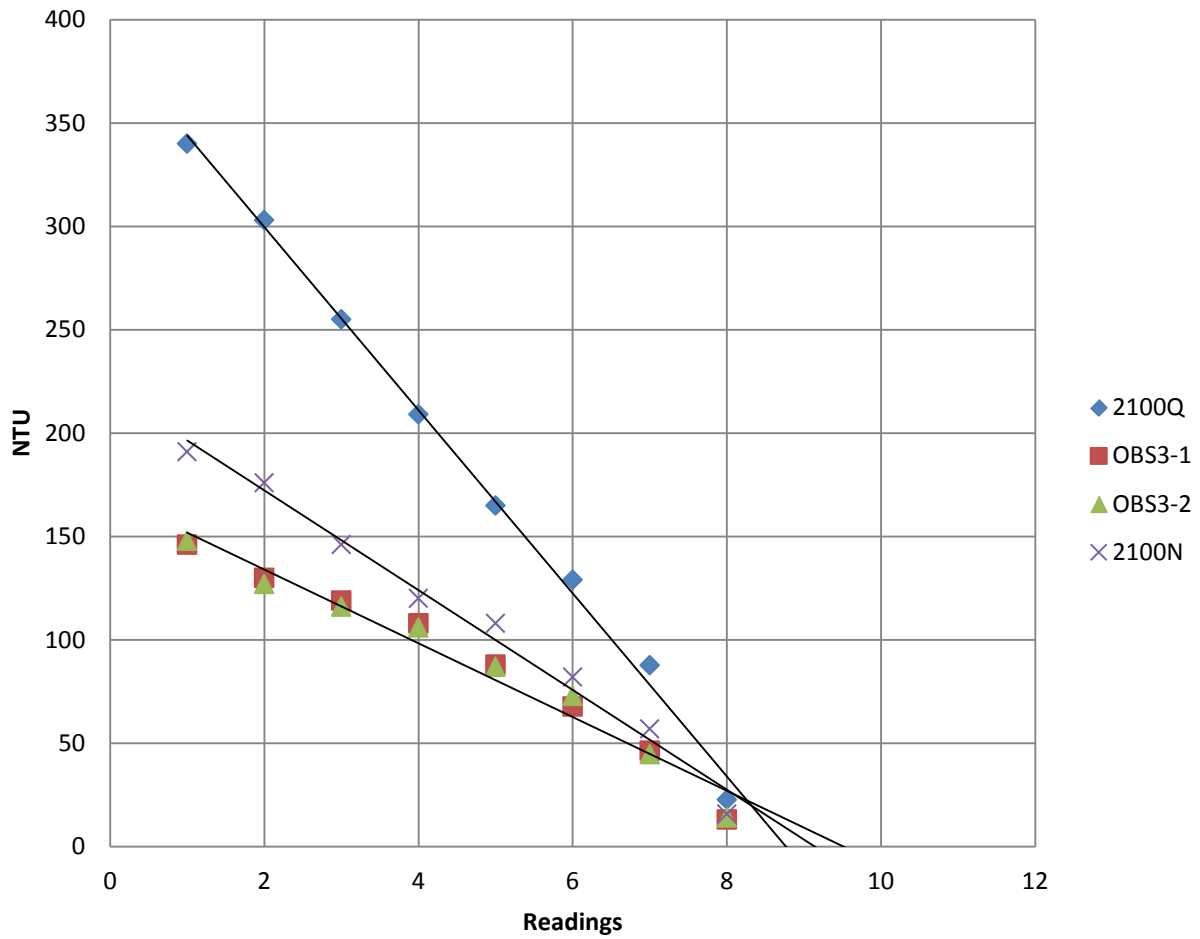
Figure 5.21. Comparison of turbidity meters in a settling tank

The OBS3+ data more closely matches the 2100N data than the 2100Q data. For a given reading the 2100Q meter reading sixty to one-hundred percent higher than the OBS3+ probes. The 2100N read ten to thirty percent higher than the OBS3+ probes. Figure 5.22 is a scatter plot which can be used to convert the readings back and forth between the OBS3+ probes and the two 2100 meters.
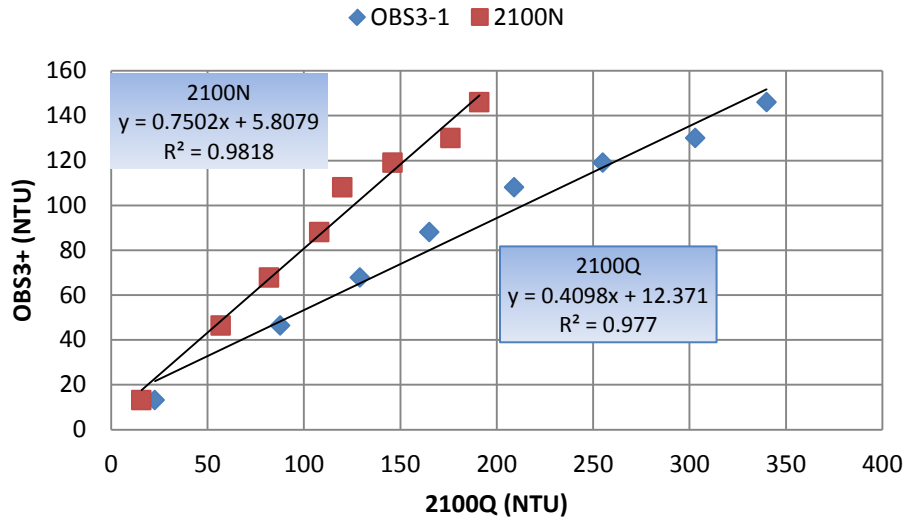
Figure 5.22. Plot of OBS3+ probes versus both the 2100N and 2100Q meters

Description of Field Sites and Events

Two construction sites were monitored as part of the field study. At one site, in Arden Hills, MN, the monitoring efforts were largely focused on an overpass constructed for Interstate-694. The second site was located west of Bloomington, MN for a constructed interchange at the intersection of Interstate-494 and Highway-169. Several large detention ponds were constructed that were able to contain most of the stormwater from the site. Table 5.1 contains information about the sampling events recorded as part of this project.

Table 5.1. Summary of data collection events from two construction sites

Site	Dates	Location	Data collected	Turbidity Sensor	Events with runoff
Snelling/694	11/2/2011-12/19/2011	Culvert upstream of construction site	Stage and grab samples	None	None
Snelling/694	5/1/2012-5/3/2012	Rock filter and ditch	Turbidity, rainfall, grab samples	Analite 495, YSI 6136	2

Snelling/694	8/2/2012-8/4/2012	Culvert downstream of construction site	Turbidity, automated samples, stage	YSI 6136	1
169/494	9/23/2011-10/28/2011	Ninemile Creek Up and Down stream of construction site	Turbidity	Analite 495	None
169/494	5/8/2012-6/20/2012	Ditch on construction site	Turbidity,rainfall,	OBS 3+	4
169/494	6/18/2012-6/29/2012	Culvert outfall from stormwater pond	Turbidity,rainfall	OBS 3+	1
169/494	6/21/???	Simulated runoff	Turbidity,sediment samples	OBS 3+	None
169/494	8/3/????-8/20/????	Ditch on construction site	Turbidity,rainfall,sediment samples	OBS 3+	1

The monitoring location at the Snelling/694 site was at or near the outfall from which runoff left the construction site, thus recorded values represent turbidity levels leaving the construction site. At the 169/494 site storm water runoff was contained in a series of settling ponds. Very little concentrated runoff left this construction site. Thus, monitoring locations at 169/494 measured turbidity levels from onsite construction activities only. Figures 5.3, 5.4, and 5.9 used to illustrate the field application of the turbidity box correspond to the monitoring setups at the Snelling/694 site. Figure 5.5 and the new Figure 5.23 show the monitoring setups at the 169/494 construction site.

Figure 5.23. Turbidity monitoring setup at 169/494 after rainfall event

Field data analysis

Turbidity data generated by consecutive rainfall events of 0.47 inches and 0.74 inches were collected at two locations at the Snelling/694 construction site in May 2012. The monitoring locations were downstream of the construction site shown in Figure 5.24. Runoff from the construction site was first intercepted by a soil berm and rock filter which allows water to seep from behind the berm after ponding. The first turbidity box was installed at the rock filter (Figure 5.25). It was instrumented with an Analite 495 turbidity probe with a range of 0 to 1000 NTUs. This location provides data on the turbidity of the runoff water treated only by the settling time at the ponded berm. After passing through the rock filter, runoff travels down slope into a ditch covered with erosion control blanket. The second turbidity box can be seen installed in the ditch in Figure 5.26. This box was instrumented with an YSI 6136 turbidity probe with a range of 0 to 1000 NTUs. This second turbidity box was set in place to measures the effect of the erosion control blanket in removing sediment from the runoff and to measure turbidity levels leaving the construction site. Water flows from the ditch into a concrete control structure before it flows underneath the freeway off site.

Figure 5.24. Construction site at Snelling/694

Figure 5.25. Turbidity box in rock filter with Analite 495 probe

Figure 5.26. Turbidity box in ditch at Snelling/694 site just above outfall off the construction site

Figure 5.27 shows the turbidity data measured at the turbidity box in the rock filter for both storm events. The turbidity readings were recording every 5 minutes. The turbidity went from zero to above the 1000 NTU maximum range of the probe immediately after runoff started for both the May 1st and 3rd storm events. Construction site activities that occurred while runoff water was still seeping from the site can also generate turbidity. Turbidity spikes were recorded at 6:00 am when workers arrived on site and again at 2:00 pm when addition erosion control blanket was installed.
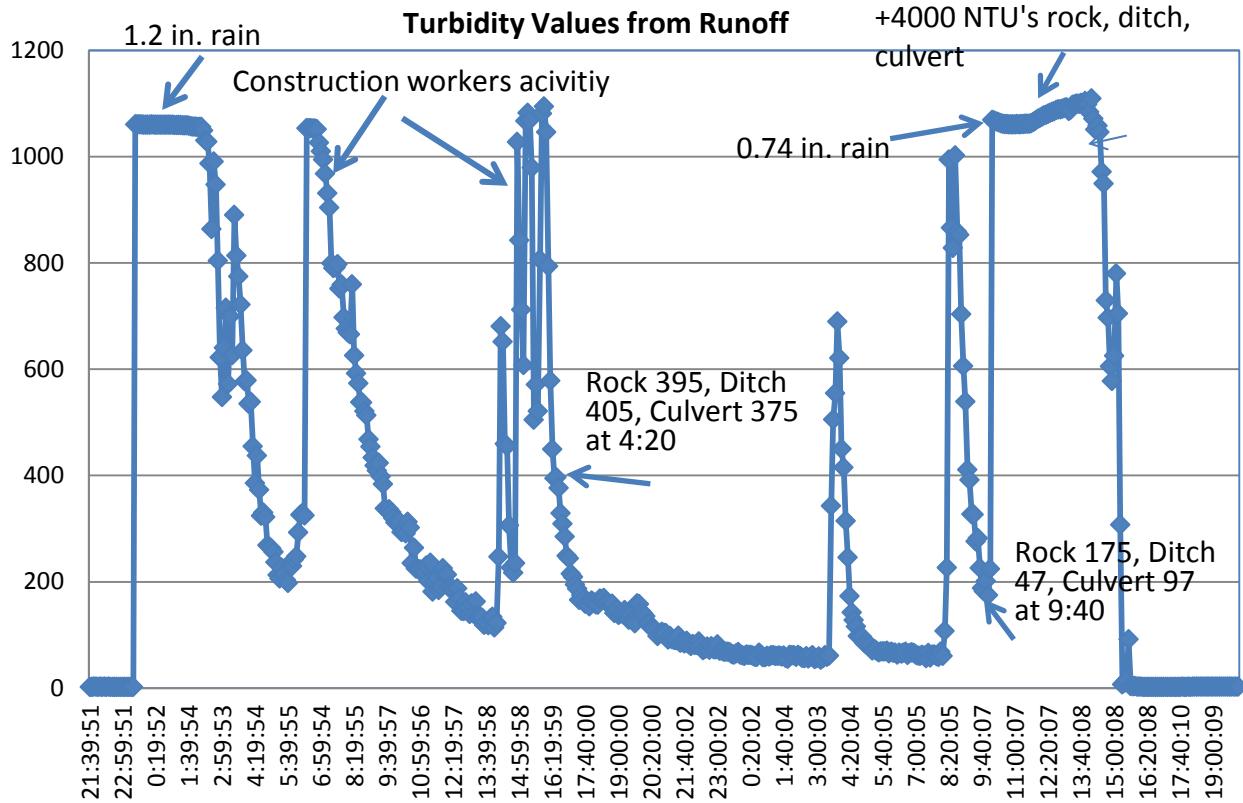
Figure 5.27. Turbidity values from two consecutive storm events at Snelling/694 construction site

To compare turbidity readings between locations and better understand the maximum turbidity generated from the site, grab samples were collected at three different times during the runoff event (Table 5.2). The sampling times are shown in Figure 5.27.

Table 5.2. Grab sample turbidity reading from May storm events at the Snelling site

Time	Turbidity values		
	Rock filter	Ditch	Culvert outfall
May 2 1600	395	405	375
May 3 1030	147	47	95
May 3 1200	+4000	+4000	+4000

All the grab samples were collected in one liter bottles and analyzed for turbidity by a HACH 2100 bench top turbidity meter. Grab samples were taken at the rock filter on May 2 at 1600 hours. This was on the receding limb of the first storm event hydrograph. The laboratory turbidity value of 395 NTUs matches closely the turbidity values recorded at the time of sampling by the Analite probe (about 400 NTUs). There was little difference in turbidity

values between the rock filter (395 NTUs) and the turbidity value recorded downstream in the ditch of 405 NTUs. This suggests little treatment for suspended sediment by the erosion control blanket in the ditch. There was also little change in turbidity between the ditch reading (405 NTUs) and the culvert outfall off site. (375 NTUs). The samples collected during the runoff event on May 3rd at 1200 hours all were collected during the peak of the runoff event and all exceeded the maximum most turbidity probes are capable of recording of 4000 NTUs.

Figure 5.28 compares the turbidity reading from the rock filter and the ditch monitoring location. Because the maximum turbidity range of 1000 NTUs was quickly surpassed on the rising limb of the runoff event comparison between the two sites can only be seen on the receding limb of the second storm event.
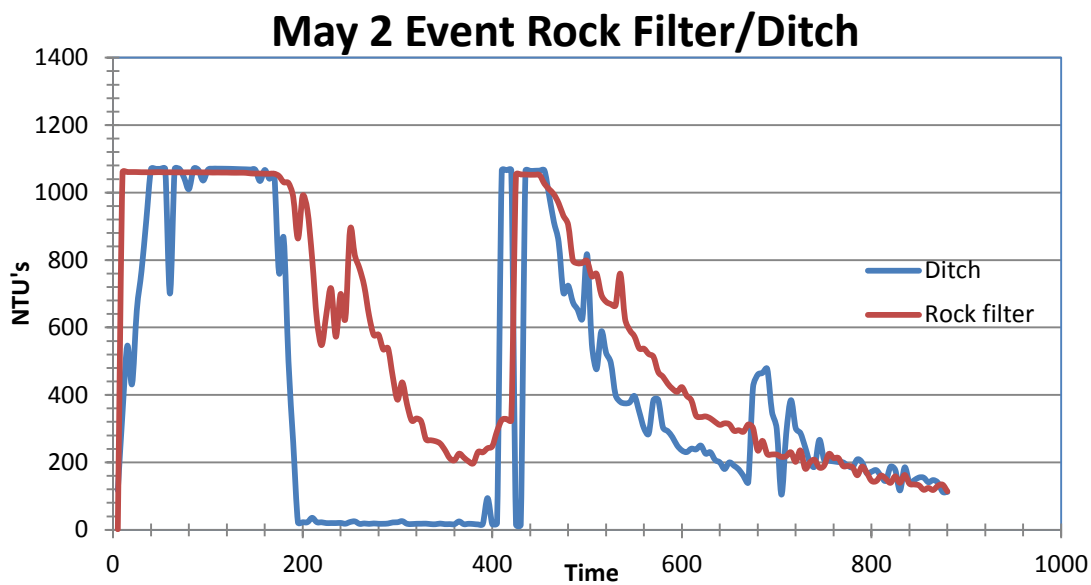

Figure 5.28. Comparison of turbidity values between the rock filter and the ditch. The rock filter was upstream of the ditch.

Given the high turbidity reading recorded at the Snelling/694 site, a Campbell Scientific OBS3+ with a range of 0 to 4000 NTUs was used to monitor 169/494 site. The monitoring location and setup is shown in Figure 5.23. Figure 5.29 shows turbidity and rainfall data from

a 2.7 inch rainfall event which occurred over a period of nineteen hours. Rainfall and turbidity readings were recorded every five minutes.
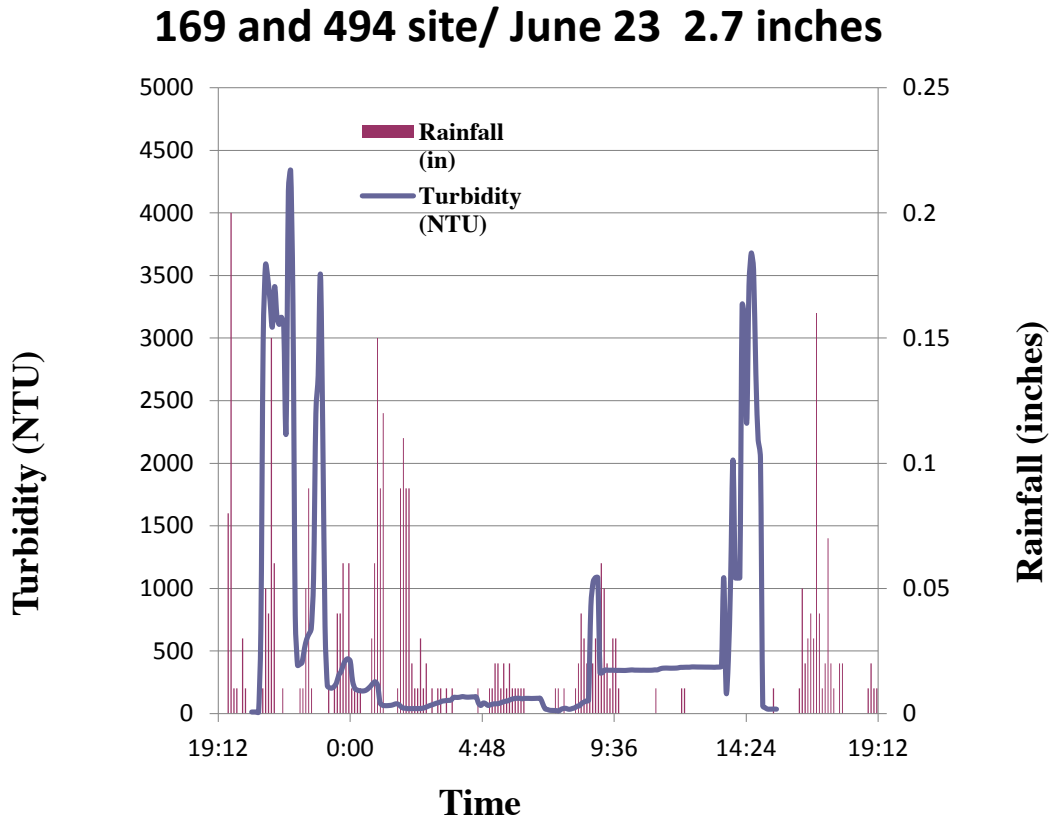

Figure 5.29. Turbidity and rainfall data from 169 and 494 construction site for a 2.7 inch rain event.

Turbidity values from this storm event peaked in the range of 3000 to 4000 NTUs. The low turbidities recorded between midnight and 7:00 am were the result of debris blocking the turbidity box. The condition of the erosion control blanket at the time of the storm depicted in Figure 5.20 was deteriorating. A new blanket was installed. On June 17th a second storm of 1 inches produced runoff from the site. Even with the new blanket in place the turbidity values during the runoff hydrograph still exceeded 3500 NTUs which is similar to that measured before the blanket was replaced (Figure 5.30).
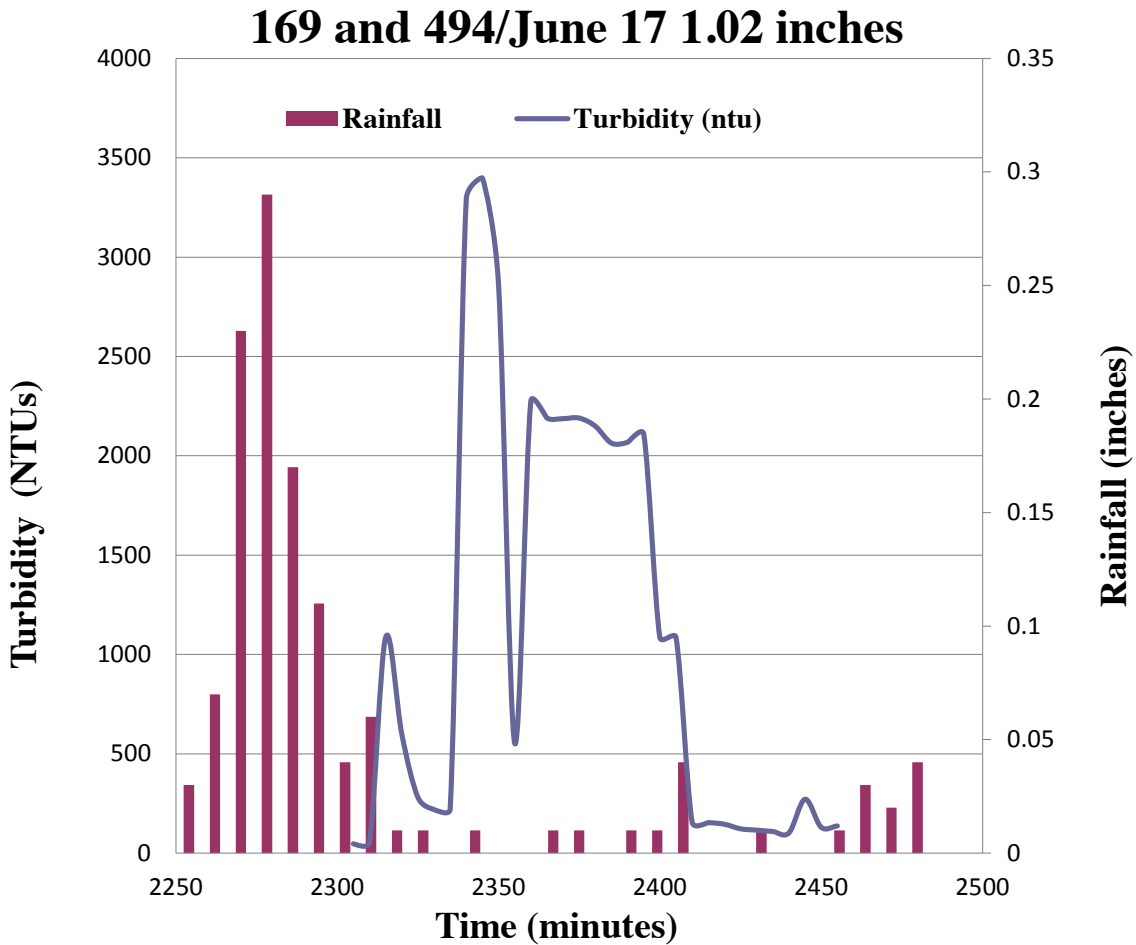
Figure 5.30. Turbidity values generated from 1.02 inch rain event after new blanket had been installed

Data from sediment pond discharge was recorded at the 169/494 site by a turbidity box mounted on the culvert outfall from the pond (Figure 5.5). The data from a 0.62 inch rainfall event at this location is shown in Figure 5.31. Because of the buffering effect of the storm water pond turbidity peaked after the rainfall had stopped. Even with the detention time of the pond of about one hour the turbidity values reached 1000 NTUs.
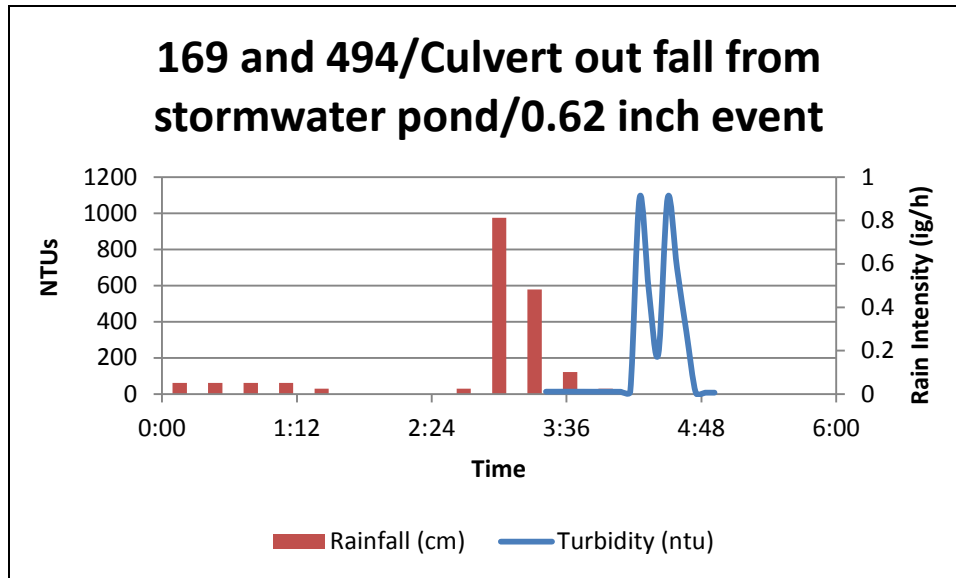
Figure 5.31. Turbidity and rainfall data at culvert outfall from storm water pond at the 169/494 site.

Comparison of Field and Laboratory Dilution Curves

To compare field and laboratory data, grab samples from both sites were brought to the lab and were analyzed using the same process described in Chapter 3 to create dilution curves. An ISCO model 3700 water sampler at the Snelling/694 site collected 1000 mL every five minutes during a rainfall event on August 3, 2012. A total of 24 samples were brought into the lab to be analyzed. A turbidity reading was taken for every sample, but all of the readings were greater than the maximum possible turbidity reading of our instruments of 4000 NTUs. Three temporally representative samples were chosen to develop observed dilution curves. An ISCO model 3700 water sampler was also placed on the 169/494 site for the same storm, but there was not enough runoff to trigger the sampler. A single grab sample was collected and brought into the lab for analysis with the Arden Hills samples.

One of the soils used in the laboratory experiments was from the Arden Hills site, allowing for a comparison of the field and laboratory turbidity data. The field samples collected on August 3 are best represented by the subsoil collected from that site. Figure 5.32 shows the dilution curves for the laboratory and field samples. There were two replicates done on the Arden Hills subsoil in the laboratory. Since the laboratory methods collected samples at six different times, there are a total of twelve time-dependent dilution curves. For the six dilution

curves from the first replicate, the average power value, shown as β_1 in Figure 5.33, was 1.40. For the second replicate, the average power value, β_2, was 1.38. The field data had an average power value of 1.37. The scaling factor α for the laboratory and field samples ranged from 0.01 to 0.07 and 0.08 to 0.1, respectively.
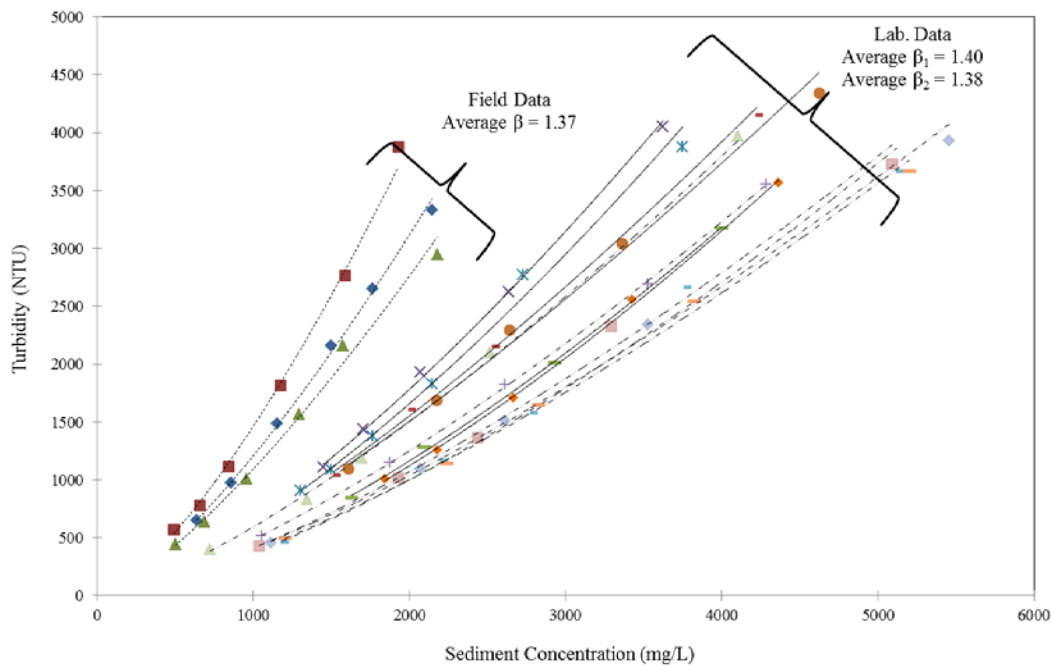

Figure 5.32. Snelling/694 dilution curves for laboratory and field sample

The β values found in the field are similar to those found in the laboratory. This result suggests that the power values obtained in the laboratory study are representative of field conditions. The α values of the field samples are noticeably larger than values reported for the laboratory data. This result is not surprising. Deposition of larger sized particles is likely at the construction site. Changes in particle-size distributions were shown in Chapter 4 to decrease the power coefficient and increase the scaling factor. Differences between field and laboratory dilution curves are consistent with both of these trends. Observed differences in laboratory and field α values are within the range of expected shifts in α with finer sediment for the Arden Hills subsoil given in Chapter 4.

A dilution curve was created for the single sample from the 169/494 site (Figure 5.33). There is no laboratory data to compare to this dilution curve, but it does show the same strong power relationship between turbidity and concentration and a β value of nearly 7/5.
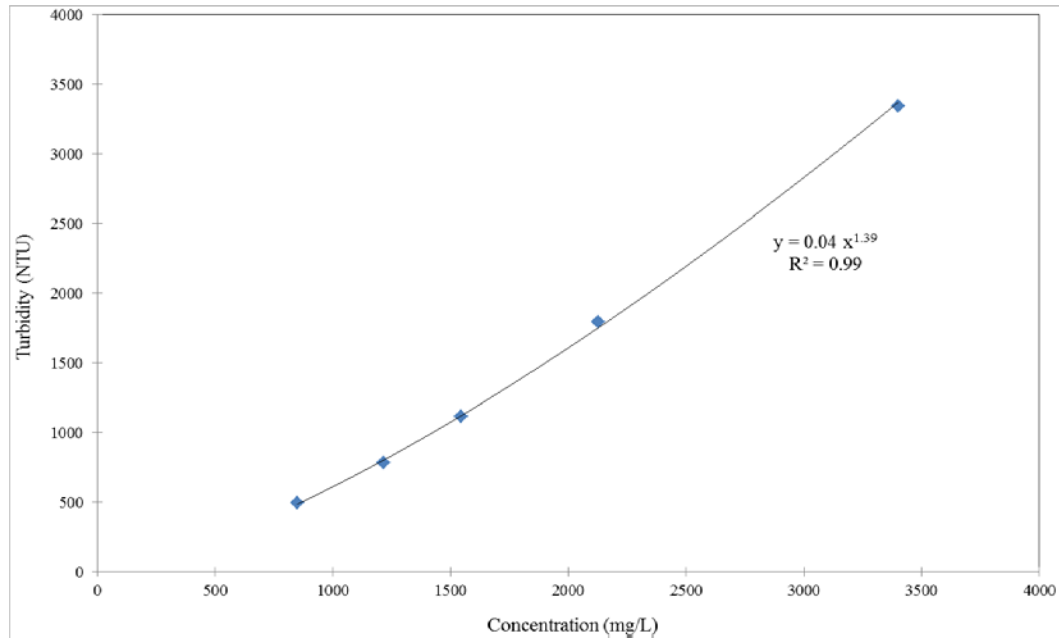

Figure 5.33. Dilution curve for 169/494 construction site.

Example Applications

Turbidity-TSS relationships developed with this study are useful to (1) estimate turbidities from measured sediment concentrations and (2) estimate sediment concentrations from measured turbidities. The first type of application will be illustrated using the data collected at the Snelling/694 site. This application is particularly useful for the assessment of turbidity water quality standards from measured or predicted TSS. Determination of concentrations from measured turbidities will be illustrated using data collected at the 169/494 site. This application is of interest in the assessment of a TSS water quality standard from turbidity data. With the additional use of an observed or predicted hydrograph, sediment load can be obtained from the estimated concentrations. The impact of a turbidity standard on the reduction in sediment loads to lake and streams can then be assessed.

Estimating Turbidity from Observed Concentrations

The simplest application of Equation 3.1 is to predict turbidity from a known concentration. On a construction site, turbidity is more likely measured then concentration data. However, process-based simulation models, such as SEDIMOT II (Wilson et al., 1984) and WATER (Wilson et al., 2008) can predict concentrations. These models can be used to assess the effectiveness of different sediment control measures. Equation 3.1 can then be used to determine the impact of these measures on turbidity and their effectiveness in meeting potential turbidity standards.

The estimation of turbidity from concentrations will be done using the 24 samples collected on August 3rd at the Snelling/694 site. The observed concentrations are plotted with time in Figure 5.34. To use Equation 3.1, the α and β coefficients need to be determined. As previously discussed, setting $\beta = 7/5$ is a reasonable assumption for Minnesota construction site soils. Three approaches are available to estimate α. They are (1) estimate α using Equation 3.3 (Model 1), which requires soil properties of percent silt, interrill soil erodibility, and the NRCS maximum abstraction depth, (2) estimate α using Equation 3.4 (Model 2) using only percent silt, and (3) solve for α directly from an observed pair of concentration and turbidity values using a $\beta = 7/5$. The third approach is preferred, but often data from individual storm events are unavailable. Equation 3.3 is the more accurate regression model for determining α, but it requires information that may not be readily available for construction sites. If a simple approximation is adequate, Model 2 can then be used to determine α.

Differences between the two methods can be assessed using all of the soil property information for the Snelling/694 site determined in the laboratory experiment. Both Model 1 and Model 2 were evaluated for Snelling/694 subsoil to obtain α of 0.027 and 0.025, respectively. The α values for the field samples were higher than these values, ranging from 0.08 to 0.1. Based on a particle size analysis, the soil is comprised of 46% sand and 54% silt. Using the relationships for v_d and ω_d from Chapter 4 and assuming sand was removed from the runoff prior to sampling, the scaling factor α increased to 0.046 and the power β decreased to 1.32. This shows that deposition plays an important role in estimating turbidity.

Figure 5.34 shows the estimated turbidity using Model 1 and Model 2 and estimated turbidity if sand were removed from suspension for the grab samples collected at Snelling/694. The predicted turbidity values are larger than the range of turbidities obtained in the laboratory study. All samples would likely violate any turbidity standard established by the State of Minnesota. Percent differences in predicted turbidities obtained for the two different estimates of α are reasonable; however, absolute difference are substantial.
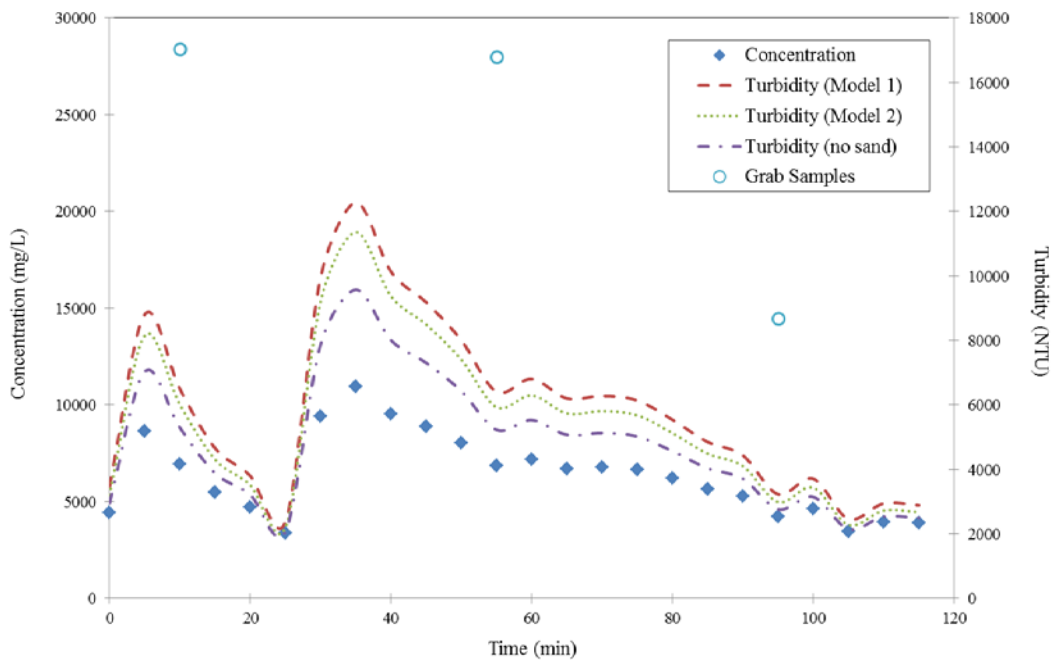

Figure 5.34. Predicted turbidity values for the August 3rd storm on the Arden Hills construction site

Dilution curves were created for three grab samples for this storm. Those curves were used to estimate the turbidity based on the concentration of sediment in the sample. These values were also plotted on Figure 5.34 to compare the predicted turbidities with the actual turbidities. The predicted turbidities are significantly lower. This discrepancy may be attributed to the August 3rd storm being larger than the control storm used in the laboratory experiment or changes in the soil's particle-size distribution.

Estimating Sediment Loads

90

On a construction site, it is more likely that turbidity is being monitored and not TSS concentration. By using relationships developed as part of this study, continuously monitored turbidity data can be converted into concentrations and used to determine sediment loads from a site. This conversion requires values for α and β for the storm event. By rearranging Equation 3.1, concentration is related to turbidity in the following format:

$$C = \left(\frac{T}{\alpha}\right)^{5/7} \tag{5.1}$$

Continuously monitored turbidity data and rainfall data were collected in a ditch on the Bloomington site during a 19 hour rainstorm on May 23, 2012. The observed turbidity-concentration data shown in Figure 5.33 were used to estimate α for this storm. The estimated concentration using Equation 5.1 is shown with the corresponding turbidity data in Figure 5.35.

A hydrograph was created for the May 23 rainstorm using an estimated time of concentration and flow rate determined with the SCS curve number method (Wurbs and James, 2001). The calculations for the hydrograph are given by Perkins (2013). Figure 5.36 shows the estimated concentration data and hydrograph for the May 23rd rainstorm. With the estimated concentration and hydrograph, sediment load at each time step can be calculated with the following equation:

$$Sediment\ Load = Q\ C \tag{5.2}$$

where Q is the flow rate and C is the concentration of sediment in the runoff.
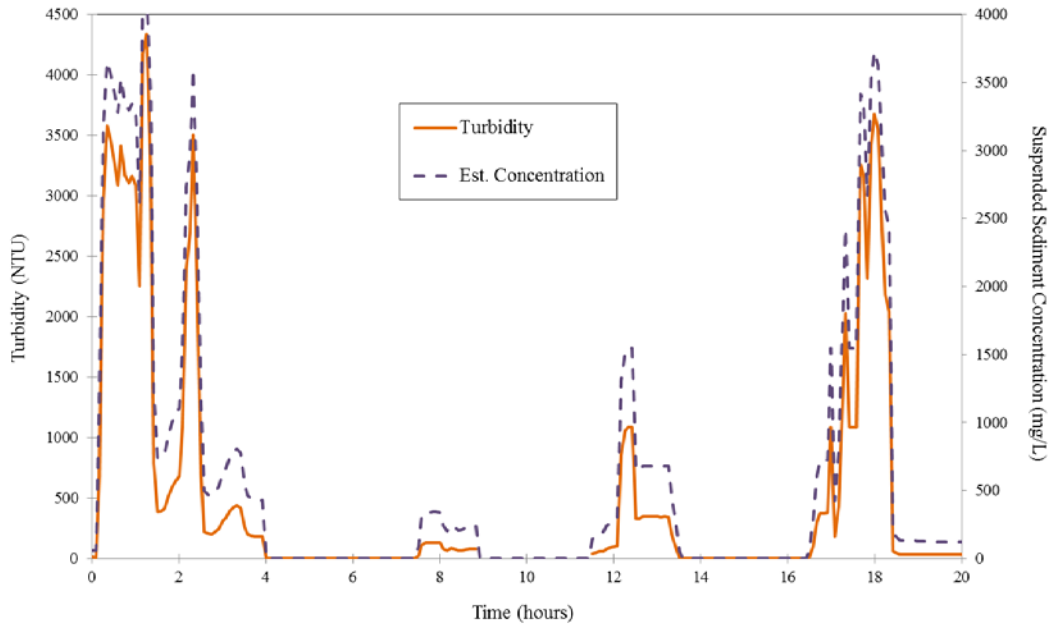
Figure 5.35. Estimated concentration values corresponding to the turbidity data collected on the Bloomington site for the rain storm on May 23, 2012.
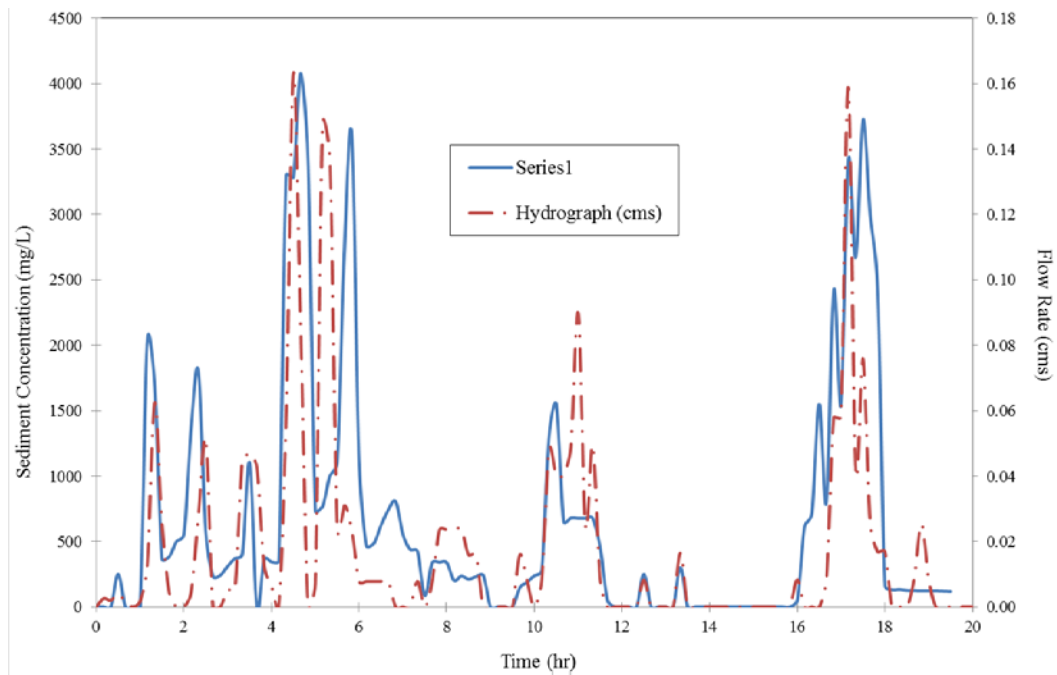

Figure 5.36. Estimated concentration data and hydrograph for May 23 storm on Bloomington site

92

Figure 5.37 shows the sediment load in tons for the May 23rd storm in Bloomington. To determine the total sediment load passing the monitoring location, the product of flow rate and concentration is simply integrated over the storm duration using the following integral:

$$Total\ Sediment\ Load\ =\ \int_o^t Q(t)\ C(t)\ dt \tag{5.3}$$

Integrating to find the area under the curve in Figure 6.6 determined that the monitoring location on the Bloomington site had a sediment load of approximately 3.5 kg during the May 23rd storm.
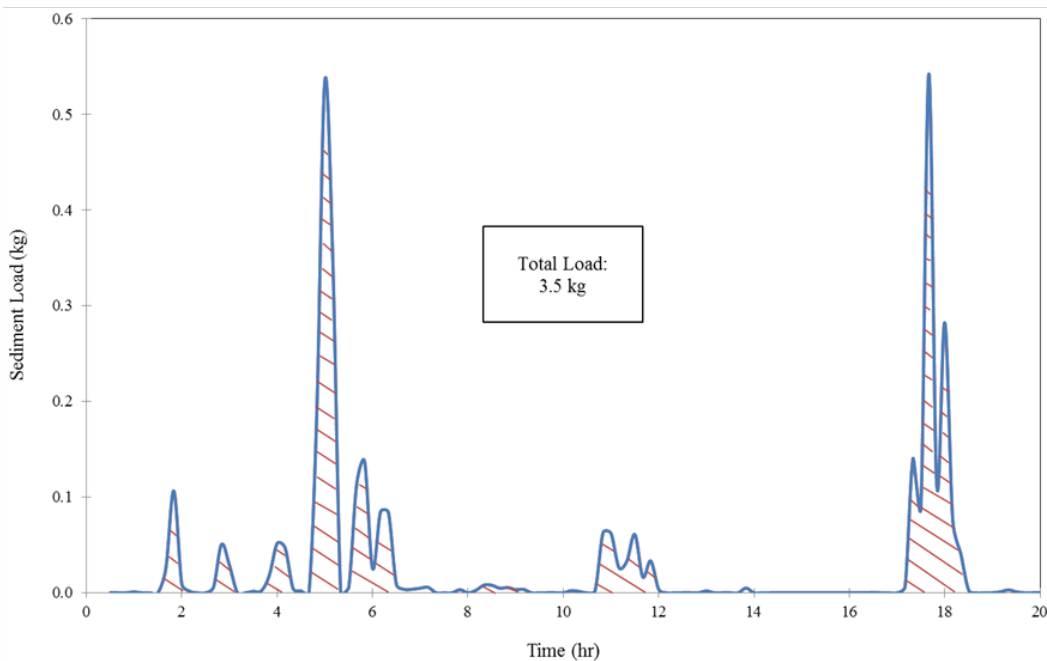

Figure 5.37. Sediment load on the 169/494 site during the May 23 storm

Impact of a Non-linear Turbidity-Concentration Relationship

Several studies, previously mentioned in Chapter 1, concluded that turbidity and concentration vary linearly. Our analysis of turbidity-concentration relationships for Minnesota construction soils resulted in non-linear power functions. To evaluate the implication of a non-linear relationship, two scenarios will be discussed. First, let's consider a percent reduction in turbidity to meet a turbidity standard. Implementation of sediment control

practices is likely required to meet this standard. We are therefore interested in differences in the corresponding percent reductions in sediment concentrations using a linear or non-linear relationship. A single flow –weighted sample is often collected for a given storm to reduce the cost of water quality analysis. Our second scenario examines the error obtained estimating the average turbidity for the storm using the single sample if turbidity varies linearly or nonlinearly with concentration. The first scenario was evaluated using the laboratory concentration and turbidity data for the Snelling/694 subsoil. Both linear and nonlinear relationships for this soil are shown in Figure 5.38. The second analysis used the turbidity and estimated concentration data for the May 23rd storm in Bloomington.

For the first scenario, three turbidity values were chosen for the analysis: 4000, 2000, and 500 NTUs. The concentrations corresponding to each turbidity value were calculated with both the linear and non-linear relationship for the soil. The percent reduction was calculated assuming the turbidity was reduced from 4000 NTU to 2000 NTU and from 4000 NTU to 500 NTU. The percent reduction was found with the following equation:

$$\% \ reduction = 100 \left(1 - \frac{reduced \ value}{inital \ value} \right) \tag{5.4}$$

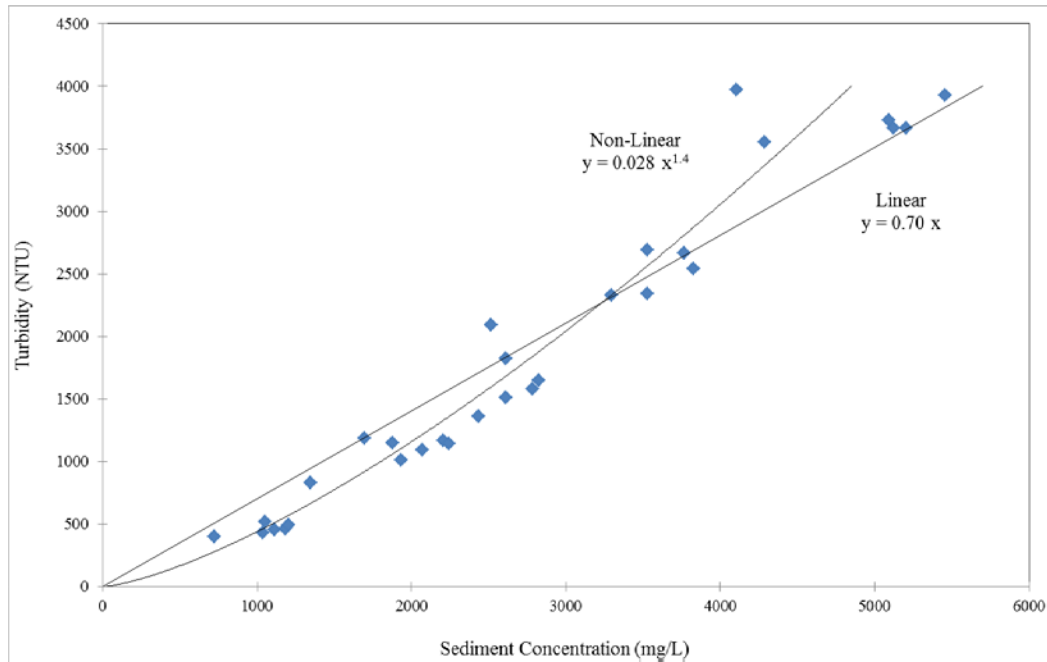The results of this analysis are shown in Table 5.3.

Figure 5.38. Linear and non-linear relationships for Arden Hills subsoil.

Table 5.3. Percent reduction in concentration with a linear and non-linear relationship.

Turbidity (NTU)		Linear		Non-Linear	
Actual	% Reduction	Concentration (mg/L)	% Reduction	Concentration (mg/L)	% Reduction
4000	-	5698.0	-	4846.3	-
2000	50.0	2849.0	50.0	2953.9	39.0
500	87.5	712.3	87.5	1097.4	77.4

As expected, the percent reduction in sediment concentration for the linear relationship is exactly equal to that of turbidity. However for our non-linear function, the percent reduction in concentration is less than the percent reduction in turbidity. If turbidity standards are adopted, then the difference between a linear and non-linear relationships could have important implications on the selection of target goals of sediment control practices.

95

For the second scenario, flow-weighted mean turbidity and concentration was found for the May 23rd storm on the Bloomington site. The linear and non-linear relationships for the data presented in Figure 5.30 were used to estimate the average turbidity and concentration for the storm. The percent error between the actual and estimated values was calculated as

$$\% \ Error = 100 \ \frac{|Estimated - Actual|}{Actual} \tag{5.5}$$

The results of this analysis are shown in Table 5.4.

Table 5.4. Percent error when estimating an average turbidity and concentration with a linear and non-linear relationship.

Flow-Weighted Mean		Linear		Non-linear	
		Estimate	% Error	Estimate	% Error
Concentration (mg/L)	1643.4	1557.5	5.2	1838.2	11.9
Turbidity (NTU)	1379.0	1455.1	5.5	1180.1	14.4

A linear function has less error then a non-linear function when estimating the average turbidity from a known average concentration and an average concentration from a known average turbidity.

Summary

Field data were collected and analyzed at two construction sites. A portable monitoring system was designed and built to assist in this data collection. The turbidity box proved adaptable and successfully monitored turbidity values at a rock filter, two ditches and two culvert outfalls on two different construction sites. It is relatively easy to setup using simple hardware. A silt fence installed above the turbidity box along with mounting the upstream end of the box slightly above the soil surface is suggested to reduce the chances of plugging the bedload slot. Also, some elevation drop is necessary between the downstream end of the box

and the soil surface to reduce the chances of sediment backing up into the turbidity box. An alternative design allowed the flow rates to also be measured.

A monitoring system was also designed to measure turbidity during de-watering. This system was easy to setup and recorded flow accurately. However, the initial design failed to accurately measure turbidity readings at high flow rates. An alternative design was tested in the laboratory. This design gave reliable measurement of turbidity.

Turbidity values generated from the two construction sites investigated, significantly exceeded acceptable limits of turbidity, often exceeding 3000 NTUs even with erosion control measures in place. If threshold monitoring (< 1000 NTUs) is all that is required the Analite 495 and YSI 3136 (0 to 1000 NTUs range) work well because they are self- logging probes that don' require additional instrumentation. If an absolute value of turbidity is desired a probe with a range of 0 to 4000 NTUs such as the Campbell Scientific OBS+3 is recommended. The drawback to higher range probes is the need to support them with a data logger and extra batteries, thus requiring more setup time and expense.

The laboratory analyses were evaluated and applied using limited information collected at the two construction sites. Comparisons of laboratory and field data suggest that the power relationship is valid for samples collected on construction sites. The prediction of α based on laboratory data is a reasonable first approximation to field values, especially considering possible changes in sediment sizes with deposition. Using the experimental relationship developed for Minnesota soils, turbidity and concentration can easily be estimated from field data with Equation 3.1 and a proper α value determined from Model 1 or Model 2. Once concentration is estimated for a site, the total sediment load can be determined using a hydrograph for the discharge point. Through a simple integration, the total sediment load can be determined at discharge point on a site and the needed sediment removal can be determined based on a turbidity standard. Proper erosion control practices can then be chosen based on sediment removal needs. The impact of using a non-linear turbidity-concentration relationship instead of a linear relationship was evaluated. Results showed that less reduction in concentration is needed to reduce turbidity by a specified amount when using a non-linear

relationship. There was also less error when using a non-linear relationship to estimate average turbidity and concentration values.

Chapter 6

Summary and Conclusions

The overall goal of the project was to gather information on turbidity from construction site and to investigate possible designs of monitoring systems. Soils from construction sites around the state of Minnesota were used to determine a soil dependent relationship between turbidity and sediment concentration using a well-defined set of laboratory measurements. The impact of particle settling on the relationship was evaluated through a separate laboratory experiment. A field study on two construction sites in the Twin Cities of Minnesota was performed during the project duration. The field study allowed for a comparison of turbidity data from real runoff, and synthetic runoff, provided insight into the application of relationships obtained from laboratory data, served to test two different monitoring systems and recorded turbidity values from a number of different construction site activities

A rainfall simulator in the laboratory was used to collect runoff data from fourteen Minnesota construction site soils. A strong power relationship between turbidity and TSS concentration was found to represent all of the time dependent runoff samples collected for each soil. The power value, β, was relatively constant, only varying slightly between soils. A single β value of 7/5 was chosen to represent all of the Minnesota soils in the final relationship for turbidity and TSS. The intercept on a log-log graph, α, varied significantly between soils, but only varied slightly within soils. A relationship for α was determined through an extensive multiple linear regression using soil properties for each site. The results of this regression determined a relationship using percent silt, maximum abstraction, and interrill erodibility (Model 1) that explained nearly 65% of the variability in α. Because of the complexities involved in evaluating maximum abstraction and interrill erodibility, a simple relationship using only percent silt (Model 2) was also determined. Both models showed promise in determining α for the laboratory soils. Model 1and Model 2 had R^2 values of 0.70 and 0.55, respectively. Model 1 had a small Relative Mean Error and a considerably smaller Normalized Mean Square Error.

Once a suitable relationship for turbidity and TSS concentration was determined for Minnesota construction site soils, the effect of particle settling was evaluated. A pipette test was performed on the total runoff sample from each soil. This test created a particle size distribution for the runoff samples. Samples were thoroughly mixed and then allowed to settle. While particles settled, small samples were extracted at a specific depth. The turbidity and concentration of each sample were determined for primary particles: sand, silt, and clay. From these samples, an extensive analysis was performed to determine how α and β changed with particle settling. Relationships for the dimensionless correction factors v_d and ω_d with fraction finer were determined. These relationships were used to estimate the turbidity for each particle class for each soil. The estimated total turbidity was compared to the actual total turbidity found in the laboratory study. The median percent error in the estimated turbidity was 3.2%.

Grab samples were collected from the two field sites in the Twin Cities and laboratory procedures were repeated to determine the turbidity and TSS relationship for field samples. The relationship for the field samples varied only slightly from the relationship determined in the laboratory for the same soil. Field samples had a strong power relationship with β values near 7/5 but α values that were slightly higher than laboratory soils. Particle settling can potentially explain the discrepancies in α.

The relationship created through the laboratory procedure shows great potential for several field applications. It can simply estimate turbidity values from known or estimated concentration data. More importantly, it can estimate concentration from continuously monitored turbidity data collected on a site. With estimated concentration data and known flow rates at the monitoring location, sediment load can be determined through a simple integration. Sediment reduction can then be calculated from based on a turbidity standard for the site. Knowing this information allows for better erosion control BMP planning and execution on a construction site.

The application of the information generated by the laboratory study relies on field generated turbidity or concentration data. To address the challenges of collecting accurate field data, two

different turbidity monitoring systems were developed. The first was a turbidity box designed to monitor turbidity levels from overland flows and the second was designed to monitor turbidity values during de-watering activities. The turbidity box proved adaptable and successfully monitored turbidity values at a number of different locations at two construction sites. Some upstream control to intercept trash and particles greater than 12 centimeters in diameter and a slight drop at the downstream end of the box is recommended to prevent plugging. The box was also instrumented to support water sample collection by an automated water sampler from which sediment concentrations were calculated. An alternative design in the design of the box allowed measurement of flow rate as well. The de-watering monitoring system was easy to setup and recorded flow accurately. However, an alternative design was needed to accurately measure the turbidities at higher flow rates. This design performed well in laboratory tests.

Turbidity values generated by five different turbidity sensors on five different soil textures were compared. As expected both differences in soil texture and probe configuration had an impact on accuracy of turbidity readings. When compared against turbidity values given by the 2100N at a concentration of 2500 mg/L differences in turbidity due to changing soil textures ranged from 60 to 142 NTUs. Differences in probe configurations generated a range of turbidities between 18 and162 NTUs. The difference between the OBS3+ sensor and the 2100N turbidities was the least of the four sensors at 18 NTU's compared to 108 NTUs for the OBS500, 112 NTUs for the YSI 6136 and 162 NTUs for the Analite NEP495.

Turbidity values generated from the two construction sites investigated, significantly exceeded acceptable limits of turbidity, often exceeding 3000 NTUs even with erosion control measures in place. If threshold monitoring (< 1000 NTUs) is all that is required the Analite 495 and YSI 3136 (0 to 1000 NTUs range) work well because they are self- logging probes that don' require additional instrumentation. If an absolute value of turbidity is desired a probe with a range of 0 to 4000 NTUs such as the Campbell Scientific OBS+3 is recommended. The drawback to higher range probes is the need to support them with a data logger and extra batteries, thus requiring more setup time and expense. Mixing probe types will make comparison of data sets more challenging. To eliminate some of the errors

associated with different probe configurations it is recommended that one type of probe be chosen to do the monitoring Also, to reduce the effect of soil texture on turbidity values a calibration of sediment concentration and turbidity for each soil is recommended.

References

Anderson, C. W. (2005). Turbidity. *U.S. Geological Survey techniques of water-resourcesiInvestigations* (A6.6). Retrieved from water.usgs.gov

Ankcorn, P. D. (2003). Clarifying turbidity – the potential and limitations of turbidity   as a surrogate for water-quality monitoring. *Georgia Water Resources   Conference*. Athens, GA: Georgia Water Science Center Publications.

Coduto, D. P., Yeung, M. R., & Kitch, W. A. (2010). *Geotechnical engineering: Principles and practices*. Saddle River, NJ: Prentice Hall.

Elliot, W. J., Licbenow, A. M., Laflen, J. M., & Kohl, K. D. (1989). *A compendium of   soil erodibility data from WEPP cropland soil field erodibility experiments 1987   & 1988*. Ohio State University & USDA Agricultural Research Service.

Faucette, L. B., Jordan, C. F., Risse, L. M., Cabrera, M., Coleman, D. C., & West, L. T.   (2005). Evaluation of stormwater from compost and conventional erosion   control   practices in construction activities. *Journal of Soil and Water Conservation*,   60(6), 288-297.

Ferguson, R. J. & Church, M. (2004). A simple universal equation for grain settling   velocity. *Journal of Sedimentology Research*, 74(6), 933-937.

Holliday, C. P., Rasmussen, T. C., & Miller, W. P. (2003). Establishing the relationship   between turbidity and total suspended sediment concentration. *Georgia Water   Resources Conference*. Athens, GA: Georgia Water Science Center Publications.

Holman, J. P. (1989). *Experimental methods for engineers*. St. Louis, MO: McGraw-Hill.

Jastram, J. D., Zipper, C. E., Zelazny, L. W., & Hyer, K. E. (2009). Increasing precision   of turbidity-based suspended sediment concentration and load estimates. *Journal   of Environmental Quality*, 39, 1306-1326.

Klute, A. (Ed.). (1986). *Methods of Soil Analysis Part 1: Physical and Mineralogical   Methods*. Madison, WI: Soil Science Society of America.

Lewis, Jack (2007). Comparisons of turbidity data collected with different instruments. Report on a cooperative agreement between the California Department of Forestry and Fire Protection and USDA Forest Service--Pacific Southwest Research Station (PSW Agreement # 06-CO-11272133-041).

Marshall, J. S. & Palmer, W. M. (1948). The distribution of raindrops with size. *Shorter   Contributions*, 165-166.

National Cooperative Highway Research Program (NCHRP), 2012. Turbidity reduction and monitoring strategies for highway construction projects. NCHRP Project 25-25(74) Final Report.

Neter, J., Kutner, M., Wasserman, W., & Nachtsheim, C. (1996). *Applied linear   statistical models*. New York, NY: McGraw-Hill/Irwin.

Omar, A. F. B. & MatJafri, M. Z. B. (2009). Turbidimeter design and analysis: A review on optical fiber sensors for the measurement of water turbidity. *Sensors*, 9(10),   8311-8335.

Omega Engineering, Inc. *Technical reference and selection guide*. Retrieved from
        www.omega.com/techref/

Onstad, C. A., Radke, J. K., & Young, R. A. (1981). An outdoor portable rainfall erosion
        laboratory. *Florence Symposium*. Florence, Italy: IAHS.

Packman, J. J., Cornings, K. J., & Booth, D. B. (1999). Confronting uncertainty: Managing change in water resources and the environment. *Canadian Water   Resources Association Annual Meeting*. Vancouver, BC.

Patil, S. S., Barfield, B. J., & Wilber, G. G. (2011). Turbidity modeling based on the concentration of total suspended solids for stormwater runoff from construction   and development sites. *World Environmental and Water Resources Congress   2011*. Palm Springs, FL: ASCE.

Rasmussen, P. P., Gray, J. R., Glysson, G. D., & Ziegler, A.C. (2009). Guidelines and
        procedures for computing time-series suspended-sediment concentrations and   loads from in-stream turbidity-sensor and stream flow data. Reston, VA: U.S.   Geological Survey.

Sadar, M. (2007). Turbidity revealed. *Opflow*, 33(1), 24-26.

Sadar, M. Turbidity measurement: A simple, effective indicator of water quality
        change. Retrieved from www.hacchhydromet.com

Sheppard, B. E. (1990). Measurements of raindrop size distributions using a small
        Doppler radar. *Journal of Atmospheric and Oceanic Technology*, 7, 255-268.

Tolhurst, T. J., Black, K. S., Shayler, S. A., Mather, S., Black, I, Baker, K., & Paterson,   M. D. (1999). Measuring the *in situ* erosion shear stress of intertidal sediment   with the cohesive strength meter (CSM). *Estuarine, Coastal and Shelf Science*,   49, 281-294.

United States Department of Agriculture. (1978). *Predicting rainfall erosion losses: A   guide to conservation planning*. Washington, DC: GPO.

United States Environmental Protection Agency. (1999). *EPA guidance manual: Turbidity provisions*. Washington, DC: GPO.

United States Environmental Protection Agency. (2011) Industry effluent guidelines:
        Construction and development. Retrieved from water.epa.gov

United States Weather Bureau. (1961). Rainfall atlas of the United States. Technical
        paper no. 40. Washington, DC: GPO.

Wilson, B. N., B. J. Barfield, A. D. Ward, & I. D. Moore. (1984). A hydrology and sedimentology watershed model. Part I: Operational format and hydrologic component. *Transactions of the ASAE, 27*(5), 1370-1377.

Wilson, B. N., B. J. Barfield, I. D. Moore, & R. C. Warner. (1984). A hydrology and sedimentology watershed model. Part II: Operational format and hydrologic component. *Transactions of the ASAE, 27*(5), 1378-1384.

Wilson, B. N., A. Y. Sheshukov, & R. Pulley. (2006). Erosion risk assessment tool for construction sites (Minnesota Department of Transportation Research Report No. MN/RC-2006-27).

Wilson, B. N., A. Y. Sheshukov, & A. Mendez. (2008). Design tool for controlling runoff and sediment from highway construction (Minnesota Department of Transportation Research Report No. MN/RC-2008-35).

Wurbs, R. A. & James, W. P. (2001). *Water resources engineering*. Saddle River, NJ: Prentice Hall.

Appendix A
Soil Properties

Chapter 2 explains the soil properties that were used in the regression performed to determine α. This appendix includes Table A.1 that has the soil property values for each soil used in the regression analysis. Figures A.1 through A.16 are the particle distributions for each soil that were determined using a standard hydrometer test. These figures were used to determine the percent sand, silt, and clay of each soil. Figures A.17 through A.27 show the proctor test results. This information was used to determine the optimum moisture content of each soil. The final pages of this appendix contain the information for Soil A and B, which were attained from the MN DOT. These soils were already evaluated by the MN DOT to obtain a particle size distribution and optimum moisture content.

Table A.1. Soil property values for each soil.

Soil Name	USDA Classification	β	A	α, β=1.4	% Sand	% Silt	% Clay	I (in/hr)	BD (g/cm³)
AHS	Silt Loam	1.40	0.037	0.036	45.9	54.1	0.0	1.29	1.30
AHS 2	Silt Loam	1.39	0.028	0.025	45.9	54.1	0.0	1.31	1.29
AHT	Loam	1.48	0.011	0.021	47.6	34.7	17.6	1.29	1.28
AHT 2	Loamy Sand	1.39	0.013	0.012	74.2	25.8	0.0	1.22	1.16
AHT 3	Loamy Sand	1.44	0.008	0.011	73.3	25.6	1.1	1.22	1.54
AHT 4	Loamy Sand	1.40	0.008	0.008	71.0	28.0	1.1	1.22	1.55
AHT 5	Sandy Loam	1.43	0.006	0.008	67.2	31.8	1.0	1.22	1.64
CTYS	Sandy Loam	1.35	0.033	0.023	49.5	48.5	2.1	1.31	1.46
CTYT	Loam	1.39	0.015	0.014	42.7	37.5	19.8	1.38	1.27
DulS	Silt Loam	1.37	0.062	0.050	33.3	59.1	7.5	1.31	1.60
DulT	Loamy Sand	1.12	0.040	0.004	79.7	12.2	8.1	1.38	1.56
HastS	Sandy Loam	1.39	0.007	0.006	61.9	34.5	3.6	1.29	1.72
HastT	Sandy Loam	1.30	0.016	0.007	70.4	23.5	6.2	1.43	1.65
OVS	Silt Loam	1.44	0.062	0.080	23.5	73.5	3.1	1.36	1.37
OVT	Silt Loam	1.36	0.050	0.037	43.4	56.6	0.0	1.29	1.23
Soil A	Silt	1.40	0.007	0.009	7.5	84.0	8.5	1.43	1.59
Soil B	Silt Clay Loam	1.35	0.016	0.049	7.5	66.5	26.0	1.43	1.58
THS	Sandy Loam	1.48	0.010	0.014	69.7	19.1	11.2	1.43	1.49
THT	Loam	1.44	0.072	0.023	34.3	47.5	18.2	1.43	1.20

Soil Name	K_i (kg-s/m⁴)	CN	S (in)	w (%)	OMC (%)	TES (g)	τ (Pa)	V_t (mL)	Q (in³/hr)
AHS	1.08E+06	96.79	0.33	29.61	13.0	15.55	1.50	1975	241.04
AHS 2	1.76E+06	98.34	0.17	26.26	13.0	26.08	1.50	2625	320.37
AHT	1.32E+06	96.17	0.40	23.51	11.0	19.05	1.30	1780	217.24
AHT 2	1.34E+06	95.57	0.46	23.42	12.0	17.21	1.65	1465	178.80
AHT 3	1.68E+06	95.59	0.46	26.94	12.0	21.66	1.67	1470	179.41
AHT 4	2.13E+06	97.11	0.30	27.07	12.0	27.44	1.37	1920	234.33
AHT 5	3.07E+06	98.33	0.17	26.58	12.0	39.48	1.27	2390	291.69
CTYS	3.32E+06	98.72	0.13	25.21	14.5	49.35	1.82	2800	341.73
CTYT	1.68E+06	98.21	0.18	29.26	15.5	27.71	1.62	2744	334.90
DulS	1.64E+06	97.09	0.30	18.63	13.0	24.35	1.23	2125	259.35
DulT	1.33E+06	96.32	0.38	18.46	11.0	21.94	1.40	2030	247.76
HastS	4.06E+06	97.79	0.23	11.37	9.0	58.53	1.23	2340	285.59
HastT	1.27E+06	97.00	0.31	16.69	7.3	22.48	0.87	2380	290.47
OVS	7.04E+05	89.56	1.17	35.96	12.0	11.27	0.87	665	81.16
OVT	9.93E+04	86.29	1.59	19.58	20.0	1.43	1.63	300	36.61
Soil A	2.81E+06	96.73	0.34	24.32	11.3	49.75	1.28	2285	278.88
Soil B	1.27E+06	97.01	0.31	30.60	16.7	22.47	1.03	2385	291.08
THS	1.55E+06	99.20	0.08	16.60	10.1	27.38	1.03	3179	387.99
THT	1.02E+06	95.94	0.42	22.10	14.7	18.03	1.35	1870	228.23

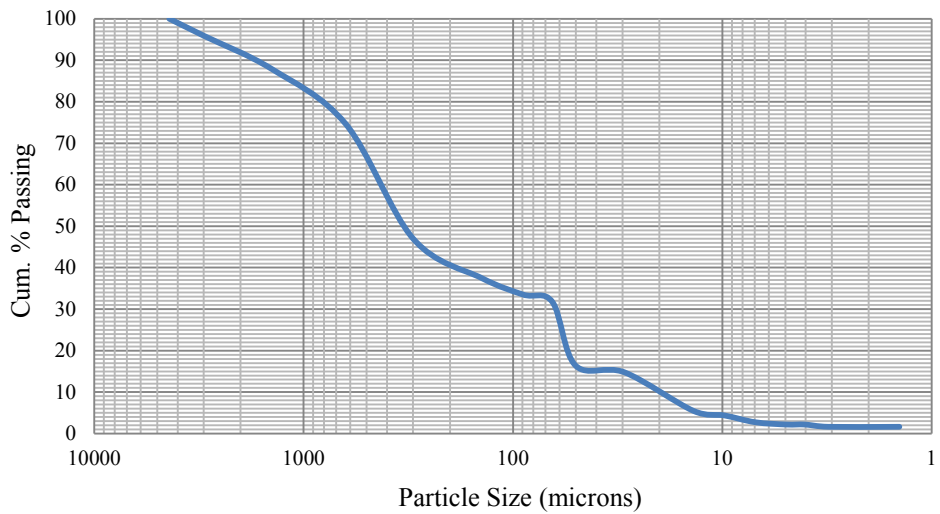**Figure A.1. Hydrometer Test, AH - S**
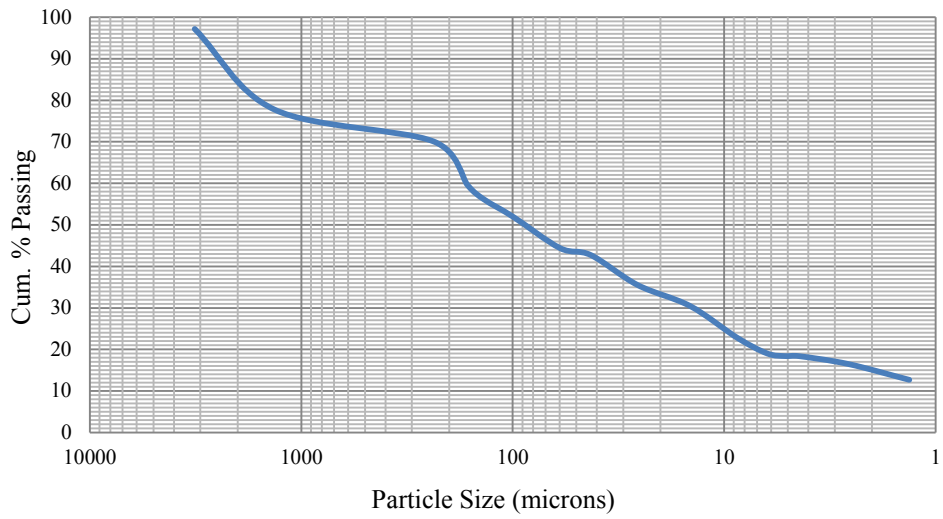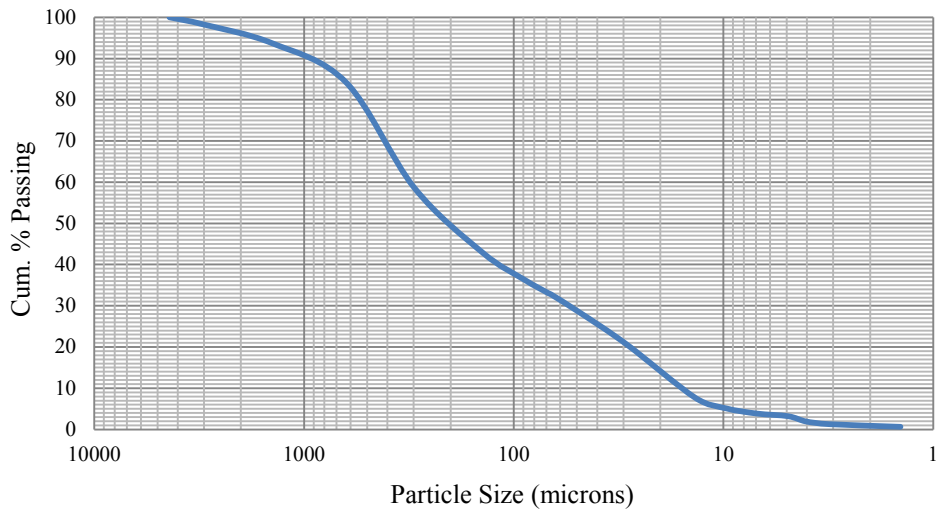

Figure A.2. Hydrometer Test, AH - T
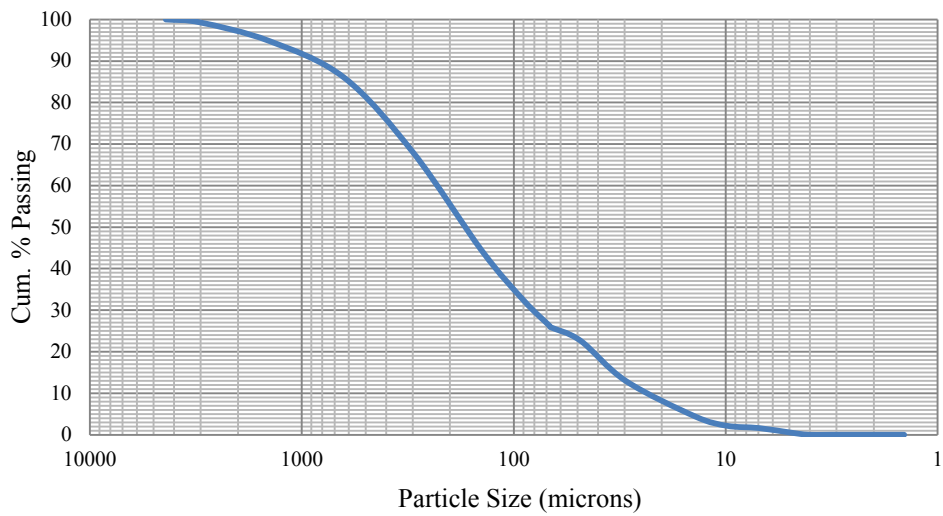
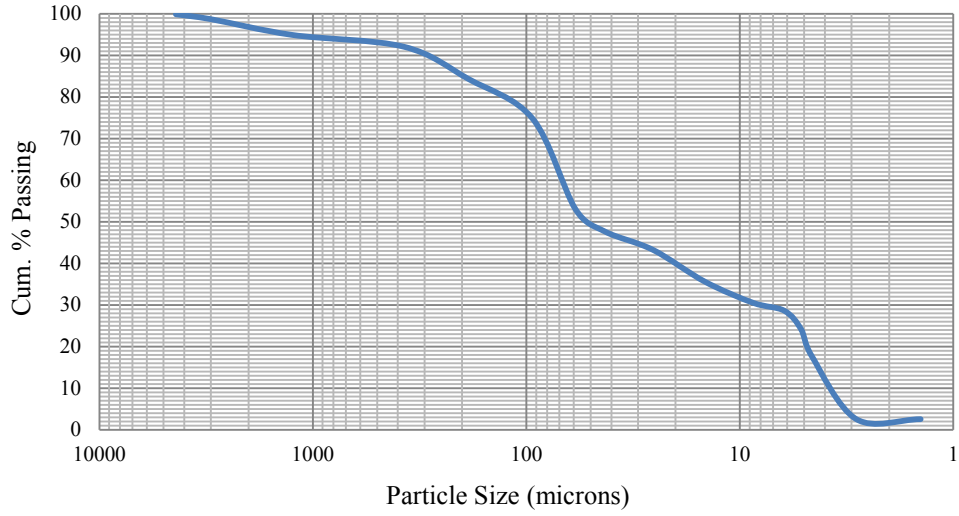**Figure A.3. Hydrometer Test, AH - T 2**
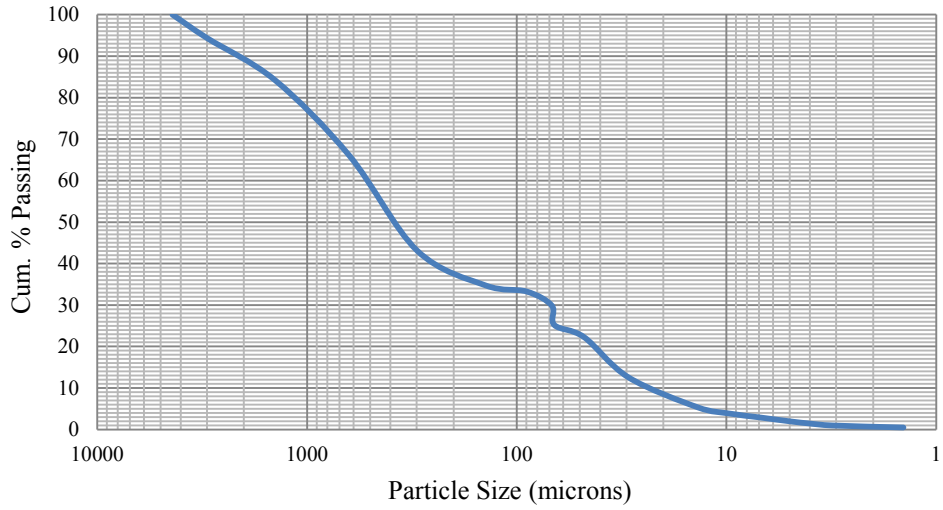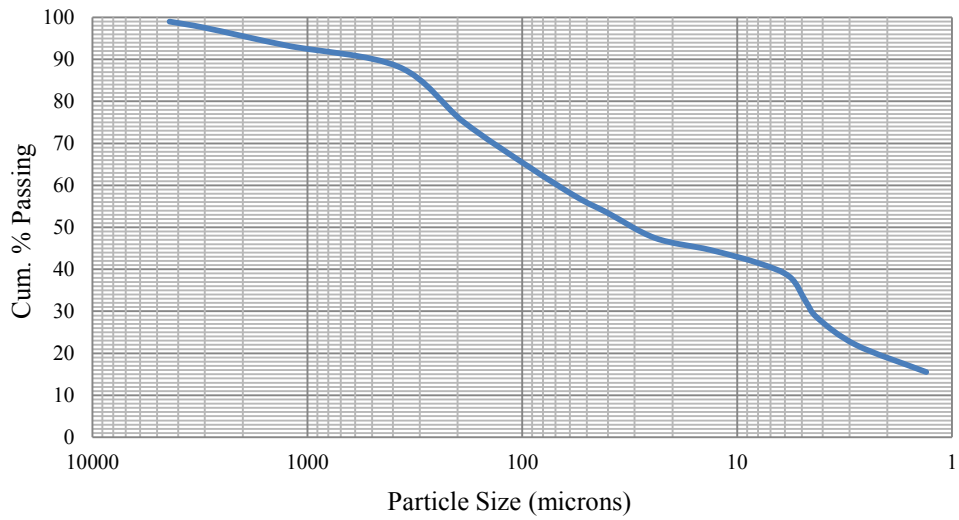
Figure A.4. Hydrometer Test, AH - T 3

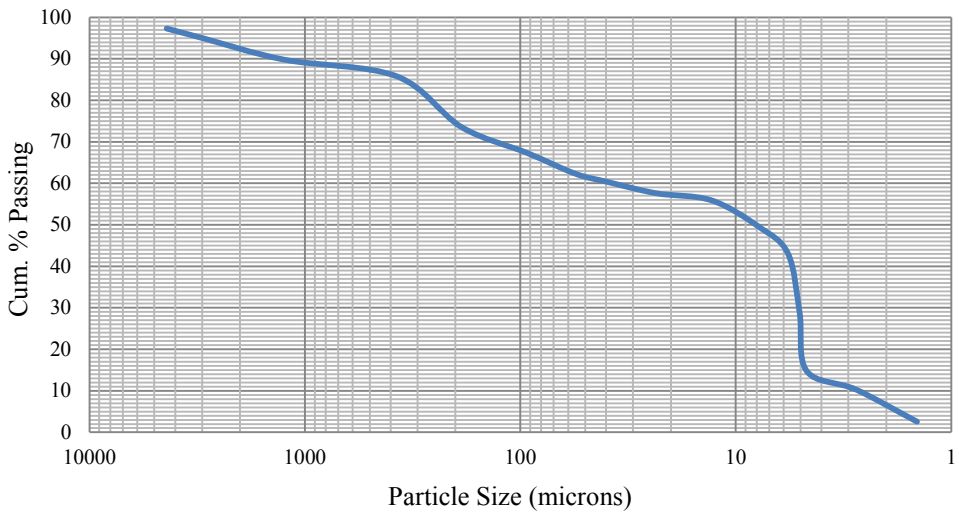**Figure A.5. Hydrometer Test, AH - T 4**
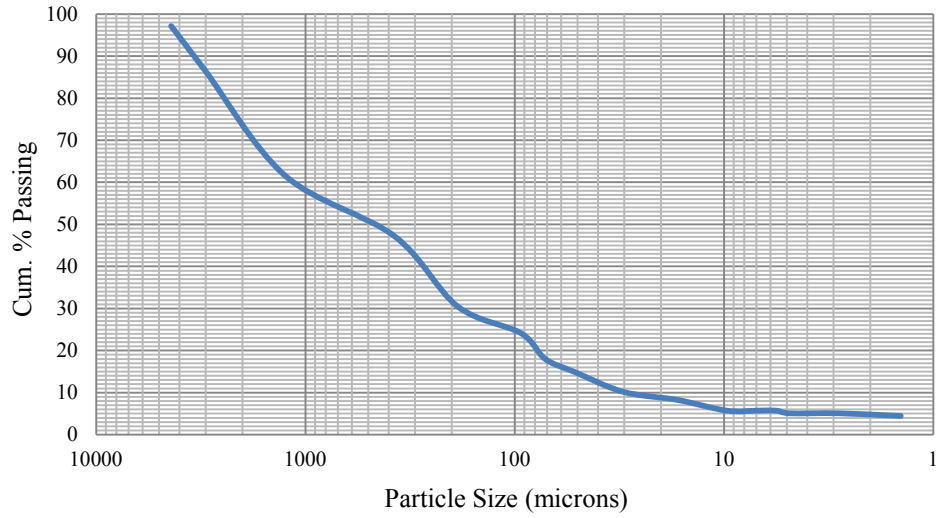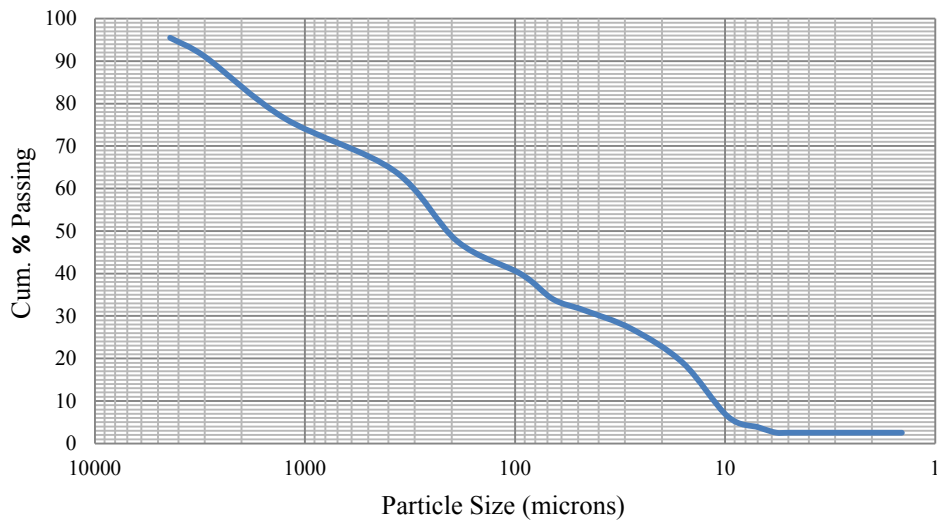

Figure A.6. Hydrometer Test, AH - T 5

109

Figure A.7. Hydrometer Test, CTY 14 - S

Figure A.8. Hydrometer Test, CTY 14 - T

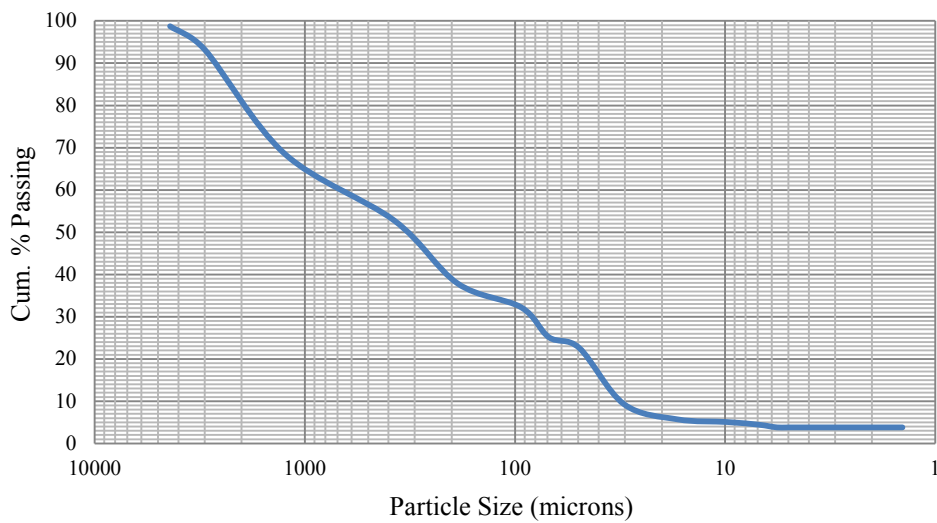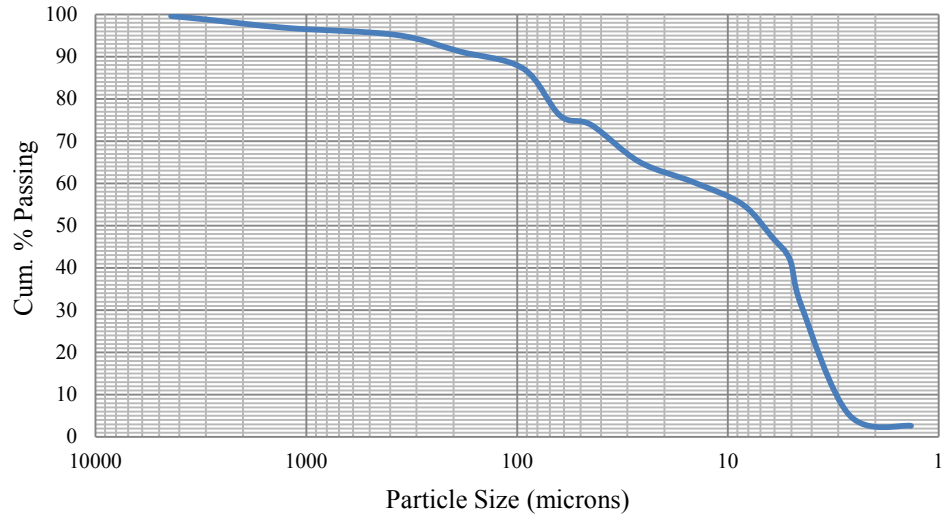**Figure A.9. Hydrometer Test, Duluth - S**
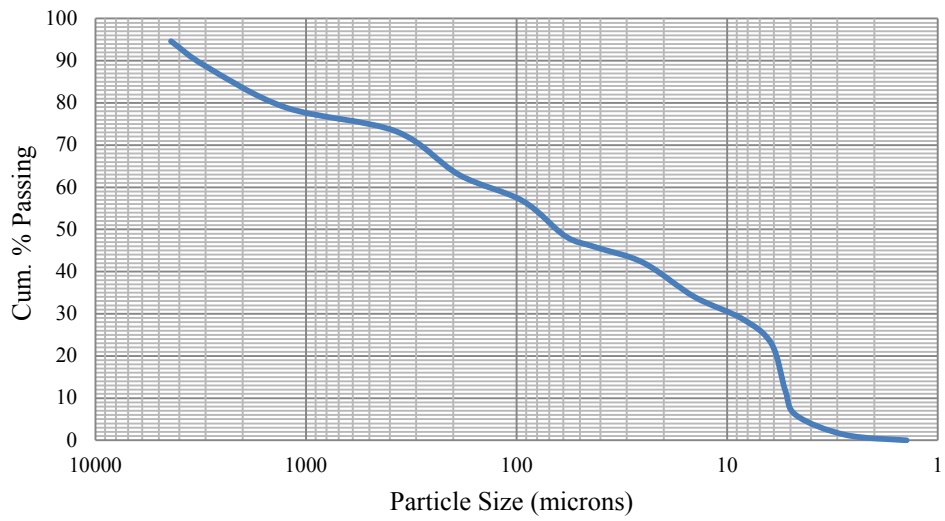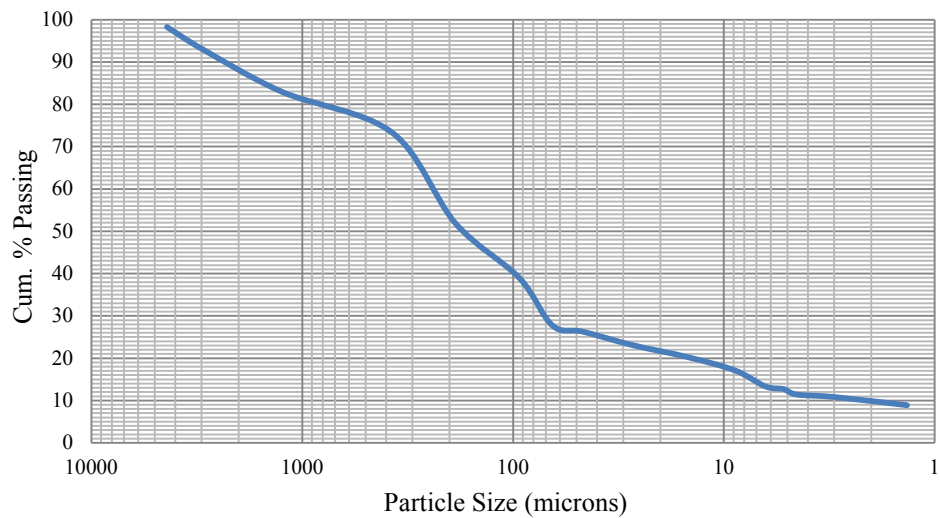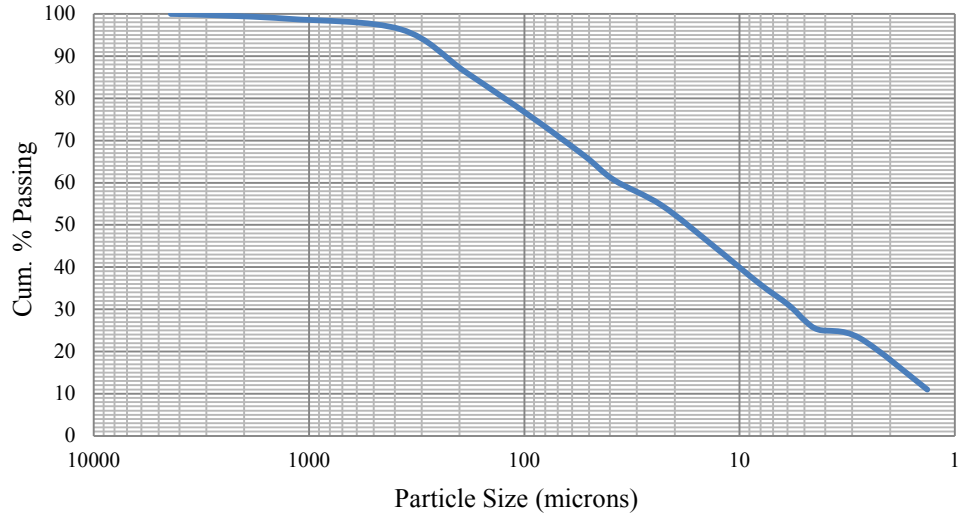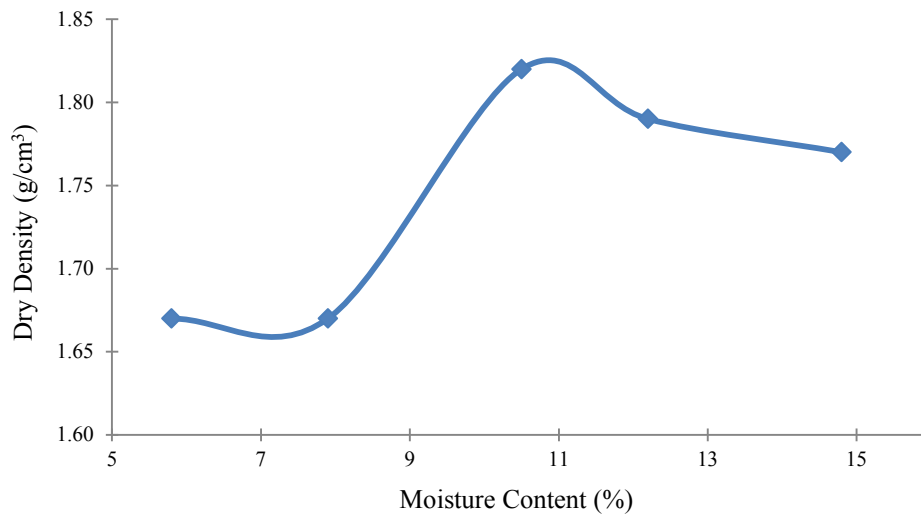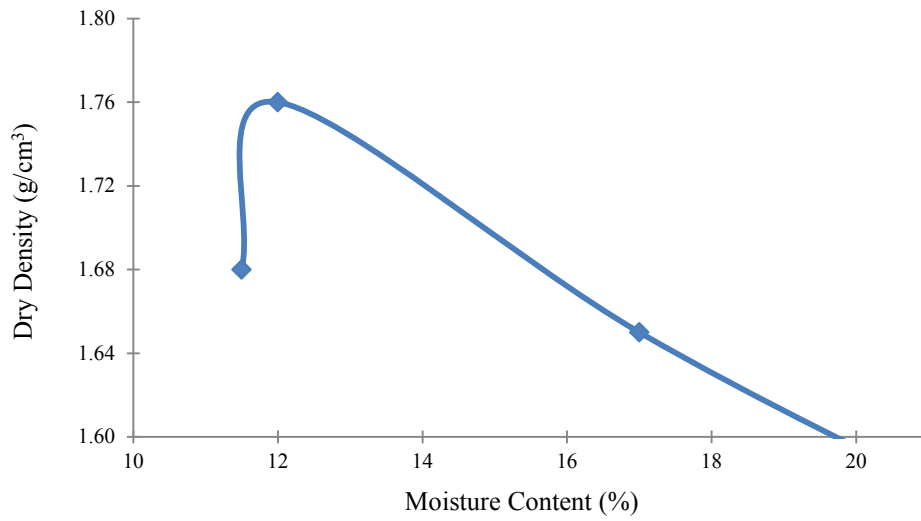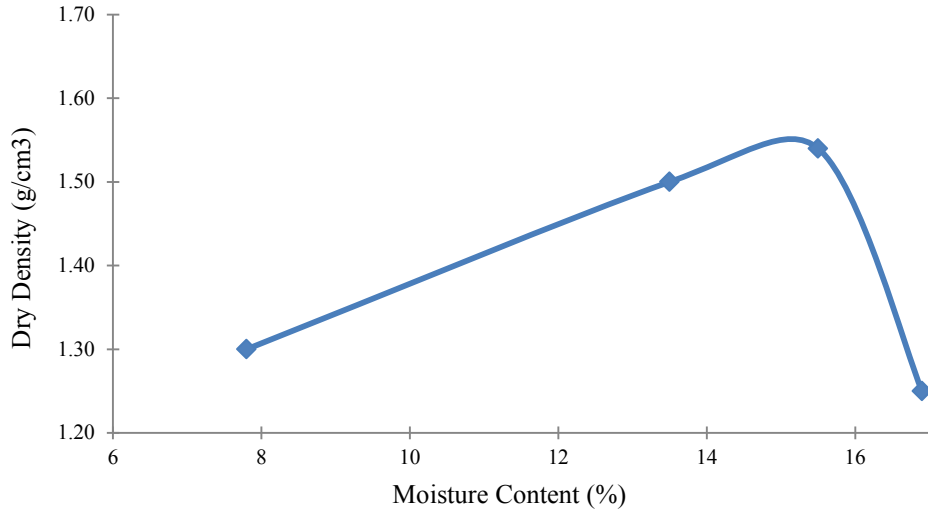
110

Figure A.10. Hydrometer Test, Duluth - T

Figure A.11. Hydrometer Test, Hastings - S

Figure A.12. Hydrometer Test, Hastings - T

Figure B.13. Hydrometer Test, OV - S

Figure A.14. Hydrometer Test, OV - T

Figure A.15. Hydrometer Test, TH23 - S
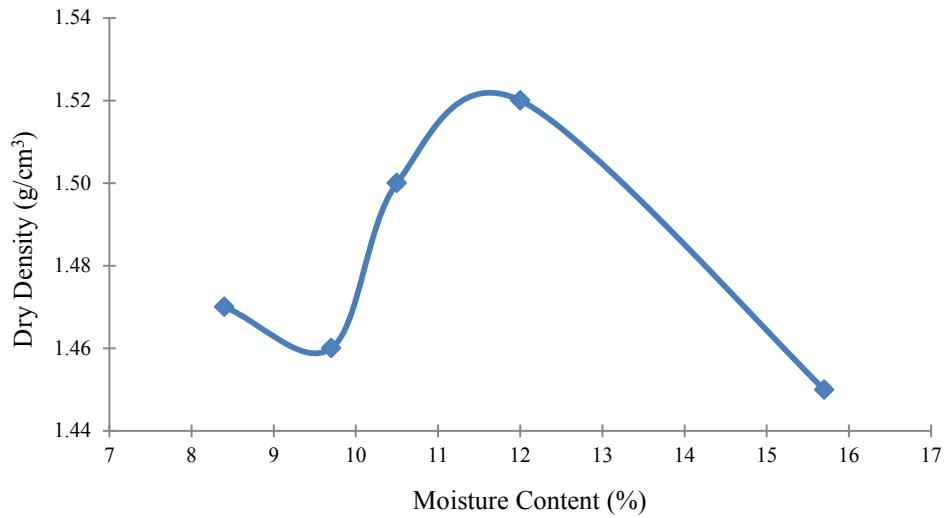
Figure A.16. Hydrometer Test, TH23 - T

Figure A.17. Proctor Test, AH - S

Figure A.18. Proctor Test, AH - T

Figure A.19. Proctor Test, AH - T rep

114

Figure A.20. Proctor Test, CTY14 - T
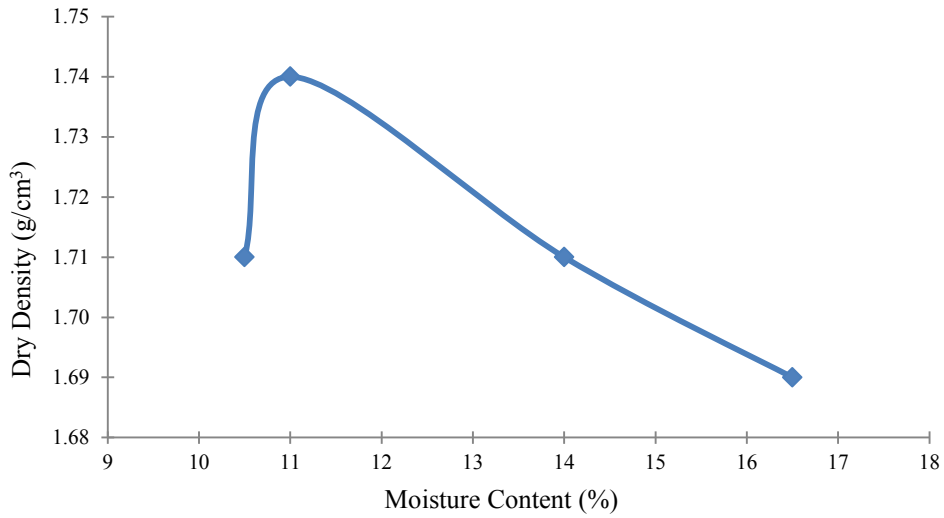
Figure A.21. Proctor Test, Dul - T
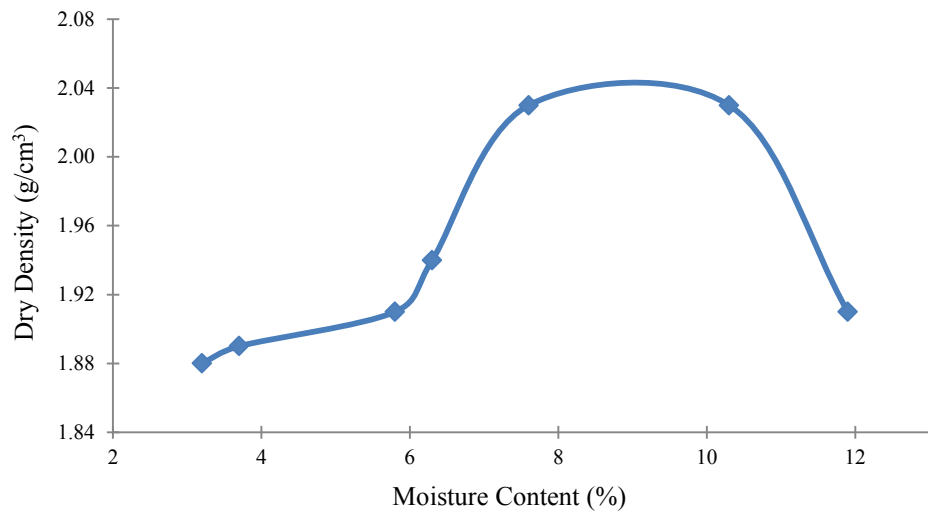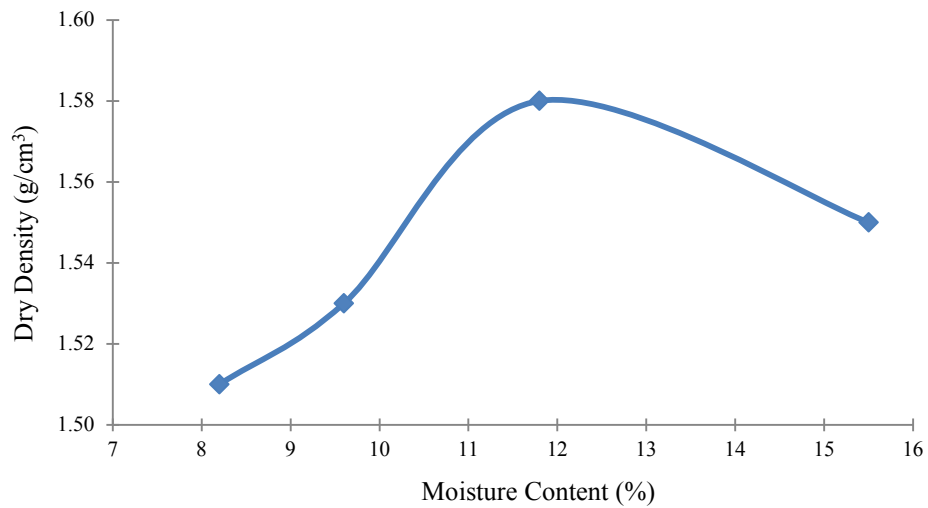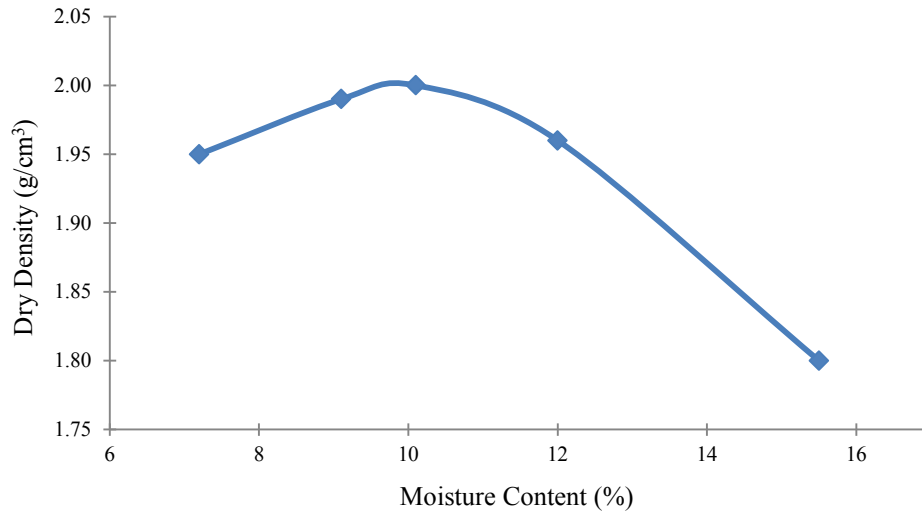

Figure A.22. Proctor Test, Hast - S
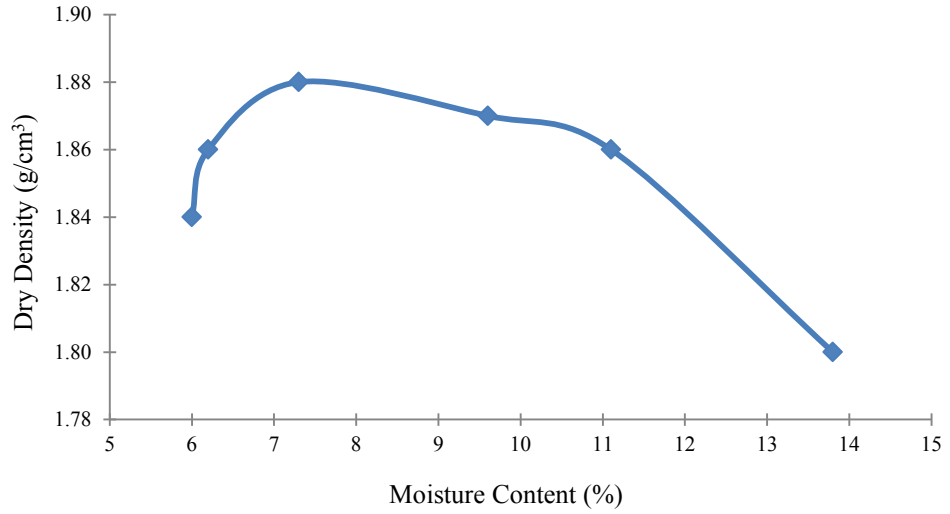
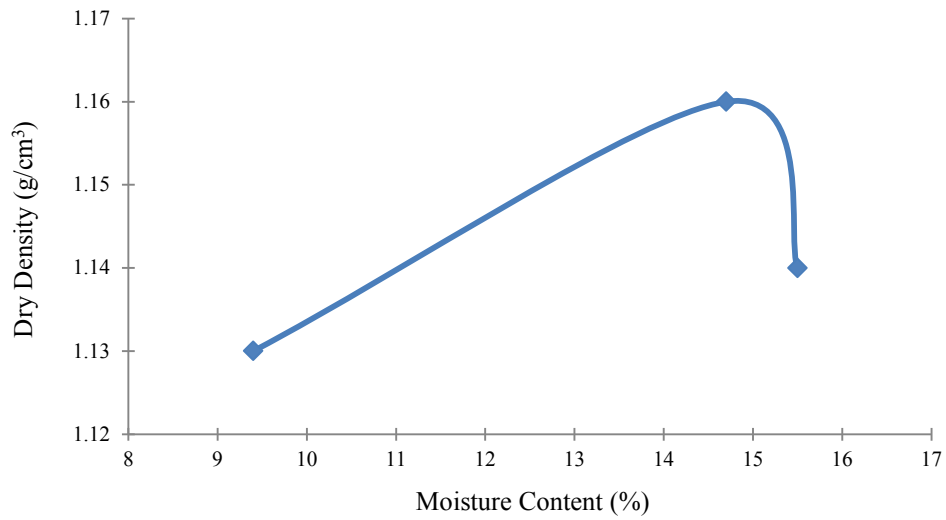**Figure A.23. Proctor Test, Hast - T**

Figure A.24. Proctor Test, OV - S

Figure A.25. Proctor Test, OV - T

116

Figure A.26. Proctor Test, TH23 - S


Figure A.27. Proctor Test, TH23 - T

117

Appendix B
Aliquot Sample Dilution Curves

Figures B.1 through B.22 show the aliquot sample analysis for each soil. Each 50 mL sample was diluted 4-6 times to create time dependent, turbidity and TSS relationships. Each soil has six relationships that were further analyzed to determine a general relationship for all of the soils. This is discussed further in Chapter 4.
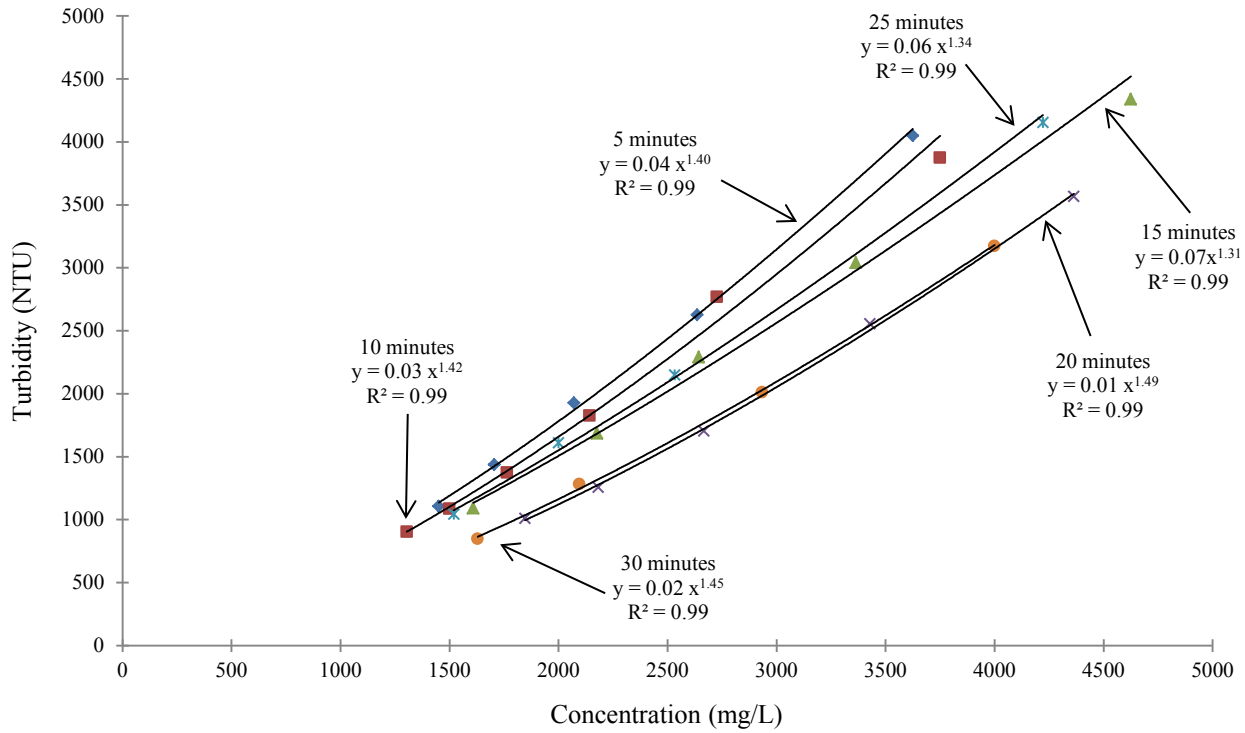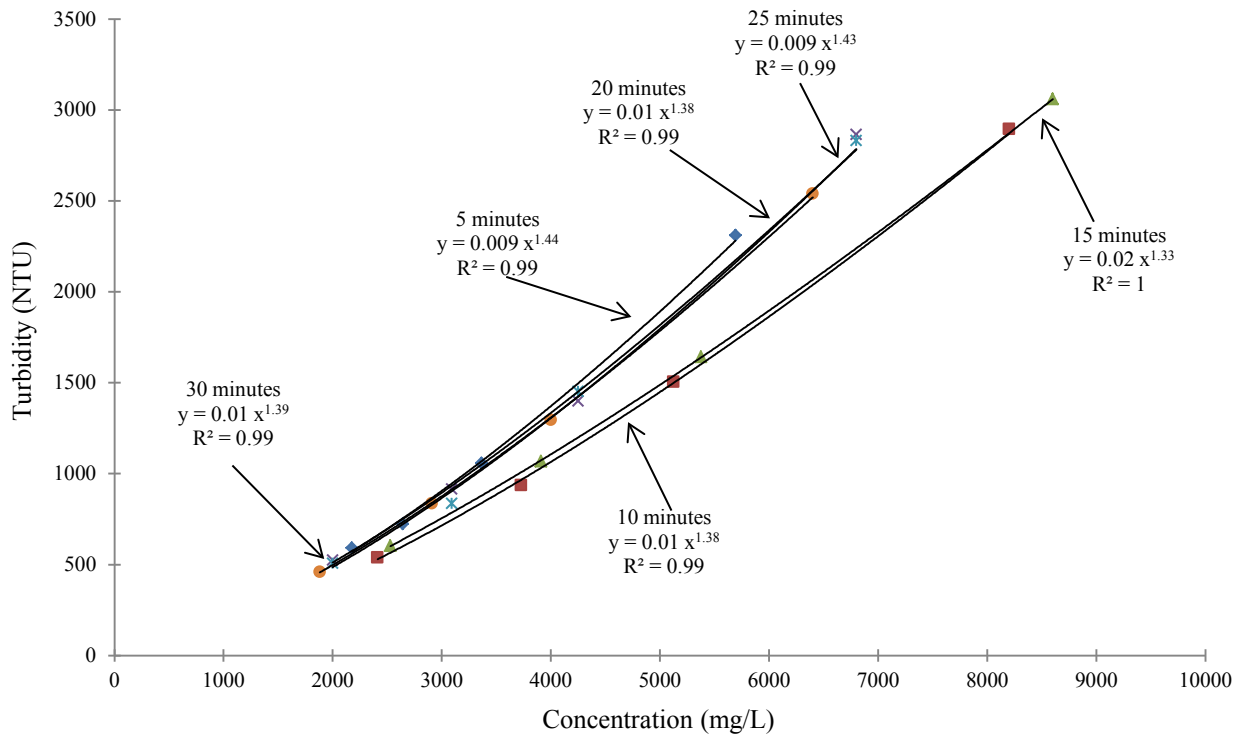
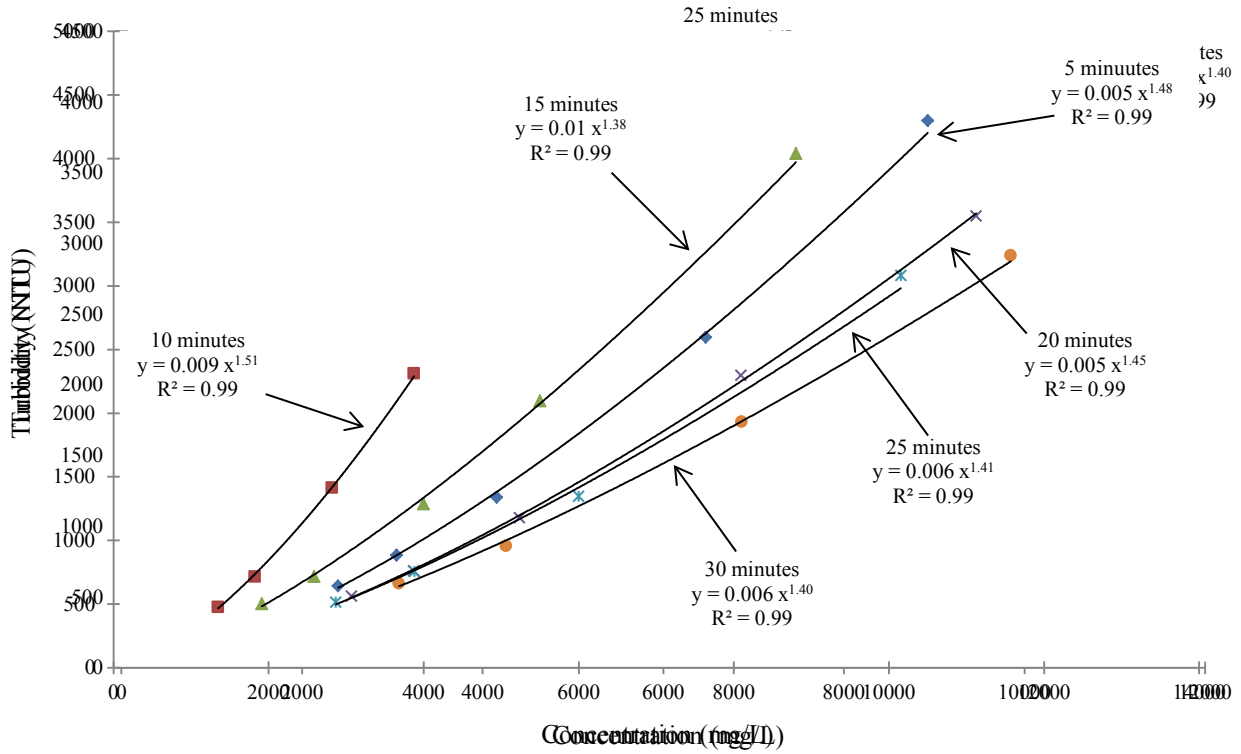**Figure B.1. AH - S (1) Aliquot Samples**
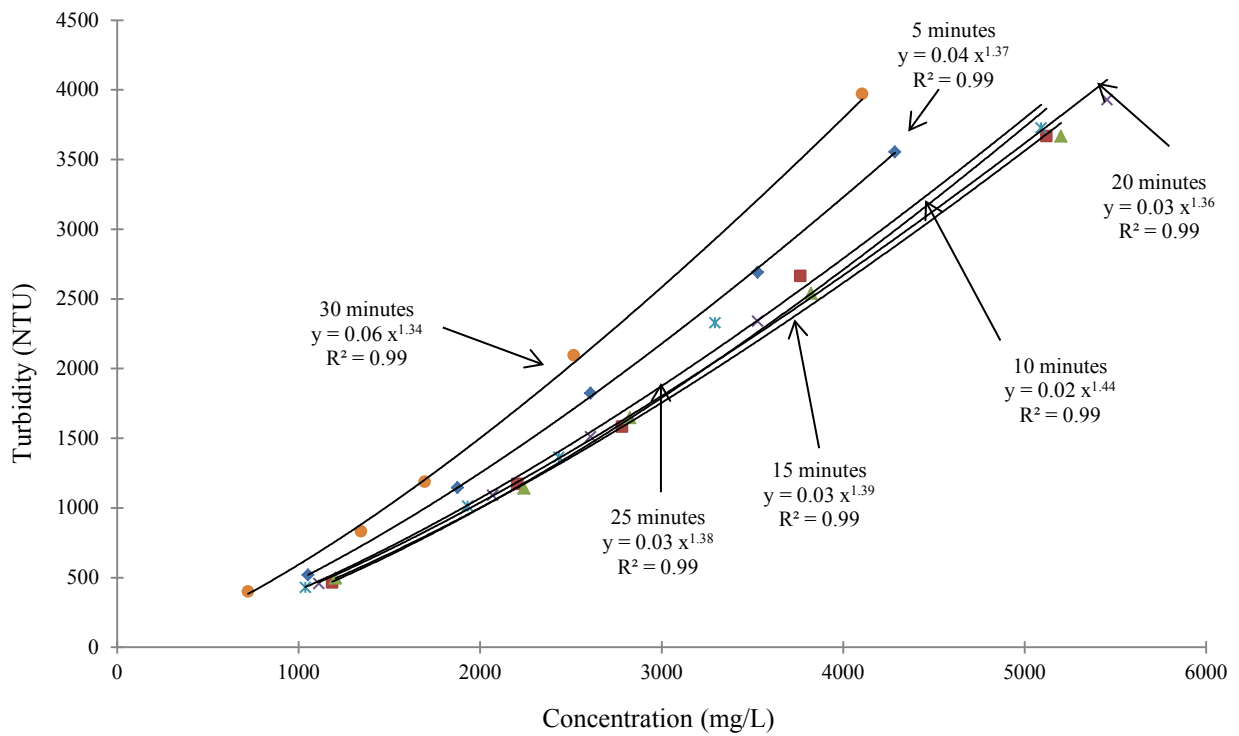
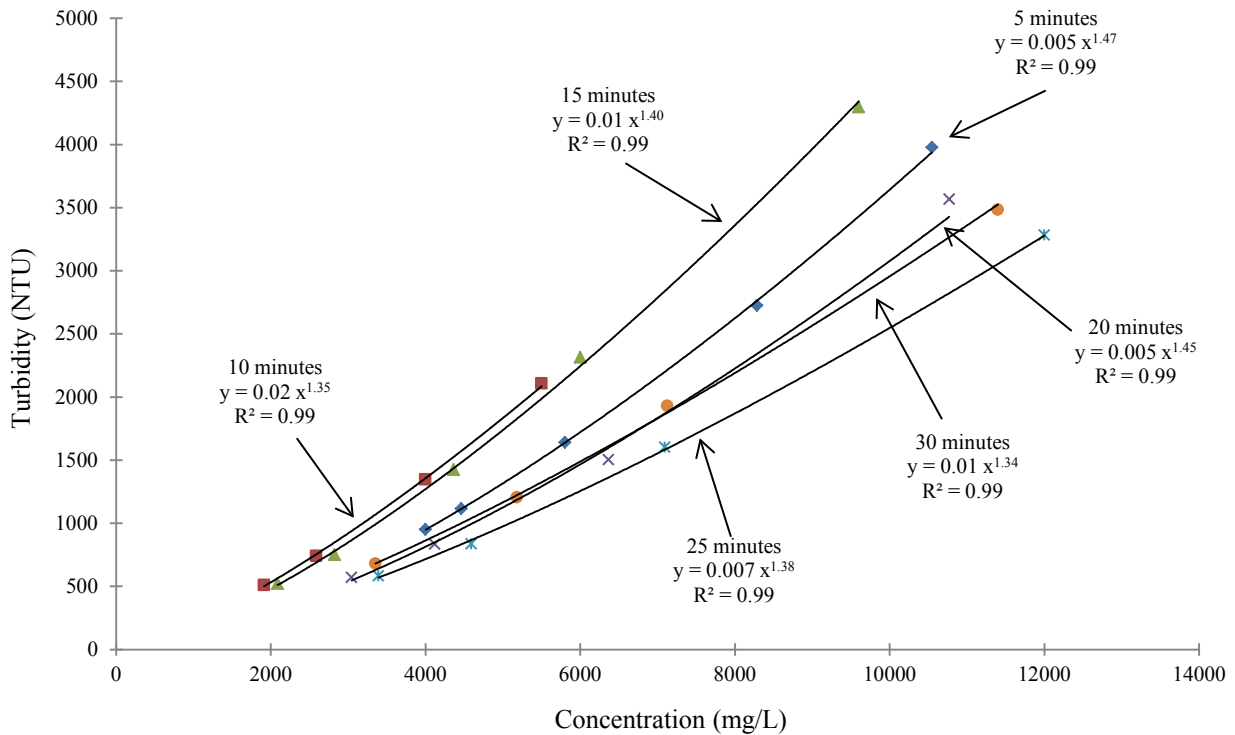**Figure B.2. AH - S (2) Aliquot Samples**

120
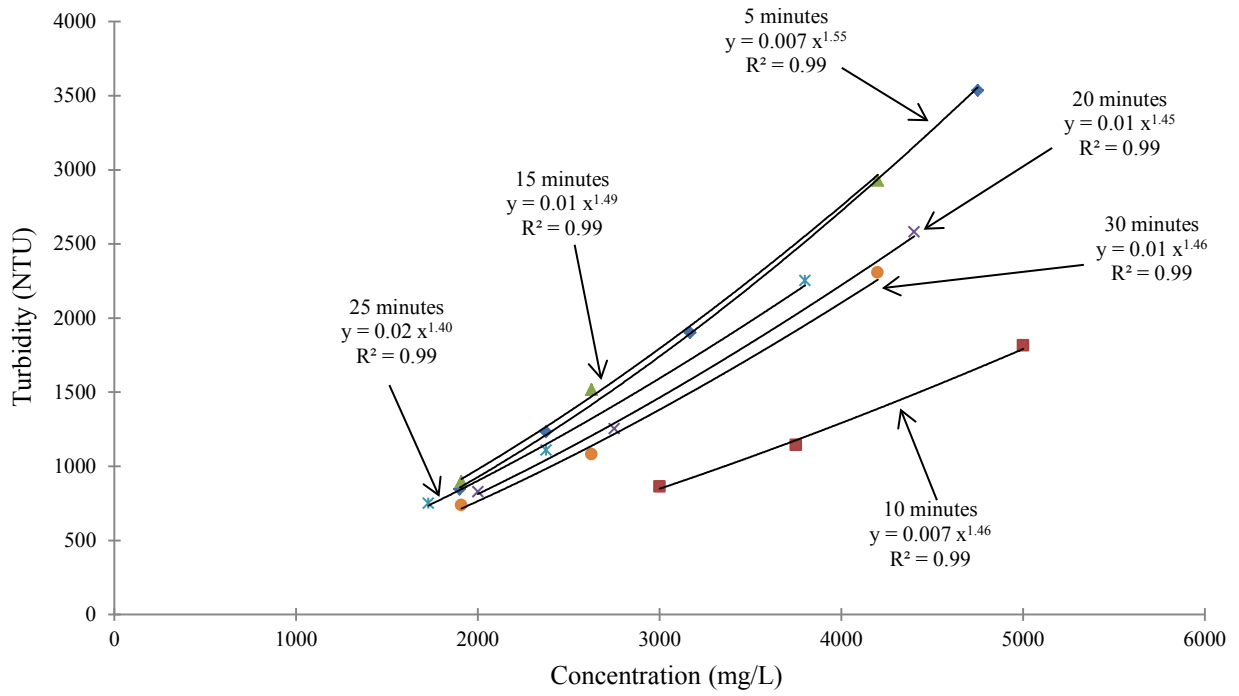
Figure B.3. AH - T (1) Aliquot Samples

Figure B.4. AH - T (2) Aliquot Samples

121

Figure B.5. AH - T (3) Aliquot Samples

Figure B.6. AH - T (4) Aliquot Samples

122
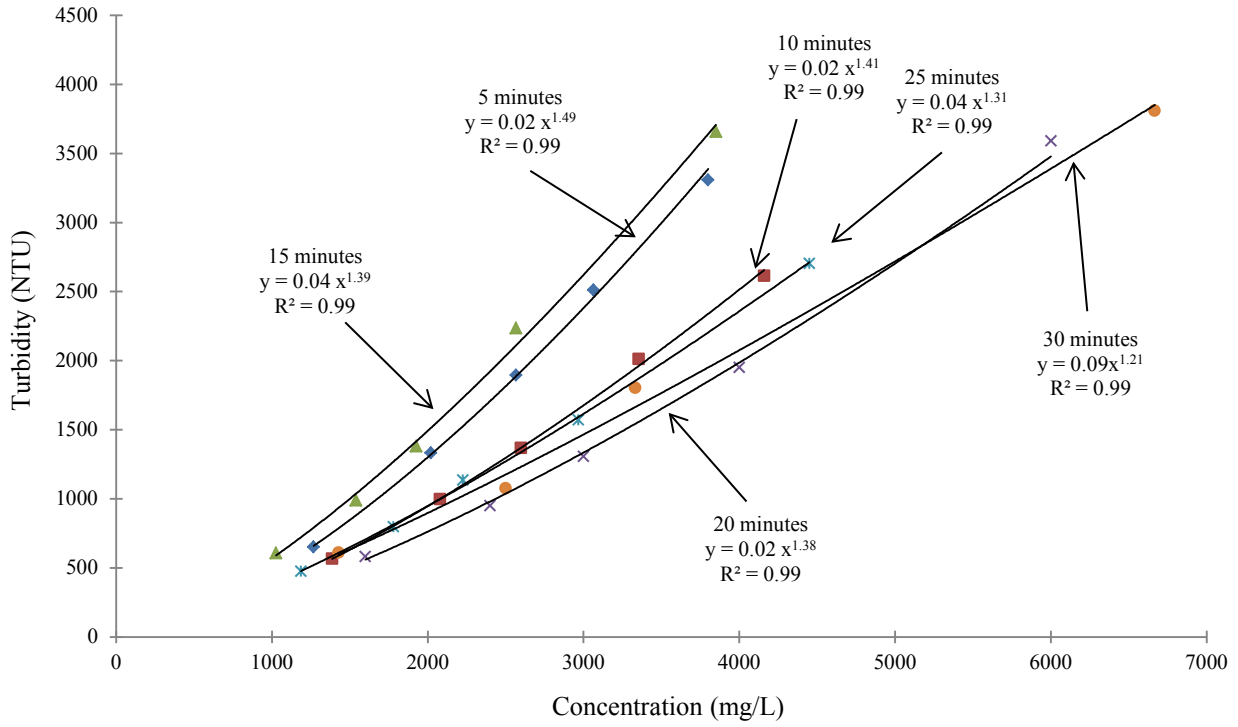
Figure E.9: CTY - S (2) Aliquot Samples
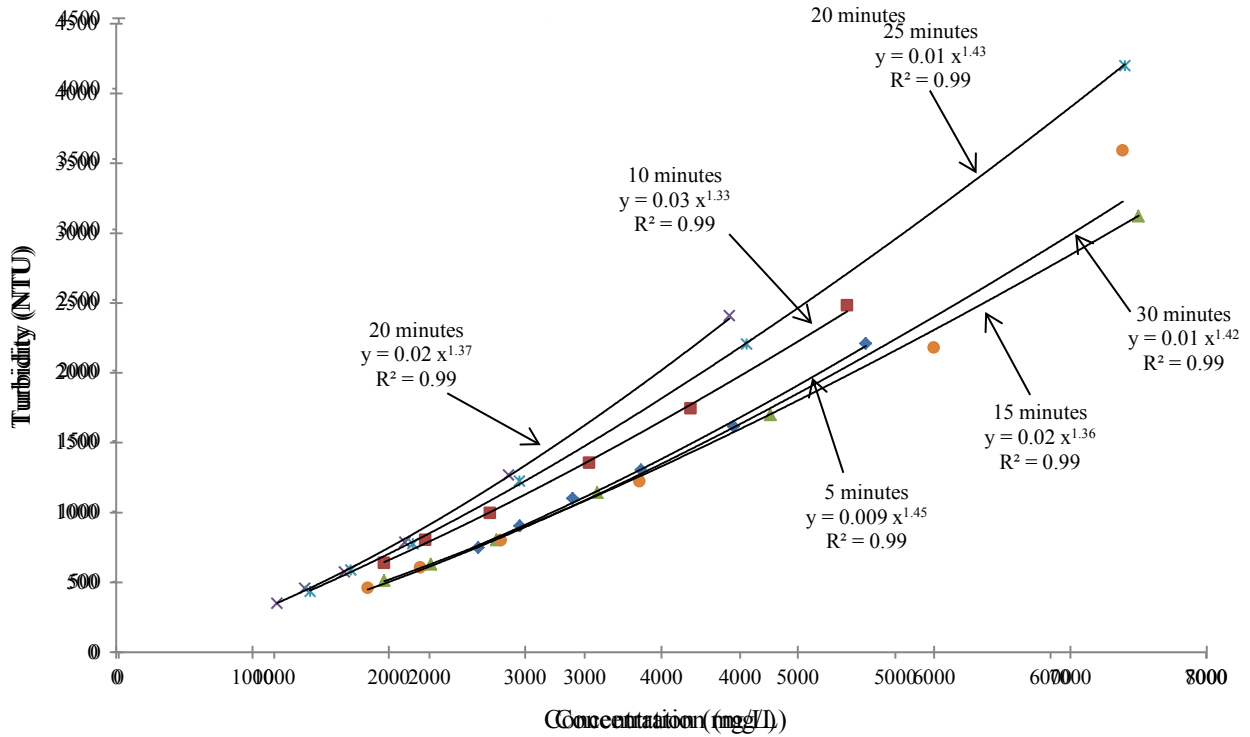
Figure E.10: CTY - S (1) Aliquot Samples

Figure B.11. Dul - S (1) Aliquot Samples

20 minutes
$y = 0.07\ x^{1.38}$
$R^2 = 0.99$

25 minutes
$y = 0.08\ x^{1.35}$
$R^2 = 0.99$

5 minutes
$y = 0.07\ x^{1.40}$
$R^2 = 0.99$

30 minutes
$y = 0.05\ x^{1.39}$
$R^2 = 1$

15 minutes
$y = 0.04\ x^{1.36}$
$R^2 = 0.9995$

10 minutes
$y = 0.06\ x^{1.34}$
$R^2 = 0.99$

Turbidity (NTU)

Concentration (mg/L)
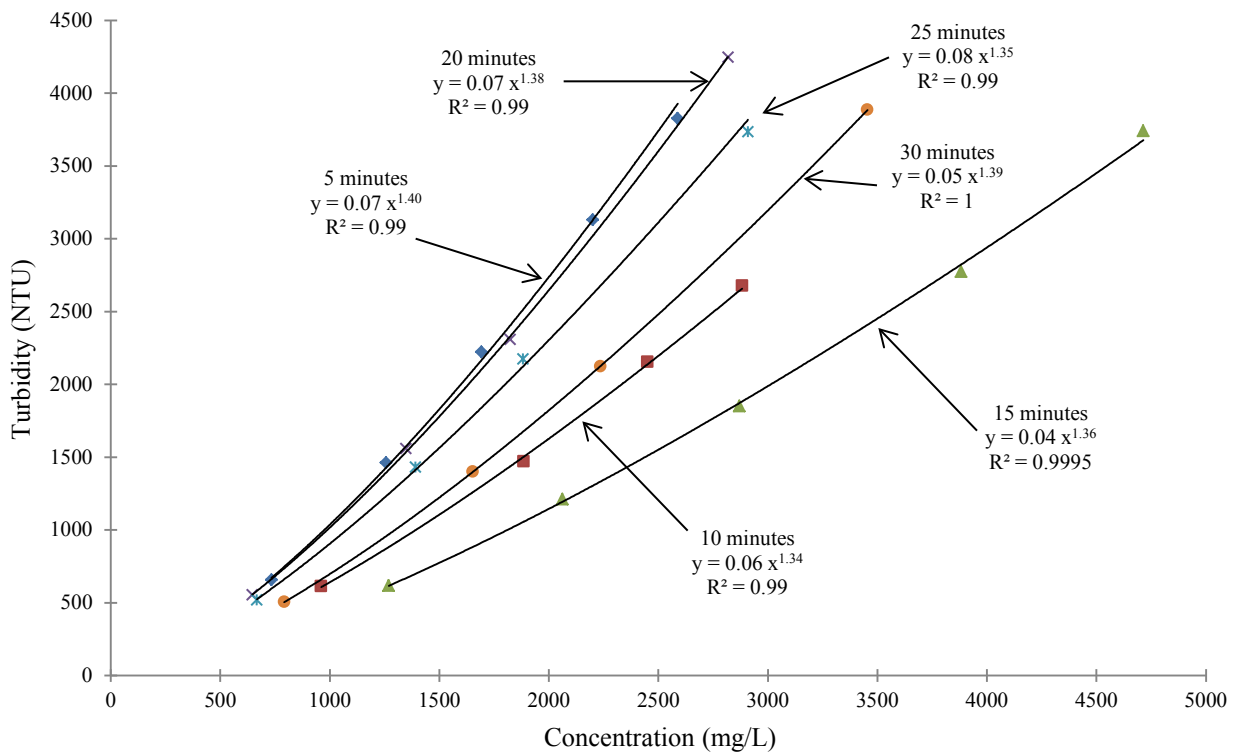
Figure B.12. Dul - S (2) Aliquot Samples

Figure B.13. Dul - T Aliquot Samples

Figure B.14. Hast - S Aliquot Samples

125

Figure B.15. Hast - T Aliquot Samples

15 minutes
$y = 0.08 \ x^{1.41}$
$R^2 = 0.99$

30 minutes
$y = 0.03 \ x^{1.56}$
$R^2 = 0.99$

20 minutes
$y = 0.08 \ x^{1.37}$
$R^2 = 0.99$

10 minutes
$y = 0.08 \ x^{1.43}$
$R^2 = 0.99$

25 minutes
$y = 0.04 \ x^{1.48}$
$R^2 = 0.99$

5 minutes
$y = 0.06 \ x^{1.43}$
$R^2 = 0.99$

Turbidity (NTU)

Concentration (mg/L)
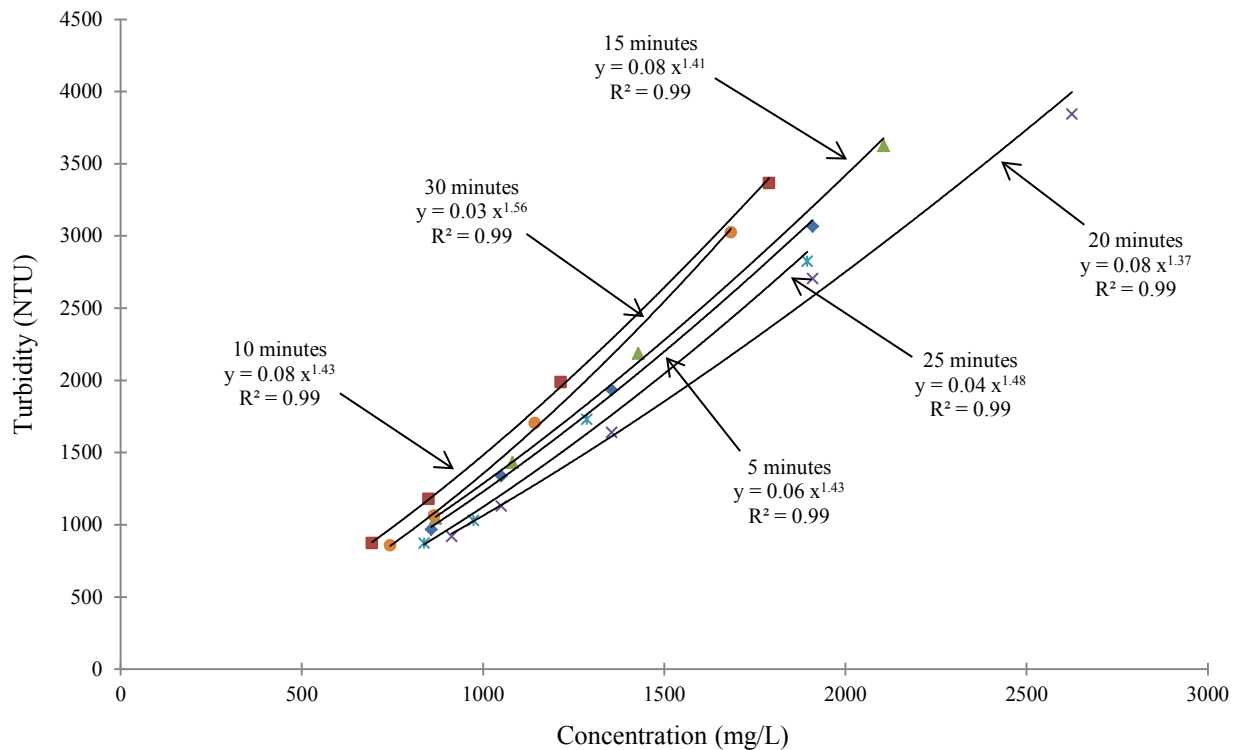
Figure B.16. OV - S (1) Aliquot Samples

126
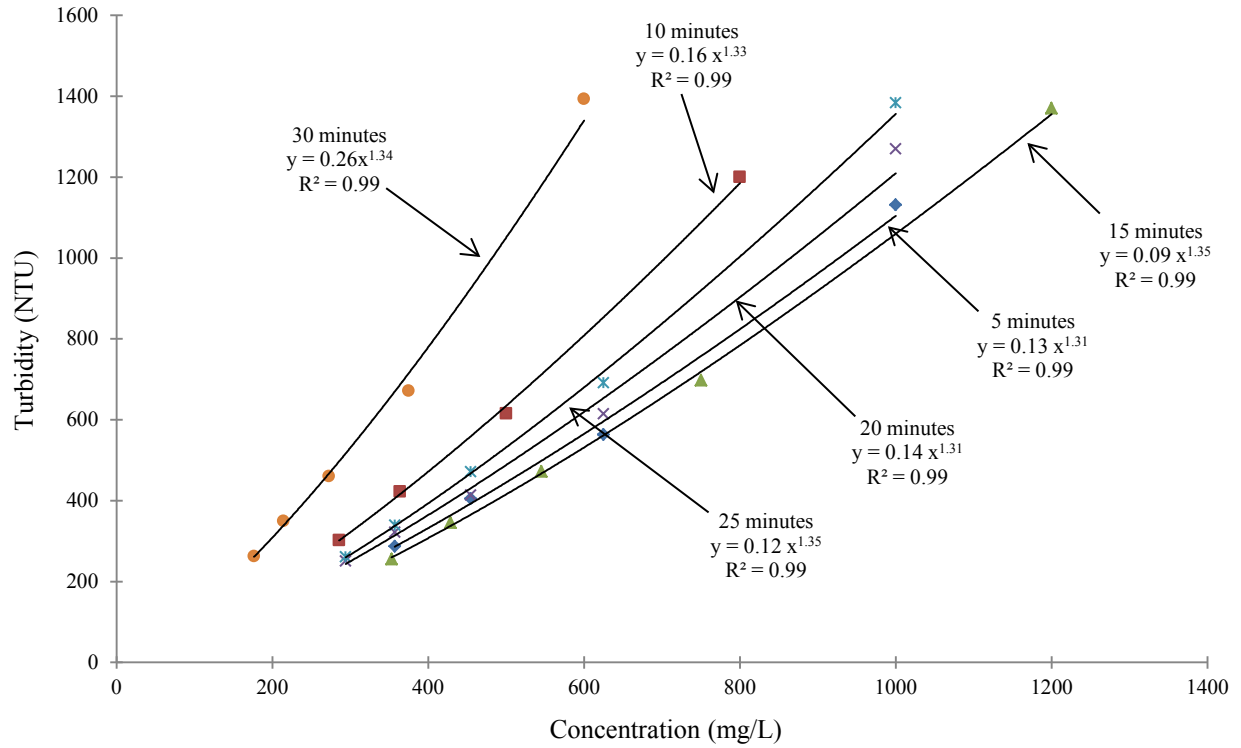
Figure B.17. OV - S (2) Aliquot Samples
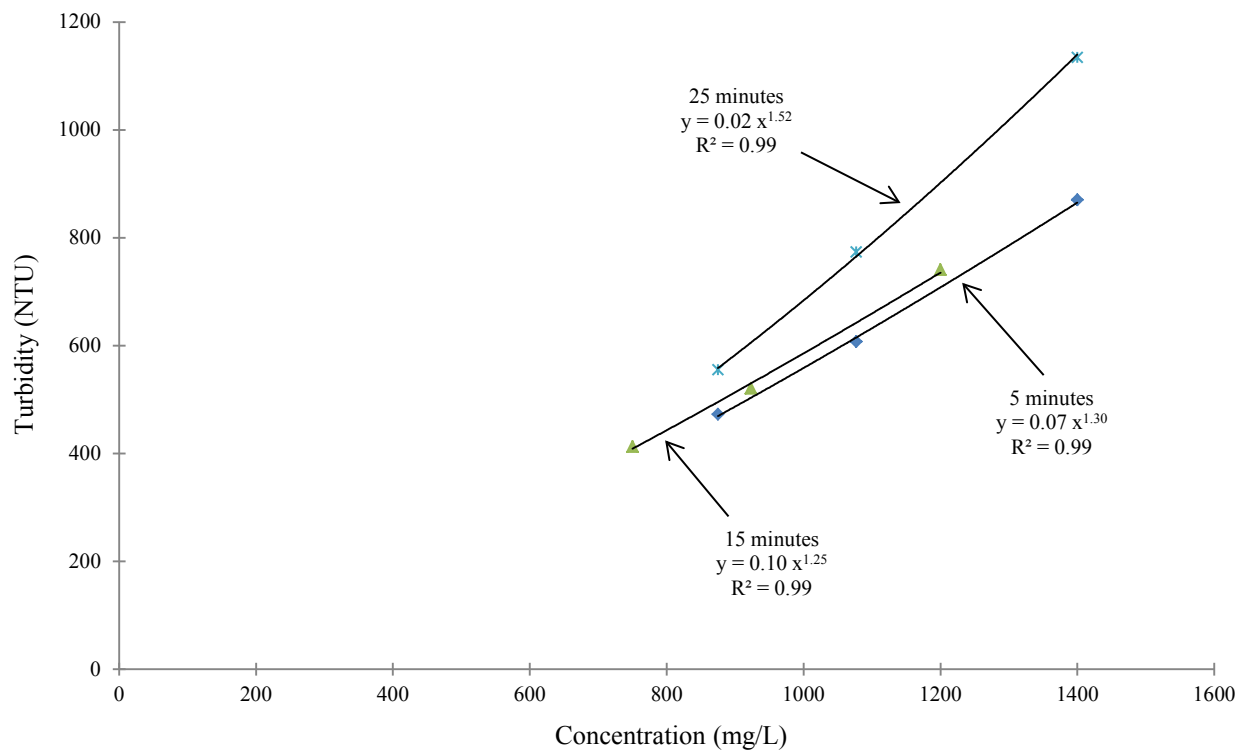
Figure B.18. OV - T Aliquot Samples
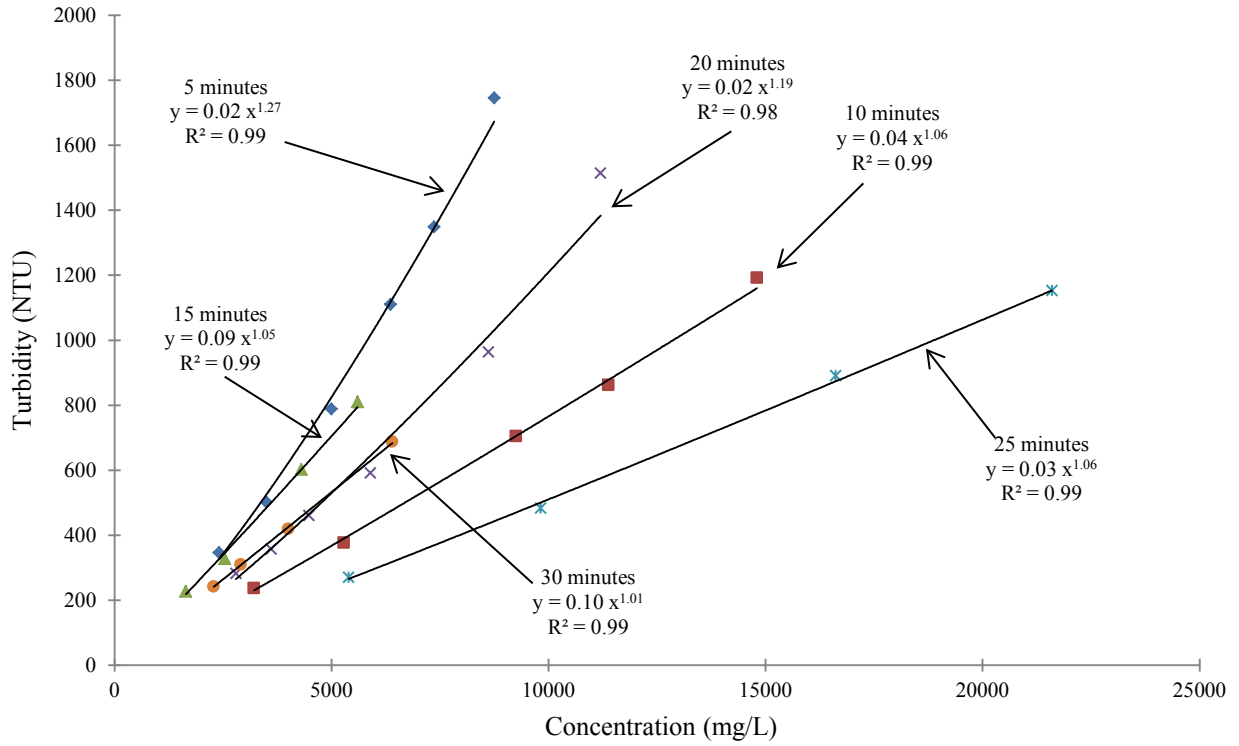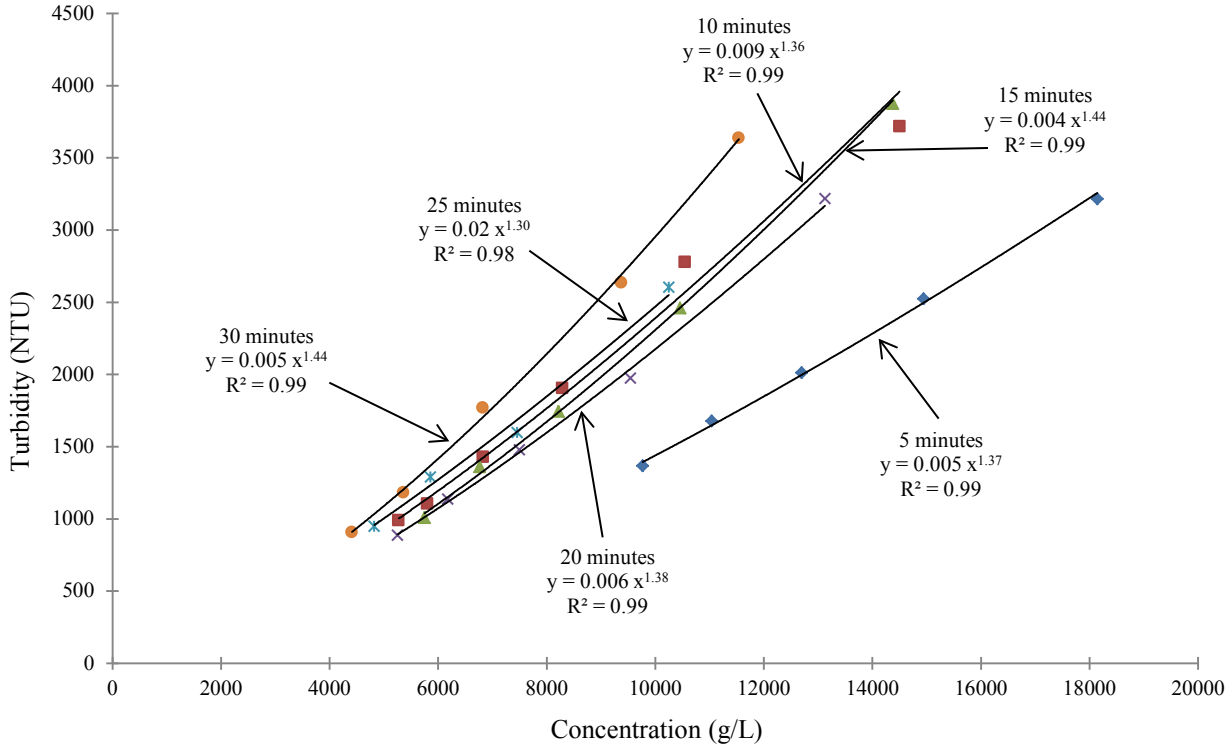
127

Figure B.19. Soil A Aliquot Samples

5 minutes
$y = 0.10\ x^{1.31}$
$R^2 = 0.99$

10 minutes
$y = 0.09\ x^{1.33}$
$R^2 = 0.99$

15 minutes
$y = 0.09\ x^{1.34}$
$R^2 = 0.99$

20 minutes
$y = 0.06\ x^{1.36}$
$R^2 = 0.99$

25 minutes
$y = 0.07 x^{1.35}$
$R^2 = 0.99$

30 minutes
$y = 0.04\ x^{1.38}$
$R^2 = 0.99$

Turbidity (NTU)

Concentration (mg/L)
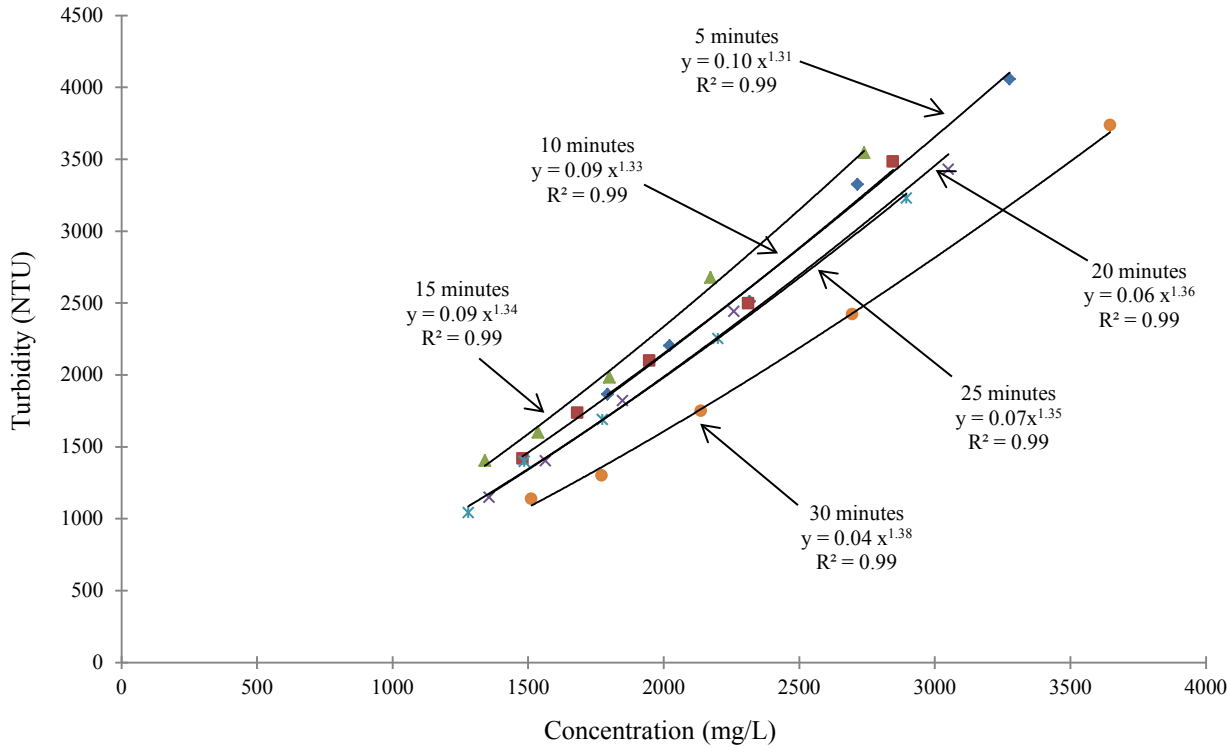
Figure B.20. Soil B Aliquot Samples

128

Figure B.21. TH23 - S Aliquot Samples
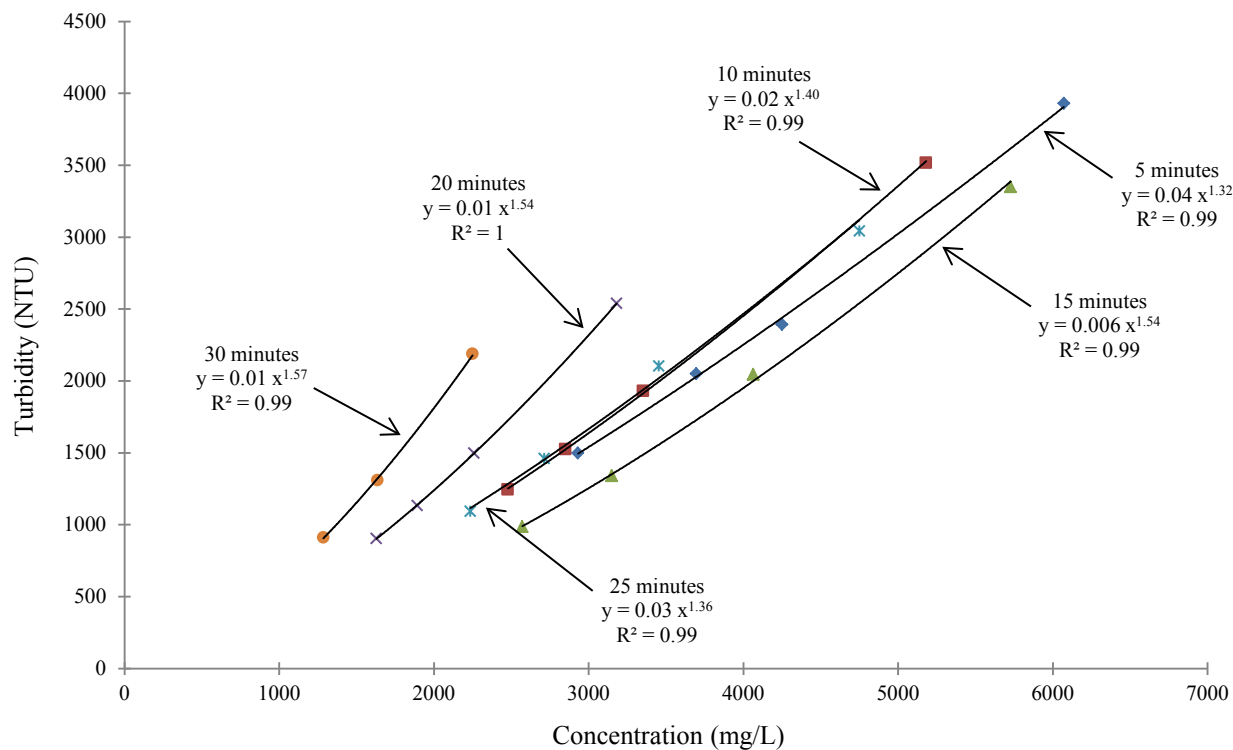
Figure B.22. TH23 - T Aliquot Samples

Appendix C
Particle Settling Data

After determining a relationship between turbidity and TSS using the methods described in Chapter 3, the effect of particle settling was explored. Chapter 4 discusses how the settlement of particle sizes over time from suspension effects the α and β coefficients in the turbidity and TSS relationship. Figures C.1. through C.15 show the non-diluted turbidity and TSS values for each sample extracted from a bucket of runoff collected from each soil. The sample for the total turbidity of the bucket, when sand settles out, and when silt settles out, representing the total, silt and clay, and clay particles still in suspension were diluted 5 times to create three independent turbidity and TSS relationships. These relationships were evaluated to determining how the coefficients change as particles settle out.

The raw data that was used to calculate dimensionless turbidity and sand, silt, and clay turbidity for each soil in Chapter 3 is shown in Table C.1.

Figure C.9. Hast - S Particle Settling
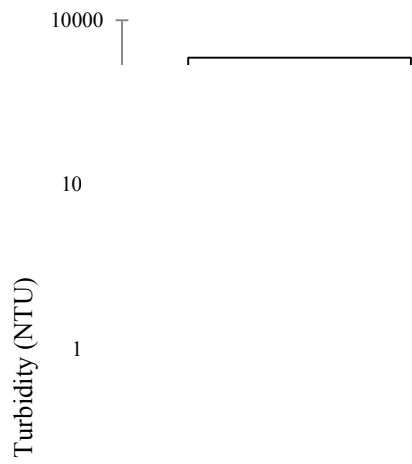
Figure C.6. CTY - S Particle Settling

Figure C.11. OV - S Particle Settling
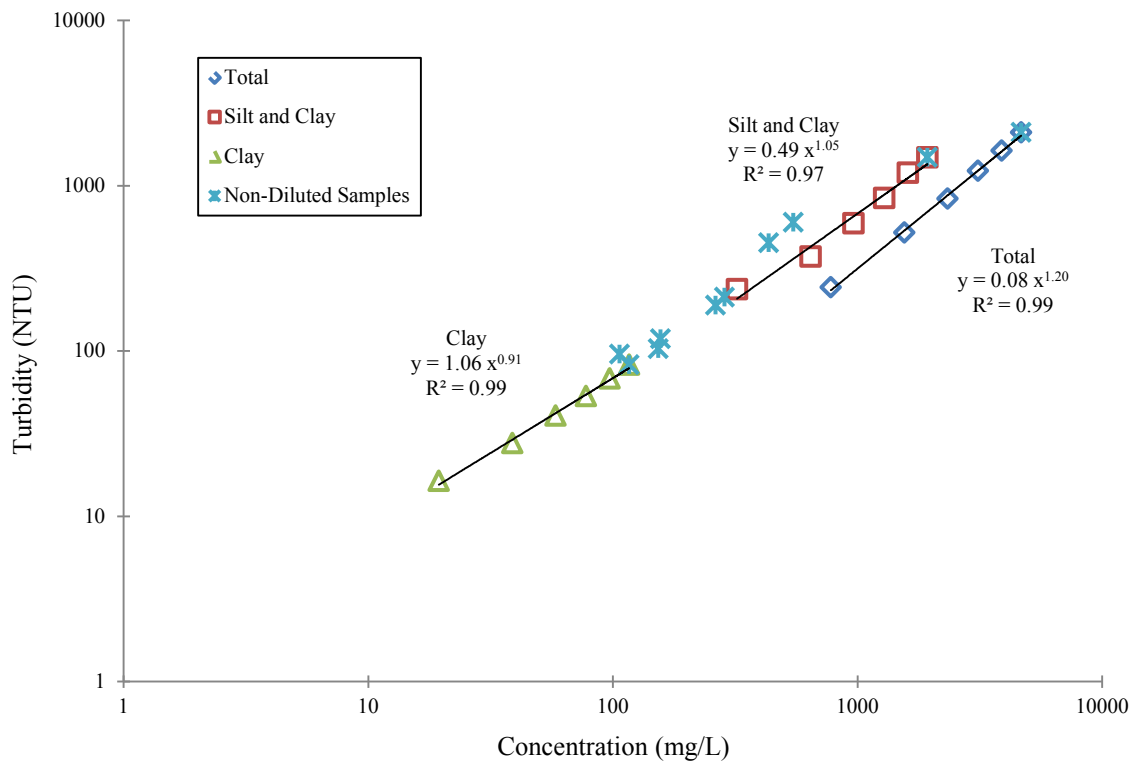
Figure C.12. Soil A Particle Settling

Figure C.15. TH - T Particle Settling

Figure C.14. contents: scatter plot with axes Turbidity (NTU) vs Concentration (mg/L), legend: Total, Silt and Clay, Clay, Non-Diluted Samples.

Silt and Clay
$y = 0.08\ x^{1.33}$
$R^2 = 0.99$

Total
$y = 0.18\ x^{1.23}$
$R^2 = 0.98$

Clay
$y = 2.23\ x^{0.89}$
$R^2 = 0.92$
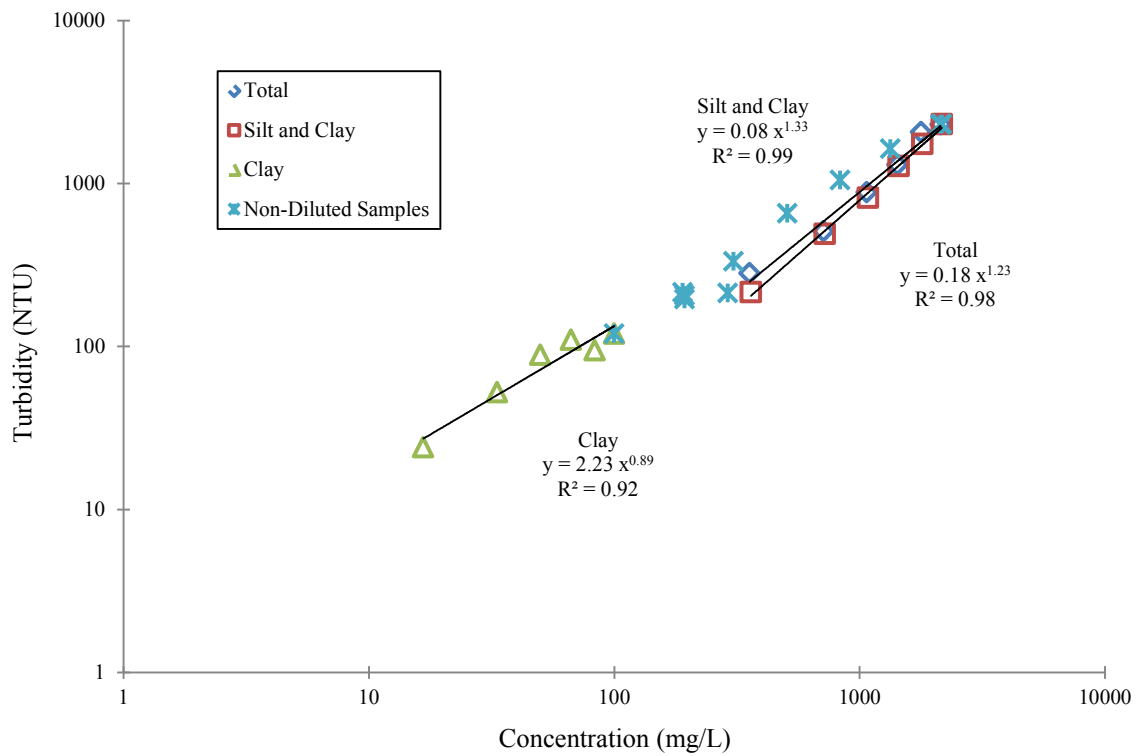
Figure C.14. TH - S Particle Settling

Table C.1. Particle settling data for each soil.

Row	Symbol	AHS	AHT 1	AHT 2	AHT 3	AHT 4	AHT 5	CTYS	CTYT
1	F_{total}	1.00	1.00	1.00	1.00	1.00	1.00	1.00	1.00
	F_{sc}	0.79	0.93	0.70	0.80	0.84	0.17	0.80	0.81
	F_c	0.007	0.037	0.063	0.057	0.029	0.012	0.079	0.048
2	T_{total}	4246.7	2605.0	1135.0	1201.3	2243.0	1058.7	2063.7	2528.3
	T_{sc}	4097.7	1900.3	911.0	1075.7	2046.3	302.0	1845.3	2311.7
	T_c	20.0	121.3	95.3	120.3	150.0	23.0	122.7	47.7
3	β_0	1.05	1.38	1.21	1.16	1.27	1.04	1.13	1.30
	α_0	0.514	0.047	0.080	0.133	0.057	0.148	0.262	0.057
4	ω_{total}	1.00	1.00	1.00	1.00	1.00	1.00	1.00	1.00
	ω_{sc}	0.98	0.99	0.97	0.98	0.98	0.84	0.98	0.98
	ω_c	0.55	0.70	0.75	0.74	0.68	0.60	0.77	0.73
5	ν_{total}	1.00	1.00	1.00	1.00	1.00	1.00	1.00	1.00
	ν_{sc}	1.22	1.07	1.35	1.20	1.16	4.44	1.21	1.20
	ν_c	70.36	16.70	10.45	11.38	20.60	42.47	8.63	13.23
6	T_{sand}	1227.4	338.5	434.2	344.9	515.9	777.7	615.4	676.7
	T_{silt}	3318.4	2185.5	605.4	774.0	1585.6	145.0	1220.2	1596.5
	T_{clay}	297.1	66.9	85.1	105.7	69.8	76.6	230.7	94.6
7	Actual	4246.7	2605.0	1135.0	1201.3	2243.0	1058.7	2063.7	2528.3
	Est.	4842.9	2590.9	1124.7	1224.6	2171.3	999.2	2066.3	2367.9
	Error	14.0	0.5	0.9	1.9	3.2	5.6	0.1	6.3
8	$T_{sand}*$	1.00	1.00	1.00	1.00	1.00	1.00	1.00	1.00
	$T_{silt}*$	0.80	0.89	0.66	0.79	0.79	0.24	0.79	0.74
	$T_{clay}*$	0.065	0.027	0.082	0.094	0.033	0.083	0.126	0.042
9	$T_{sand}*$	1.00	1.00	1.00	1.00	1.00	1.00	1.00	1.00
	$T_{silt}*$	0.96	0.96	0.90	0.94	0.93	0.95	0.94	0.91
	$T_{clay}*$	3.90	0.68	0.86	0.96	0.96	2.65	0.95	0.75
10	Sand	0	0	0	0	0	0	0	0
	Silt	20.7	7.7	34.8	19.4	18.3	297.0	19.5	22.7
	Clay	5860.6	2466.6	948.5	921.7	2791.8	3098.7	652.4	1706.7

Row	Symbol	DulS	HastS	HastT	OVS	Soil A	Soil B	THS	THT
1	F_{total}	1.00	1.00	1.00	1.00	1.00	1.00	1.00	1.00

	F_{sc}	0.50	0.54	0.47	0.95	0.41	0.96	1.00	0.69
	F_c	0.020	0.043	0.046	0.044	0.025	0.073	0.047	0.055
2	T_{total}	1902.7	3415.7	3284.3	2812.3	2094.0	4087.3	2304.3	3037.0
	T_{sc}	1270.3	2752.7	1818.7	2654.3	1483.0	3803.3	2312.7	2246.3
	T_c	40.3	77.0	124.0	44.0	82.3	139.7	119.7	198.7
3	β_0	1.07	1.26	1.34	1.35	1.20	1.35	1.33	1.49
	α_0	0.342	0.127	0.034	0.090	0.078	0.102	0.084	0.017
4	ω_{total}	1.00	1.00	1.00	1.00	1.00	1.00	1.00	1.00
	ω_{sc}	0.94	0.95	0.93	1.00	0.92	1.00	1.00	0.97
	ω_c	0.65	0.72	0.72	0.72	0.67	0.76	0.72	0.74
5	ν_{total}	1.00	1.00	1.00	1.00	1.00	1.00	1.00	1.00
	ν_{sc}	1.80	1.68	1.91	1.05	2.12	1.04	1.00	1.37
	ν_c	28.34	14.42	13.77	14.19	23.09	9.32	13.54	11.81
6	T_{sand}	1069.5	1785.1	1838.1	302.1	1378.2	470.9	94.7	1467.7
	T_{silt}	838.3	1285.5	836.9	2465.0	633.1	3620.0	2068.6	1585.9
	T_{clay}	169.7	151.6	82.0	105.0	82.0	207.4	94.2	63.1
7	Actual	1902.7	3415.7	3284.3	2812.3	2094.0	4087.3	2304.3	3037.0
	Est.	2077.4	3222.2	2757.0	2872.1	2093.3	4298.4	2257.4	3116.7
	Error	9.2	5.7	16.1	2.1	0.0	5.2	2.0	2.6
8	$T_{sand}*$	1.00	1.00	1.00	1.00	1.00	1.00	1.00	1.00
	$T_{silt}*$	0.53	0.47	0.34	0.93	0.36	0.94	1.00	0.54
	$T_{clay}*$	0.089	0.049	0.031	0.038	0.041	0.051	0.044	0.021
9	$T_{sand}*$	1.00	1.00	1.00	1.00	1.00	1.00	1.00	1.00
	$T_{silt}*$	0.90	0.81	0.74	0.97	0.80	0.98	1.00	0.81
	$T_{clay}*$	1.88	0.85	0.70	0.69	1.19	0.62	0.72	0.49
10	Sand	0	0	0	0	0	0	0	0
	Silt	70.6	74.0	115.9	4.9	124.3	4.5	0.0	49.3
	Clay	2014.4	1624.6	2189.2	1712.6	2820.8	1121.6	1544.5	2261.7

Table C.2. Row descriptions for Table C.1.

Row #	Description
1	Fraction finer values from laboratory concentration data
2	Laboratory turbidity values as each particle class is removed from suspenstion
3	α_0 and β_0 values from labortory data
4	ω estimated with fitted function: $\omega = 1 + 0.09 * Ln(F)$
5	ν estimated with fitted function: $\nu = F^{-0.85}$
6	Turbidity of individual particle classes, found using estimated ω and ν (rows 6 and 8)
7	% Error between actual total turbidity and sum of turbidities found for each particle class
8	Dimensionless T*, found with concentration
9	Dimensionless turbidity, T*, found without concentration
10	% Error between T* using concentration and T* not using concentration

Appendix D
Field Data

The turbidity and concentration data for the field samples collected during the August 3 storm on the Arden Hills site are shown in Table D.1. The estimated turbidity values using Model 1 and Model 2 and the particle settling relationships are also shown in Table D.1. Table D.2 shows the estimated α values using Model 1 and Model 2. Table d.3 shows the estimated α and β values after particle settling occurs on the site.

Table D.1. Field data

Sample #	Time (min)	Conc. (mg/L)	Turbidity (NTU)	Estimated Turbidity (NTU)		
				Model 1	**Model 2**	**No Sand**
1	0	4430	>4000	3468.1	3207.9	3052.9
2	5	8620	>4000	8807.2	8146.4	7362.4
3	10	6940	>4000	6501.7	6014.0	5527.4
4	15	5470	>4000	4659.2	4309.6	4034.8
5	20	4730	>4000	3801.3	3516.1	3329.3
6	25	3380	>4000	2374.7	2196.6	2134.8
7	30	9410	>4000	9957.5	9210.5	8267.5
8	35	10930	>4000	12279.9	11358.6	10077.9
9	40	9530	>4000	10135.7	9375.4	8407.3
10	45	8880	>4000	9181.3	8492.5	7657.4
11	50	8050	>4000	8002.8	7402.4	6725.6
12	55	6870	>4000	6410.1	5929.2	5453.8
13	60	7170	>4000	6805.4	6294.8	5770.9
14	65	6710	>4000	6202.1	5736.8	5286.5
15	70	6770	>4000	6279.9	5808.7	5349.1
16	75	6660	>4000	6137.5	5677.0	5234.4
17	80	6190	>4000	5539.8	5124.2	4751.6
18	85	5630	>4000	4851.1	4487.1	4191.6
19	90	5280	>4000	4434.2	4101.5	3850.6
20	95	4210	>4000	3229.4	2987.1	2854.1
21	100	4650	>4000	3711.6	3433.1	3255.0
22	105	3470	>4000	2463.7	2278.9	2210.3
23	110	3940	>4000	2943.2	2722.4	2614.6
24	115	3890	>4000	2891.0	2674.2	2570.8

Table D.2. Calculation of α with Model 1 and Model 2.

	Model 1	Model 2
% Silt	54	54
S	0.163	-
K_i	1.76E+06	-
α	0.028	0.025

Table D.3. Calculation of α and β with particle settling.

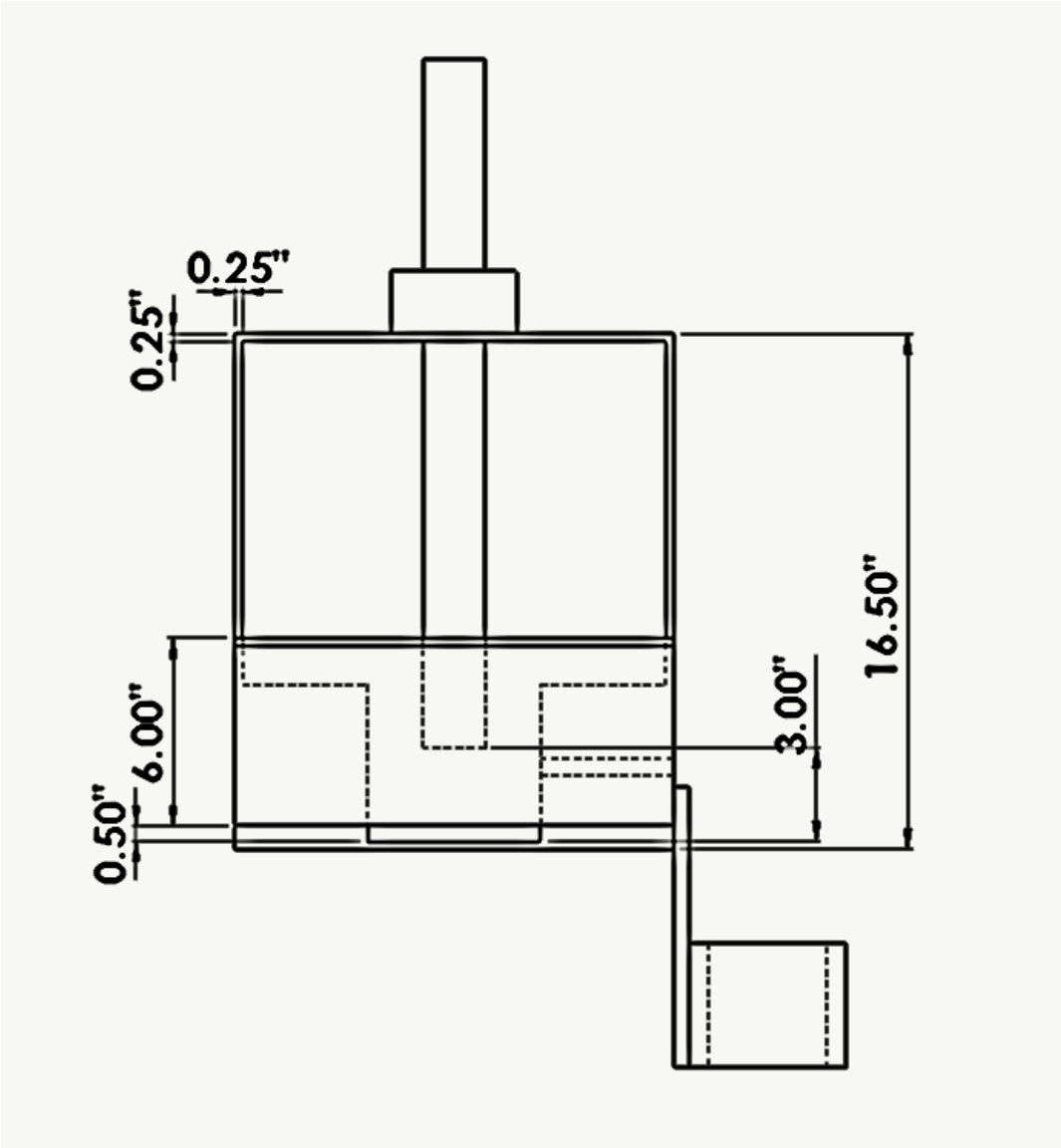|	
F_d	0.54
ν	1.689
ω	0.945
α	0.047
β	1.322

Appendix E
Dimensions of Turbidity and Flow Rate Two-Stage Monitoring Box
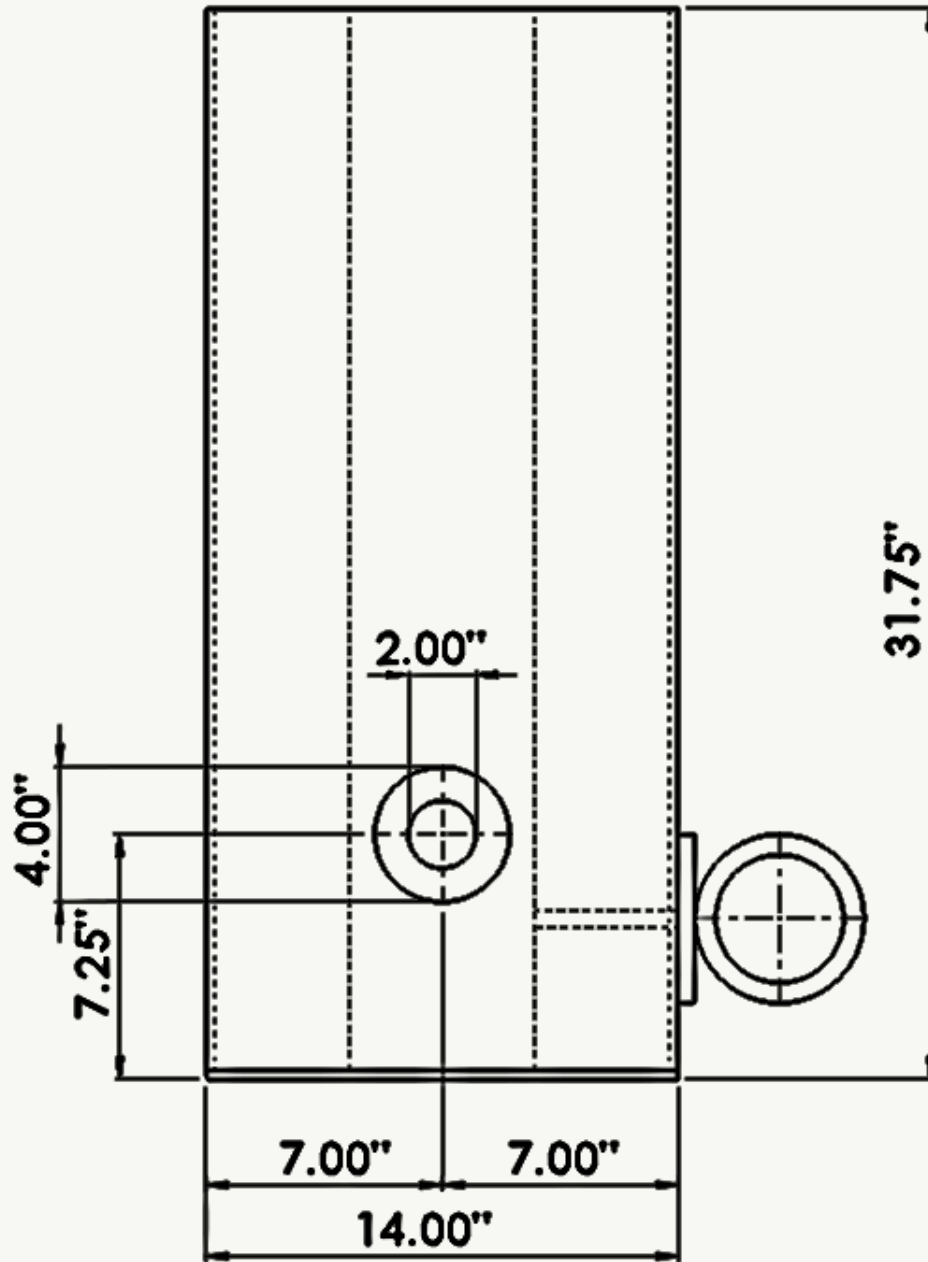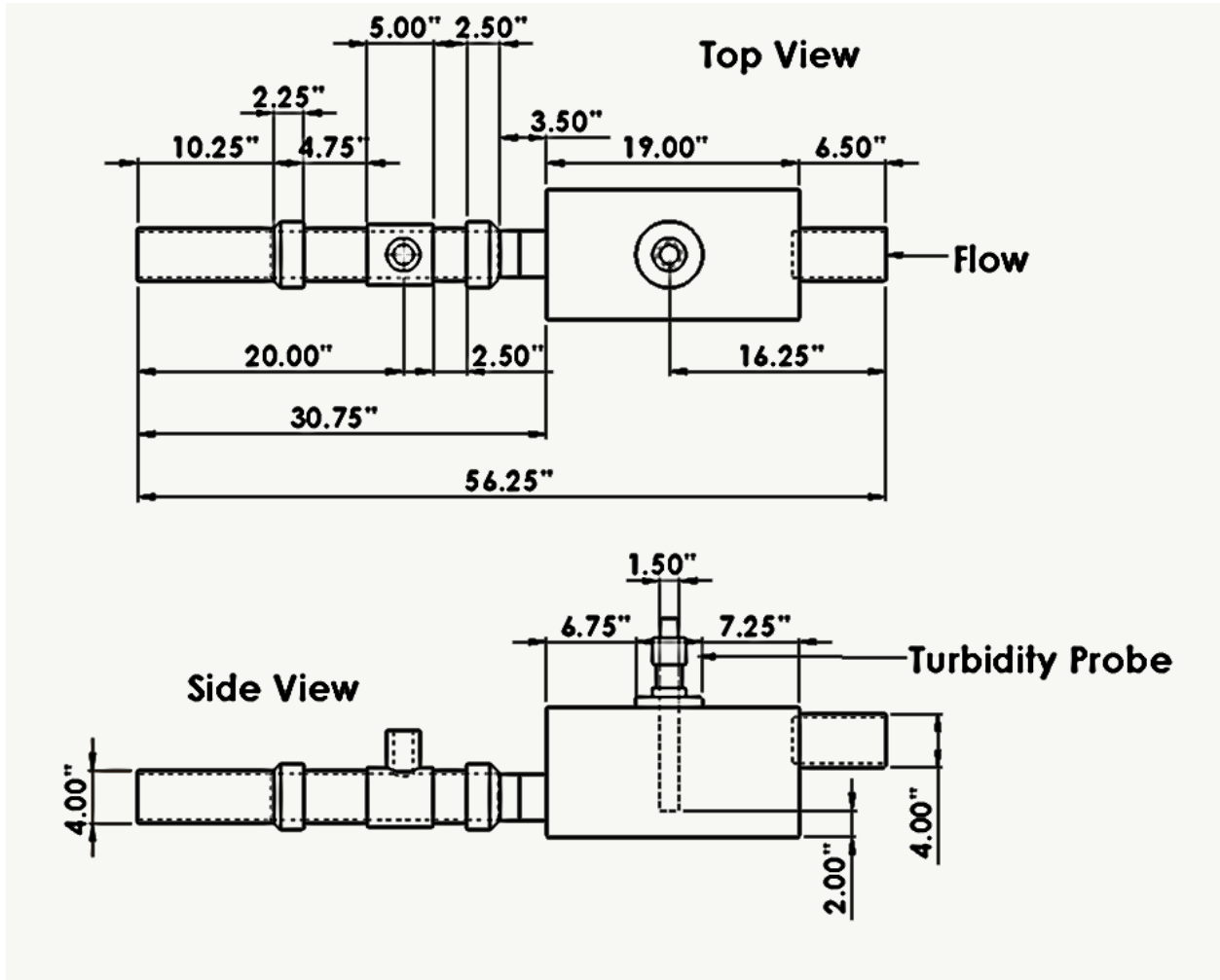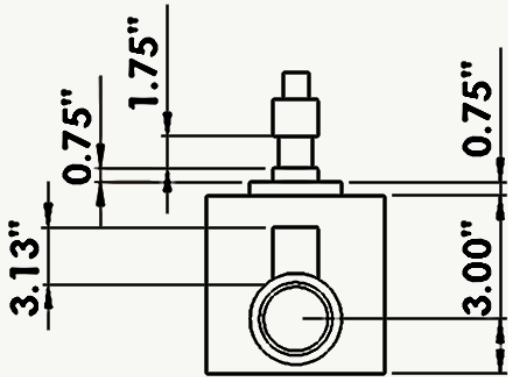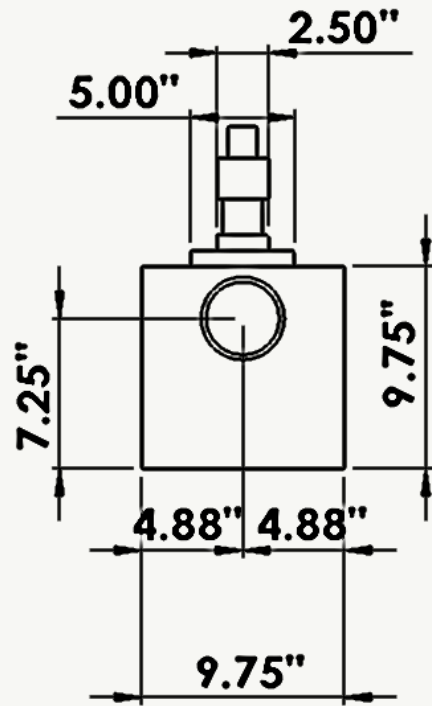
Isometric View

FLOW
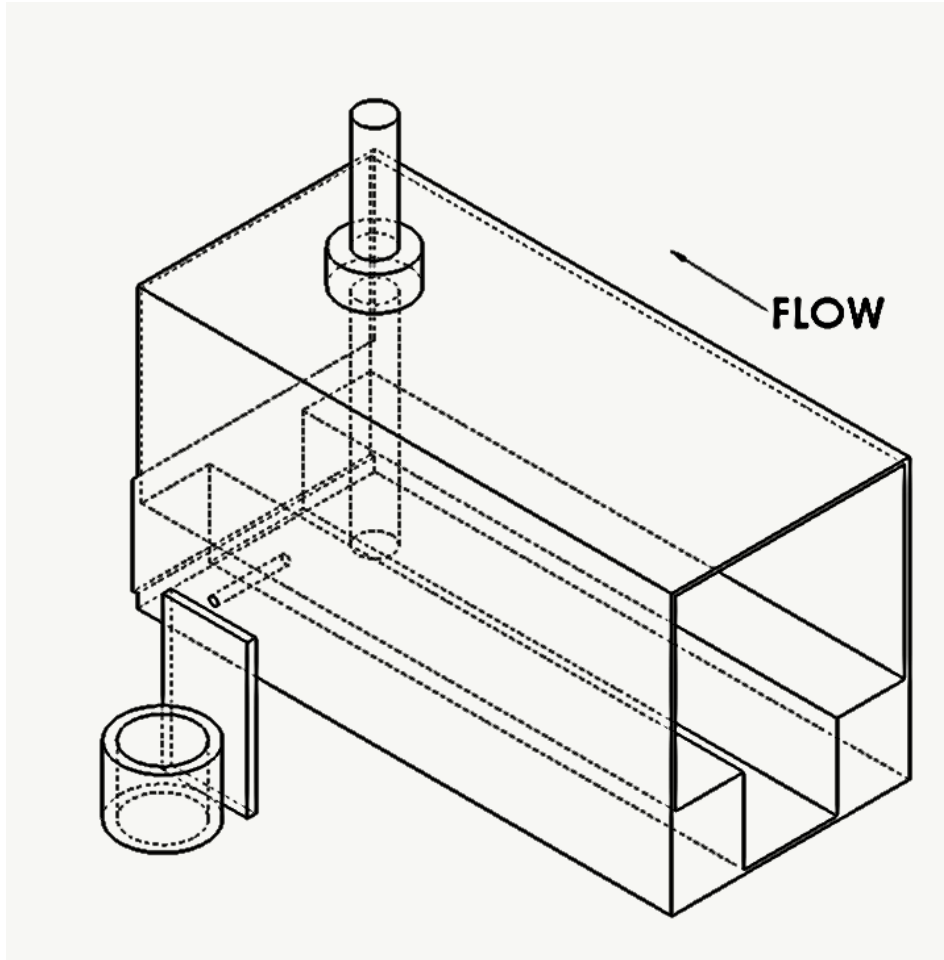
Back View

Top View

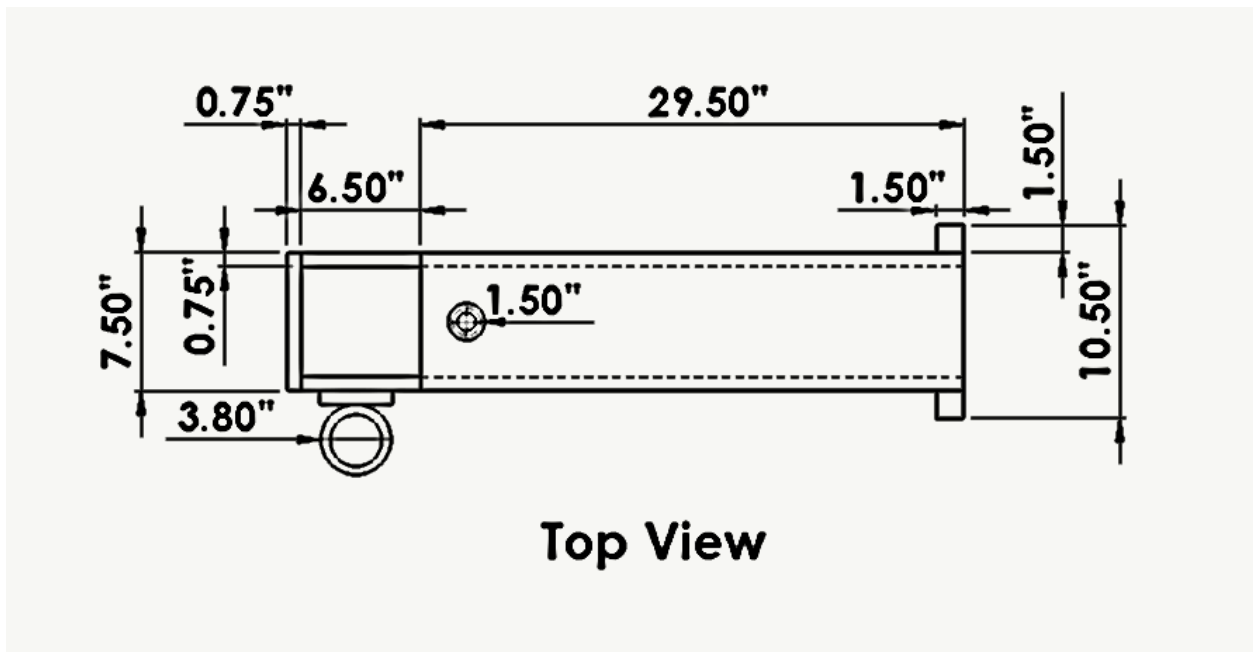**Dimensions of Turbidity Monitoring Device for De-watering**
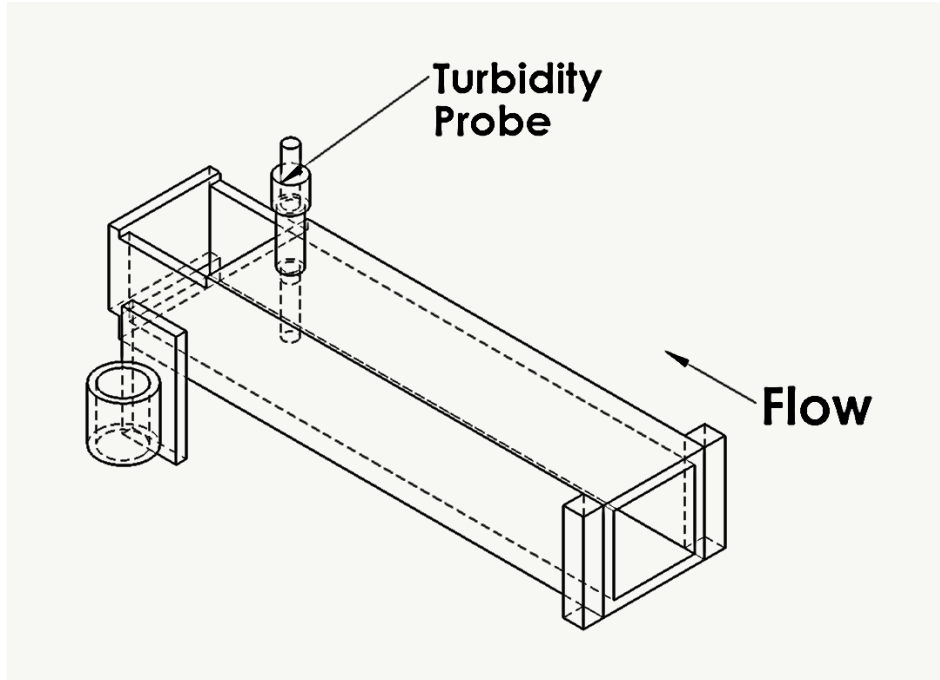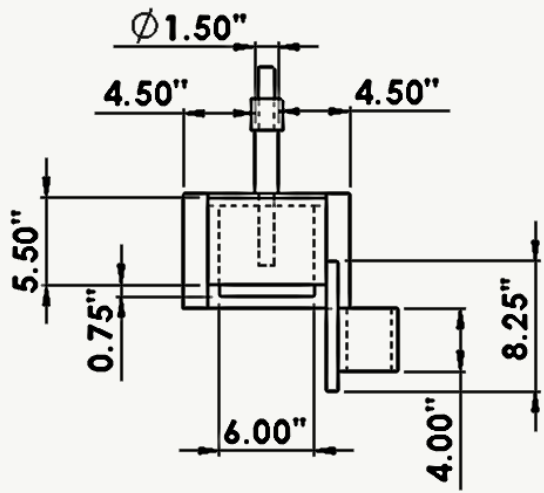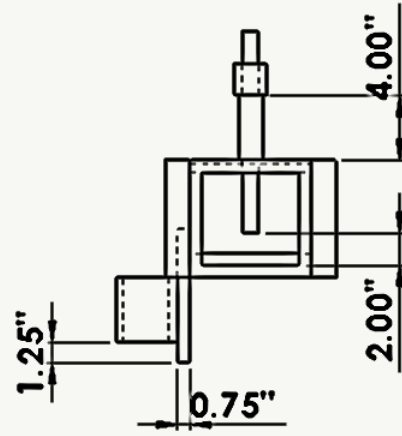
Downstream View

Upstream View

143

Dimensions of Turbidity Monitoring Box

Downstream View

Upstream View